The

PHILOSOPHICAL MAGAZINE

FIRST PUBLISHED IN 1798

OL. 46 SEVENTH SERIES No. 380 September 1955

A Journal of Theoretical Experimental and Applied Physics

PRICE 15s. 0d.
Annual Subscription £8 0s. 0d. payable in advance

ED AND PUBLISHED BY TAYLOR & FRANCIS LTD., RED LION COURT, FLEET ST., LONDON, E.C.4

CVI. *The Sensitivity of Electron Diffraction as a Means of Detecting Thin Surface Films : I*

By R. C. Newman and D. W. Pashley*
Physics Department, Imperial College, London†

[Received in revised form April 4, 1955]

Abstract

Very thin layers (0–20 Å) of silver bromide and of copper have been deposited on to smooth (111) surfaces of silver single crystals. The thickness of these layers has been determined by means of a radioactive technique. The electron diffraction patterns from the layers have been studied as a function of their thickness. The layers do not grow as uniform films but as nucleated deposits. It is found that the thinnest detectable layer is 0·4 Å in mean thickness for the silver bromide and 0·8 Å for the copper.

§ 1. Introduction

Electron diffraction provides a powerful tool for the study of thin surface films when the reflection method is used. Although information concerning crystal size, structure, orientation and lattice spacing is readily obtainable, it is extremely difficult to estimate the average thickness of a very thin layer. In particular, the minimum thickness of a detectable surface film is not known.

Various types of surface deposits, of 100 Å or less in mean thickness, are commonly studied. These layers are formed by electrodeposition, chemical attack, condensation from the vapour *in vacuo* and growth from solution. The thickness of the layers may be estimated by such methods as weighing, multiple beam interferometry and from Faraday's law in the case of electrodeposits. For film thicknesses of less than 10 Å, these methods become insensitive or unreliable.

The direct estimation of film thickness from the electron diffraction pattern is limited by :

(*a*) the lack of a detailed theory which predicts the intensities of the diffracted beams relative to the background intensity,

(*b*) the marked influence on the pattern of the substrate surface topography,

(*c*) the effect on the pattern of the mode of growth of the deposit.

Raether (1949, 1950, 1951) has considered the effect of (*b*) on the assumption that the deposit grows as a uniformly coherent film, which

* Imperial Chemical Industries Research Fellow, University of London.
† Communicated by the Authors.

follows the topography of the substrate. He considered three special cases :

(1) electron optically smooth surfaces (e.g. crystal cleavage surfaces),

(2) slightly undulating surfaces (e.g. electropolished surfaces),

(3) rough surfaces (e.g. etched or abraded surfaces).

The sensitivity for observation of the thinnest deposits decreases as the surface becomes progressively rougher. In the case of a smooth surface, the deposit will cause the diffraction pattern from the substrate to be obscured below a certain value of the angle between the electron beam and the surface (hereafter denoted by α). If this critical value of α can be determined, and if the relevant mean free path for electron scattering by the deposit material is known, then the thickness of the deposit may be estimated. Raether gives an approximate method of determination of this mean free path. The method has been used by both Raether (1950) and Lucas (1951) to estimate the thickness of zinc oxide on a cleavage surface of zinc, but it is limited and not very accurate.

Schulz (1951, 1952 a, b, c) has systematically studied the growth of alkali halides on various substrates, and he estimated the thickness of the layers, to an accuracy of $\pm 20\%$, from the radiation characteristics of the source. He calibrated this by depositing a thick layer, the thickness of which was determined either by weighing or by an optical method. He claimed that with a cleavage face as substrate an observable diffraction pattern could be obtained from a deposit only one or two Ångströms in average thickness. Seifert (see Gomer and Smith 1953, pp. 360 and 383) has expressed doubts as to whether such thin layers can be detected in this way.

An accurate and reliable method of thickness measurement is therefore required to test the validity of Schulz's conclusions concerning the sensitivity of the electron diffraction method. Now that a large number of radioactive isotopes are available, it is possible to use tracer methods for thickness measurements. Deposits have therefore been formed on flat substrate surfaces and the change of the diffraction pattern has been studied as a function of the deposit thickness in the range 0–20 Å, this thickness being measured by a radioactive method. In particular, the thinnest deposit layer which would give rise to an observable diffraction pattern has been determined. The substrate consisted of atomically smooth (111) faces of silver crystals, and the deposits consisted of (i) silver bromide grown by chemical attack of the silver and (ii) metallic copper deposited from the vapour phase.

§ 2. Specimen Preparations

The silver substrates were prepared by condensation on to a cleavage surface of mica heated to about 270°c. A detailed account of the

preparation and properties of these specimens will be given later. The main advantages for the purpose of these experiments are :

(1) the specimens are easily prepared in large numbers,

(2) the silver is well oriented, in single positioning, with its (111) face parallel to the mica surface,

(3) the surfaces are ' atomically smooth ' over areas large compared with atomic dimensions.

The specimens were mounted on small brass blocks, which were clamped directly in the specimen holder of the camera. The edges of the mica were painted with ' Aquadag ' which prevented charging up of the specimens in the electron beam, and allowed fairly low values of α to be used.

(*a*) *Bromide Layers*

The bromine was prepared by the oxidation of ammonium bromide, which had been exposed to neutrons in the Harwell pile. The bromine gas was dissolved in water to give a stock solution, from which subsequent working solutions were obtained by dilution. The silver specimens were exposed to the bromine vapour, which was in equilibrium with a given strength of solution, by suspending them above the surface of the solution. By trial and error, a strength of solution was found which gave a convenient rate of growth of the bromide of about 3 Å/min. The exposure times were varied so that specimens of different thickness were obtained ; these specimens could be stored indefinitely without any loss in the quality of their diffraction patterns.

(*b*) *Copper Layers*

The copper layers were prepared in the evacuated electron diffraction camera, by evaporation of metallic copper from a tungsten filament. The ' specpure ' copper was cut into suitably sized pieces, for subsequent insertion in the tungsten spiral, before being sent for exposure to neutrons in the pile. The evaporation was carried out with the substrate at room temperature, and the diffraction pattern from the surfaces was simultaneously observed on the fluorescent screen. The arrangement of the specimen chamber has already been described (Kehoe, Newman and Pashley 1954) ; the vacuum was about 10^{-4} mm Hg, as measured by a hot filament ionization gauge.

The rate of deposition was adjusted to a convenient value of about 0·5 Å/minute by variation of the current through the tungsten filament. Since the copper oxidizes when exposed to air, all the plates required from a given deposit were taken before the specimen was removed from the camera. The reloading of the plate holder was carried out while the vacuum was maintained immediately around the specimen by means of a special vacuum lock (Kehoe, Newman and Pashley 1954).

§ 3. Thickness Measurement

Both isotopes used (Br 82 and Cu 64) are β, γ emitters, and in the present experiments the β-rays were counted. The relevant data for these isotopes are given in table 1.

Table 1

Isotope	Br 82	Cu 64
Maximum β energies (MeV)	0·45	0·66
Half-life (hours)	35·5	12·8
Initial specific activity (mc/g)	110	50
Initial counting sensitivity (counts/min/Å above background)	110	180

The counting apparatus consisted of a G.E.C. type GM4 counter, used in conjunction with a standard power pack and scaler. The counter was housed in a lead container which halved the background counting rate. The specimen was mounted immediately behind a circular aperture $\frac{1}{8}$ in. in diameter, which was placed directly in front of the counter window. In this way, all specimens were placed in exactly the same position, and their effective areas were equal. Since the back scattering corrections were also the same for all specimens, an accurate comparison between the thickness of any two specimens was possible.

The absolute values of thickness were determined from a calibration, which was carried out after the isotopes had decayed by a factor of about a thousand. For the purpose of this calibration the ammonium bromide was converted into silver bromide, by precipitation from a silver nitrate solution. Thick layers (about 1000 Å) of the silver bromide were deposited by evaporation on to clean glass slides (1 in. $\times$ 1 in.), and the amount of bromide in these layers was determined by means of a semi-microbalance. An identical thickness of bromide was simultaneously evaporated on to one of the silver specimens ; this specimen was used for the determination of the counting rate corresponding to the measured film thickness. The counting sensitivity could then be calculated for any time during the experiment. The same procedure was used for the copper, which was evaporated as the metal.

The absolute accuracy was about $\pm 15\%$. The relative accuracy was determined only by the number of counts registered and was better than $\pm 5\%$, except for layers less than 2 Å in thickness for which measurements were accurate to $\pm 0{\cdot}1$ Å.

§ 4. The Effect of Deposit Thickness on the Diffraction Patterns

All diffraction photographs were recorded on Ilford thin film half tone plates (N50), which were developed for 2 minutes in ID2. The accelerating potential for the electrons was maintained at about 45 kv.

(a) Silver Bromide Layers

A large number of specimens was prepared, ranging in thickness from about 0·2 Å to 20 Å. After the thickness of the bromide layer had been measured, the specimen was examined in the diffraction camera and photographs were taken at various values of α (defined in § 1). In all cases where the silver bromide was observed, it was oriented with its (111) planes parallel to the silver (111) surface. The orientation was partly fibrous with a preference for the $[1\bar{1}0]$ and $[\bar{1}10]$ silver bromide directions to be parallel to the silver $[1\bar{1}0]$ direction.

Specimens covered by layers of mean thickness less than 0·4 Å gave rise to diffraction patterns which were indistinguishable from those obtained from the freshly prepared silver specimens (see fig. 1, Plate 15). Layers of mean thickness between 0·4 Å and 1·0 Å were observable by means of secondary diffraction patterns, such as that shown in fig. 2 (Plate 15), the interpretation of which is given in fig. 3. Primary diffraction spots were observed from the bromide when the thickness

Fig. 3

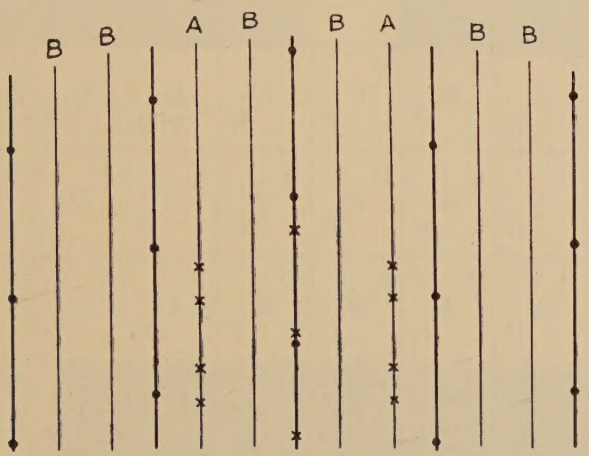

Interpretation of fig. 2 (Plate 15).

- Spots due to the substrate silver ; (111) surface, $[1\bar{1}0]$ azimuth. These spots are drawn out into almost continuous streaks due to the flatness of the surface, which restricts the penetration of the electrons to the top one or two atomic layers, when small values of α are used.

× Spots which would appear due to the oriented silver bromide ; streaks A and B are due to secondary diffraction, the silver streaks acting as sources for diffraction by the bromide.

was increased beyond 1·0 Å. Figure 4 (Plate 15) shows such a pattern from a layer 2·6 Å in thickness, at a low value of α. As α was increased, the cross-grating (primary) spots became weaker and the secondary diffraction pattern started to appear (see fig. 5, Plate 16). At higher

Table 2. Results for the Silver Bromide Layers

Thickness (Å) \ $\alpha°$	0·6	0·9	1·2	1·6	2·0	2·5	3·5	4·5
0·6	B O C	B O C	A O C	A O D	A O E	A O F	A O G	A O H
1·0	D O D	C O C	B O C	A O C	A O D	A O D	A O F	A O G
1·2	E D F	D E D	C G C	B H D	A H D	A O D	A O E	A O F
1·5	F B G	D C E	C C D	B E D	A F D	A G D	A O D	A O E
2·5	G A H	G B F	D C E	C C E	A D D	A D D	A G C	A O D
3·5	G A H	G B F	D C E	C C E	A D D	A D C	A F C	A H C
4·5	H A H	H A G	E B G	C B F	B C E	A C D	A E D	A H C
7·0	H A H	H A G	F A G	E A F	D A F	C C E	B D E	B F E
11·0	O A O	O A O	O A O	H A O	E A G	C B F	B D E	B F E
19·0	O A O	O A O	O A O	H A O	G A O	C B F	C C F	B E E

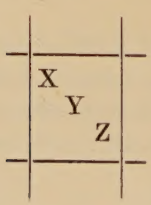

X Intensity of silver pattern
Y Intensity of primary silver bromide pattern
Z Intensity of secondary pattern

Fig. 1

Freshly prepared silver substrate.
(111) surface, [1$\bar{1}$0] azimuth.

Fig. 2

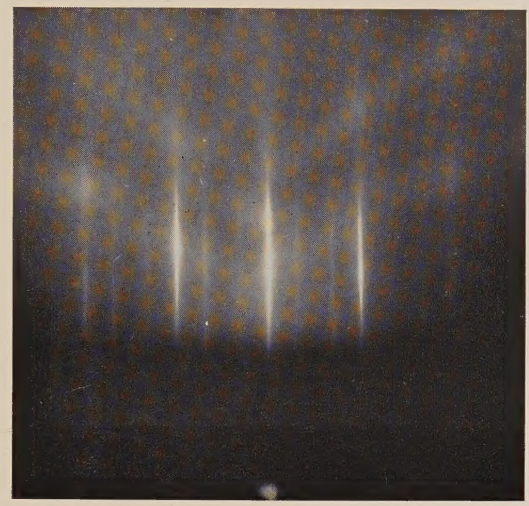

Silver substrate plus 0·6 Å of silver bromide.
α=1·8°, silver [1$\bar{1}$0] azimuth.

Fig. 4

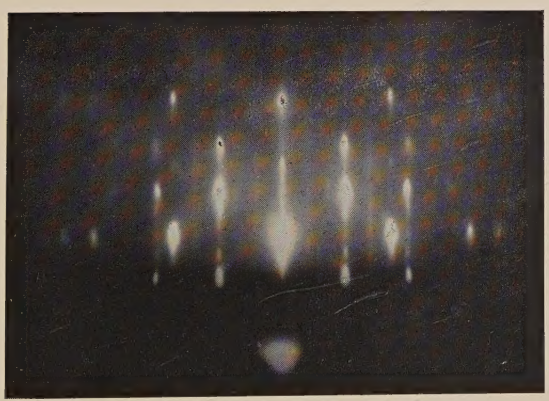

Silver substrate plus 2·6 Å of silver bromide.
α=1·0°, silver [1$\bar{1}$0] azimuth.

Fig. 5

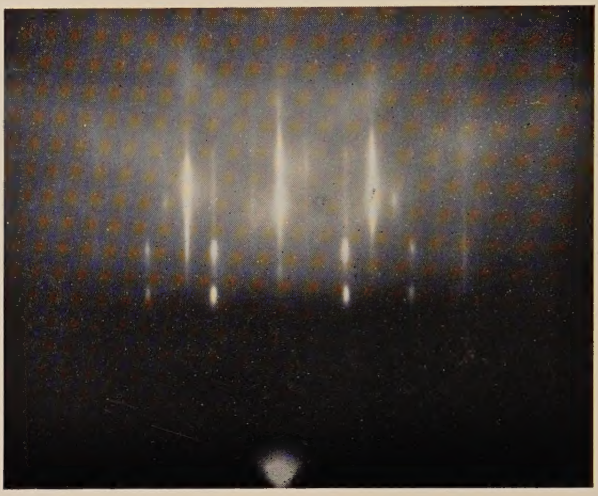

As for fig. 4, except $\alpha = 2{\cdot}2°$.

Fig. 6

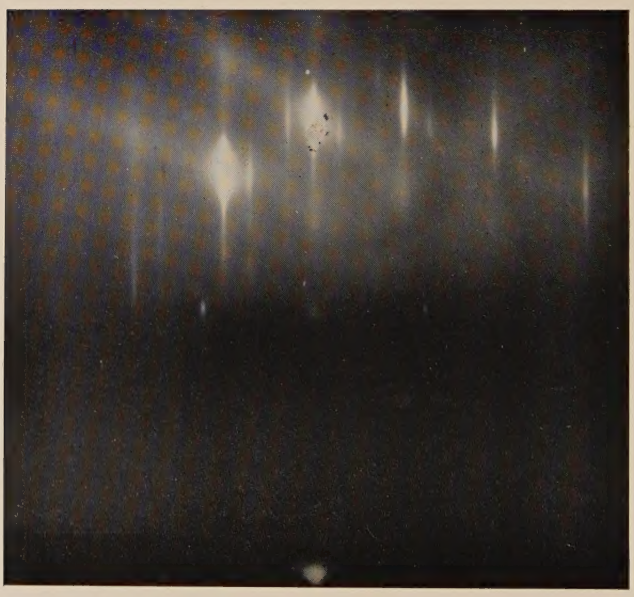

As for fig. 4, except $\alpha = 3{\cdot}4°$.

Fig. 7

substrate plus 7·0 Å of silver bromide.
$\alpha=1{\cdot}2°$, silver $[1\bar{1}0]$ azimuth.

Fig. 8

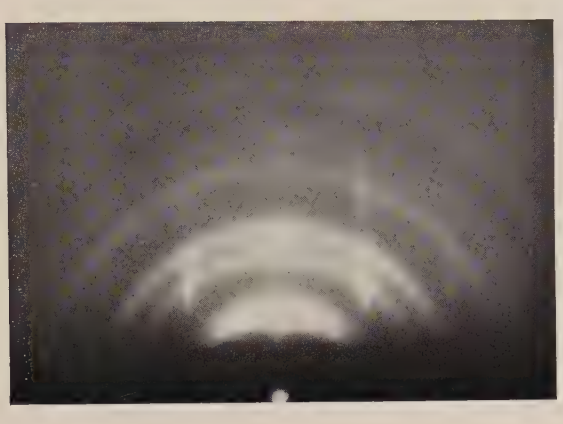

Silver substrate plus 15 Å of copper.
$\alpha=0{\cdot}9°$, silver $[1\bar{1}0]$ azimuth.

Fig. 9

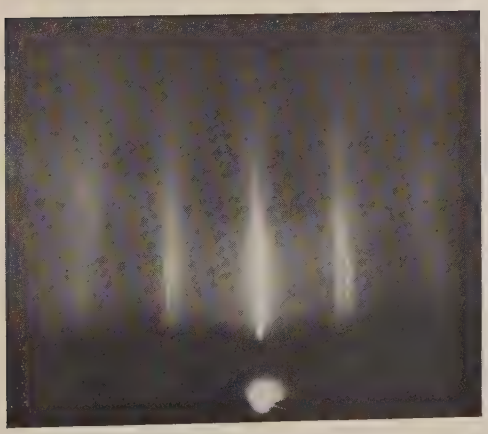

Silver substrate plus 0·9 Å of copper.
$\alpha=0{\cdot}9°$, silver $[1\bar{1}0]$ azimuth.

Fig. 11

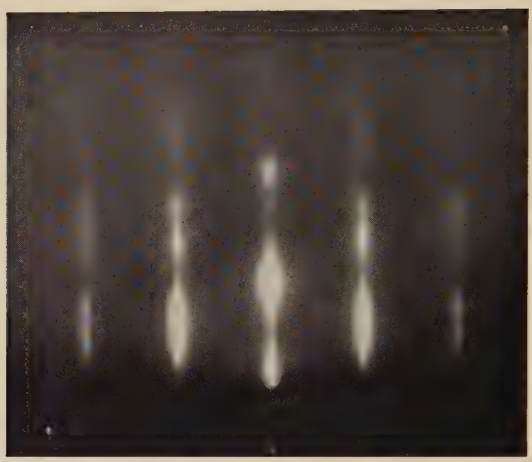

Silver substrate plus 3·3 Å of copper.
$\alpha=1°$, silver $[1\bar{1}0]$ azimuth.

Fig. 12

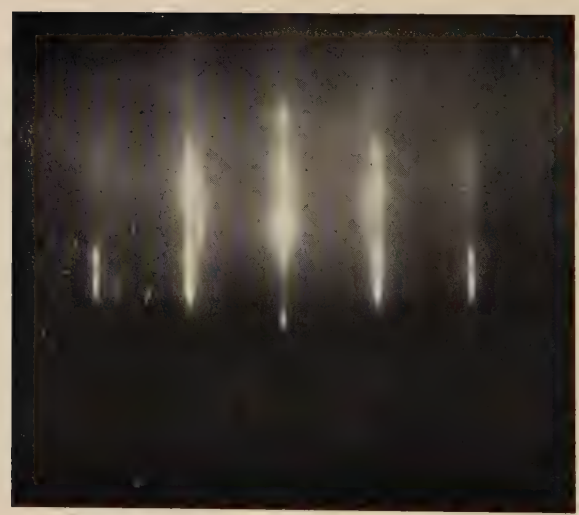

As for fig. 11, except $\alpha=2{\cdot}6°$.

values of α, as shown in fig. 6 (Plate 16), the secondary diffraction pattern predominated over the primary pattern, and a strong silver pattern was observed. With further increase of thickness, the primary diffraction pattern from the bromide became quite strong (see fig. 7, Plate 17), and was visible at all values of α up to 5°. These results are presented in table 2. The intensities of the components of the pattern are estimated qualitatively by visual inspection, and are denoted in order of decreasing intensity by means of the letters A–H. O indicates the absence of a particular component. The table is intended to show only the character of the variations of the diffraction pattern with thickness and α, and is not quantitative.

The silver substrates give rise to quite prominent Kikuchi patterns, which become slightly less distinct as the bromide is grown on the specimens. Even with the thickest layers (20 Å), these Kikuchi patterns are still easily distinguished.

Since prominent cross-grating spots are observed from bromide layers as thin as 1·2 Å, the deposits do not grow as a uniform film, but in the form of a large number of nuclei. Hence only a fraction of the surface is covered. Attempts have been made to estimate the size and shape of these nuclei. The diffraction patterns show no definite refraction effects, so that the nuclei do not possess atomically smooth surfaces. The measurement of the size of nuclei is always uncertain, particularly since the size of the diffraction spots varies considerably with photographic exposure. The size of the focused central spot on the photographic plate was small compared with the size of the diffraction spots, so that the length of the diffraction spots in any direction can be used for the measurement of the thickness of the nucleus in that direction. It has been assumed that there is no other cause of appreciable spot broadening, such as ' tailing ', for which there was no evidence. Measurements gave for the average size a height of about 40 Å and a width of about 70 Å ; it was not possible to detect any change in the size of the nuclei as the thickness of the layer was increased.

The lattice spacing of the bromide layers has been measured relative to that of the substrate silver. Because of the nature of the patterns, it was possible to measure spacings only of planes perpendicular to the surface. From measurements of the primary pattern on a large number of plates, the value of $5{\cdot}737 \pm 0{\cdot}018$ Å was obtained for a_0. This is 0·5% lower than the x-ray value of 5·768 Å. In this case the measurements from the various plates were quite consistent, within the above accuracy which was limited by the size and shape of the diffraction spots from the silver bromide. When the secondary diffraction patterns were measured, however, satisfactory consistency was not obtained. Most specimens gave values which were in agreement with the above value for the primary measurements, but some gave much higher values (by as much as 2%) which varied from plate to plate taken from the same specimen. The reason for these variations is not known.

(b) Copper Layers

A number of specimens was prepared ranging in mean thickness from 0·4 Å to 20 Å. Initially the deposited copper was always oriented with its (111) planes parallel to the silver surface, and with the $[1\bar{1}0]$ and $[\bar{1}10]$ copper directions parallel to the $[1\bar{1}0]$ silver direction. As the thickness was increased some randomly oriented copper was simultaneously formed, being just visible as broad rings at a mean thickness of about 5 Å. When the deposit thickness was increased to about 15 Å, the rings became more distinct and had approximately the same intensity as that of the spot pattern (see fig. 8, Plate 17).

Layers of less than 0·7 Å in mean thickness gave rise to no extra features in the diffraction patterns from the substrate silver. At about 0·8 Å elongated spots due to primary diffraction by copper nuclei appear. These spots increase rapidly in intensity for further small increases in thickness. A typical example is shown in fig. 9 (Plate 17); the interpretation is given in fig. 10. At about 5 Å, the silver pattern is almost

Fig. 10

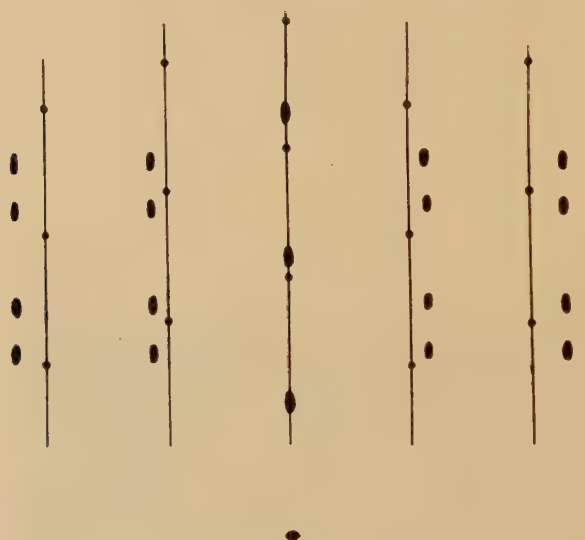

Interpretation of fig. 9 (Plate 17).

- Spots due to the substrate silver; (111) surface, $[1\bar{1}0]$ azimuth. These spots are drawn out into almost continuous streaks because of the flatness of the surface, as for fig. 3.
- Spots due to copper; (111) surface, $[1\bar{1}0]$ and $[\bar{1}10]$ azimuths.

completely obscured for all values of α less than about 2°. Most specimens of thickness less than 5 Å gave rise to secondary diffraction effects; they were much less prominent than in the case of the bromide layers. These results are given in table 3, where the same scheme is

used as in table 2. At $\alpha=1°$, quite a thin layer of copper causes the diffraction pattern from the silver substrate to be almost obscured (see fig. 11, Plate 18). The copper pattern consists of a cross-grating of strong

Table 3. Results for the Copper Layers

Thickness (Å) \ $\alpha°$	0·5	0·7	1·0	1·3	1·6	2·0	2·5	3·0
0·8	A A O	A A O	A A O	A B H	A B H	A C H	A D G	A F G
1·0	B A O	A A O	A A O	A B H	A B H	A C G	A C G	A D F
1·3	E A O	D A H	D A G	C A G	B B G	A B G	A B G	A B E
2·0	F A H	E A G	D A G	C A F	B A F	B A D	A B D	A B D
2·5	G A H	F A H	F A H	E A G	E A G	D A F	B A E	A B D
3·3	H A H	G A H	F A H	F A H	E A G	E A G	C A F	C A D
7·7	O A O	O A O	O A O	O A O	O A O	O A O	O A O	G A H

X Intensity of silver pattern
Y Intensity of primary copper pattern
Z Intensity of secondary pattern

elongated spots. Some of these spots are seen to be split into pairs in a direction parallel to the shadow edge. This fine structure fits neither with the splitting expected from the occurrence of reciprocal lattice spikes (Laue 1936, 1937) arising from crystal shape effects, nor with

effects due to refraction. No satisfactory explanation has been found. A possible explanation seems to be that dislocations are present in the copper nuclei. A more detailed examination would be necessary to check this point ; it is beyond the scope of the present work. An increase of α causes the silver pattern to become stronger, as shown in fig. 12 (Plate 18).

The Kikuchi patterns from the silver substrate became gradually less distinct as the thickness of the copper was increased. At a thickness of about 20 Å the patterns were completely obscured for $\alpha < 2°$.

The diffraction spots from the copper nuclei were not in the normal Laue positions, but were displaced towards the shadow edge of the patterns. This shift is due to refraction of the electrons during entry and exit at the crystallite surfaces. The magnitude of the shift was less than the full value to be expected for an inner potential of 14 volts, which is the value calculated by Tull (1951). This would result from an averaging effect, due to the possibility of the electrons entering the nuclei by one facet and leaving by another. A displacement occurs only as the electrons pass through the top surface, which is therefore very smooth on an atomic scale. From the size and shape of the diffraction spots it is deduced that the nuclei are plate-like, with a height of about 12 Å and lateral dimensions of about 60 Å. The measurement of the height must be taken as a lower limit, because part of the elongation of the spots might arise from variable refraction effects. No variation of spot length was observed as α was changed, so that it was deduced that the electrons were penetrating the whole depth of the nuclei. Halliday, Rymer and Wright (1954) have recently studied thin films of copper prepared by vacuum evaporation. They deduce that the films are composed of nuclei which are plate-like, with a height of 15 Å, and a diameter of 90 Å.

A nuclear thickness of 12 Å implies that, for the thinnest detectable layer of 0·8 Å, the proportion of the surface covered by the nuclei is about 7%. Measurements showed that the size of the nuclei did not increase appreciably as further copper was deposited, but that the number of nuclei increased. It is interesting to note that the non-oriented copper started to appear only after a large fraction (say $>40\%$) of the silver surface had become covered by nuclei.

The lattice spacing of the copper nuclei was measured relative to that of the silver substrate. A mean of several measurements gave $a_{Cu} = 3{\cdot}635 \pm 0{\cdot}015$ Å, which is about 0·75% greater than the x-ray value of 3·608 Å. A similar expansion of the copper lattice in thin films has previously been observed (see Shishakov 1952).

All these results were found to be independent of the rate of deposition of the copper, over the range of 4 Å/hour to 80 Å/hour, the normal deposition rate being about 25 Å/hour. It was found that the rate of deposition could be maintained at a constant value for a period of at least one hour.

§ 5. Discussion

The present experiments have shown that the radioactive method, which requires no elaborate or laborious technique, is highly accurate for the measurement of the thickness of surface layers as thin as 0·1 Å. In addition, the method allows independent measurements to be made on each specimen as distinct from methods which involve only the calibration of the rate of deposition. As a general method, however, it has the following limitations :

(1) many elements do not have a suitable isotope,

(2) an isotope with a half-life of a few hours is required where permanent apparatus is contaminated,

(3) if deposits as thin as 0·1 Å are to be measured on specimens of the size normally used in electron diffraction experiments, the specific activity of the material should be at least 5 mc/g ; this ensures that the counting time for each specimen is not prohibitively long. It is preferable to count β- or γ-particles, rather than α-particles, in order to minimize effects due to particle absorption in the deposit. The disadvantage of the use of α-particles is illustrated by the inconsistency of the counting rate, for a given film thickness, found by Antal and Weber (1952).

By means of the radioactive method described in § 3 it has been conclusively shown that layers with an average thickness of less than 1 Å can give rise to observable electron diffraction patterns. These results apply to electrons with energy of about 45 kev ; the sensitivity of detection is expected to vary with changes in this energy, but it is difficult to predict the form of this variation.

The lower limit of detection is 0·8 Å for the copper layers, and only 0·4 Å for the bromide layers. A difference of this order of magnitude is to be expected because the scattering power per unit volume of the bromide is about one and a half times that of the copper, over the employed range of scattering angles. This high degree of sensitivity agrees with the results obtained by Schulz (1951, 1952 a) and thus Seifert's doubts (see Gomer and Smith 1953, pp. 360 and 383) are not justified.

An interesting difference occurs between the diffraction patterns from the copper and the silver bromide layers. From tables 2 and 3 it is seen that for a deposit thickness of 1 Å, and for small values of α, the bromide layer gives no primary diffraction, whereas the copper gives a very strong primary pattern. This is a surprising result, since it would be expected that with equal volumes of the two deposits the bromide would give rise to stronger primary diffraction patterns than the copper, provided that (*a*) all of the nuclei have their normal crystal structure and orientation, (*b*) the nuclei are sufficiently small for multiple scattering to be negligible, and (*c*) none of the nuclei is shielded from the incident electron beam. Since conditions (*a*) and (*b*) are considered to be satisfied, the above difference appears to be due to condition (*c*) not

being fulfilled. A likely explanation is that in the initial stages the silver bromide nuclei are partially embedded in the silver substrate. This could occur as a result of the mechanism of the chemical reaction, which might be expected to lead to the diffusion of bromine into the surface layers of the silver. It might also be due to the occurrence of growth in holes, grain boundaries, steps or cracks in the surface. Under such conditions there would be a high probability of the electrons being diffracted by metallic silver before or after entering the silver bromide nuclei. This would cause the intensity of the primary diffraction pattern to be reduced and that of the secondary diffraction pattern to be increased. This interpretation would, therefore, be consistent with the observation of very strong secondary patterns from the bromide layers, compared with those from the copper deposits (cf. tables 2 and 3).

These results will now be compared with those of Schulz (1951, 1952 a). Schulz grew alkali halides, by condensation *in vacuo*, on to cleavage faces of various single crystals, and according to his interpretation the layers were of two types : (i) monolayers, (ii) nucleated deposits. The monolayers were most easily detected at low values of α, the patterns being attributed to primary diffraction. He found, in the case of the nucleated deposits, that a more sensitive method of detection was to use a strong diffracted beam from the substrate crystal as a source for diffraction by the deposit nuclei. This latter method (Schulz 1950) required the use of a somewhat higher value of α. In the present experiments, however, although the deposits grew as nuclei, it was found in all cases that the greatest sensitivity of detection was obtained at the smallest possible values of α.

In the case of copper layers, the first indication of the presence of a deposit consisted of definite primary diffraction spots. The smaller the value of α, the more intense were these primary spots, and secondary diffraction spots occurred comparatively weakly only at higher values of α (cf. table 3). It has been shown in § 4 (*b*) that the copper nuclei are plate-like in shape, and hence the copper deposits resemble Schulz's monolayers more closely than his nucleated deposits. This is consistent with the primary diffraction pattern being predominant.

In the case of the bromide layers, the first indication of the presence of the overgrowth consisted of extra streaks on the diffraction pattern (see figs. 2 (Plate 15) and 3). Streaks of type B arise only as a result of secondary diffraction, as illustrated in fig. 3, while streaks of type A could be due to a superposition of both primary and secondary diffractions. Since type B streaks were usually of the same intensity as those of type A, it is reasonable to conclude that type A streaks, and hence all of the streaks, are of secondary origin. As shown in § 4 (*a*) the bromide grows in the form of nuclei, and streaks arise in the secondary diffraction pattern simply because the silver spots acting as the sources are themselves extremely elongated. The bromide layers are similar to Schulz's nucleated deposits, and so their initial appearance by means of secondary

diffraction is to be expected from his results. The fact that Schulz used larger values of α than those found most suitable in the present work might be due to the difference in the diffraction patterns from the substrate ; the silver specimens give very good diffraction patterns even at the lowest possible values of α.

Since, in Schulz's experiments, it is reasonable to suppose that none of his deposits was embedded in the substrate, it follows that the appearance of secondary diffraction effects from the silver bromide layers is not sufficient evidence of the embedding of the nuclei. It appears that the secondary diffraction will appear anyway, provided the nuclei fulfil certain conditions on size and shape. However, it is considered, in view of other reasons given above, that the embedding of the silver bromide nuclei does occur and that there is more than one condition favourable to the appearance of the secondary diffraction.

To summarize, it is concluded that the copper nuclei are plate-like and form on the surface of the silver. The measurement of the nuclear size is uncertain because of refraction effects. The silver bromide nuclei have no well defined shape, and are partially embedded in the metallic silver. The measurement of their size is not reliable because of the embedding. Since the primary diffraction arises mainly from the protruding part of the nucleus, the measurement of the spot size will include only that part of the nucleus. It will not measure the part of the nucleus embedded in the silver.

In the case of the thicker deposits, a layer of 7·7 Å of copper completely obscures the silver substrate pattern for values of $\alpha < 3°$. However, such an effective cut-out is not produced even by 19 Å of silver bromide, unless α is reduced to less than $1\frac{1}{2}°$ (cf. tables 2 and 3). This large difference proves that the shape and size of the deposit nuclei are important factors in the determination of the conditions for the cut-out of the substrate pattern. These factors have not been considered by Raether (1949, 1950, 1951). His method of thickness measurement applies to deposits in the form of uniform layers, but very few deposits grow in this manner, and hence the method has very limited application. A theoretical treatment of the diffraction patterns to be expected from deposits on various types of surface would be extremely useful. Such a theory would have to consider the formation of both primary and secondary diffraction patterns, and also the effect of nuclear size and shape.

The measurement of the lattice spacing of the deposit during the earliest stages of growth is of importance in connection with theories of orientation. By considering the initial formation of an oriented deposit to be in the form of a monolayer, Frank and van der Merwe (1949, 1949–50) deduced that the lattice spacing of this first layer will be modified to fit that of the substrate. They maintained that the formation of such a monolayer was an essential first stage for the occurrence of an oriented overgrowth. In the present experiments,

however, the deposits have not grown as extensive monolayers, but as oriented three-dimensional nuclei. As the deposit thickness is increased, the size of the nuclei remains approximately unchanged, and the number of nuclei increases. Thus the various stages of growth of a single nucleus are not observed, even for deposits of very small mean thickness. There is, therefore, no direct evidence concerning the lattice spacing of a single nucleus during the earliest stages of its growth. All that can be stated is that the lattice spacing of the completed nuclei, although slightly modified from the value for the bulk material, is not constrained to fit that of the substrate. If, however, a deposit grows in the form of a uniform oriented 'monolayer' (see Schulz 1951, 1952 a, Gomer and Smith 1953, p. 372), the electron diffraction method is sufficiently sensitive to allow the first atomic layer to be detected, and its lattice spacing could then be measured.

Acknowledgments

The authors express their gratitude to Dr. M. Blackman for his interest and encouragement, and to Mr. J. A. W. Dalziel for the use of a semi-microbalance. One of us (R. C. N.) is indebted to the Department of Scientific and Industrial Research for a maintenance grant.

References

Antal, J. J., and Weber, A. H., 1952, *Rev. Sci. Inst.*, **23**, 424.

Frank, F. C., and van der Merwe, J. H., 1949, *Proc. Roy. Soc.* A, **198**, 205; 1949–50, *Ibid.*, **200**, 125.

Gomer, R., and Smith, C. S., 1953, *Structure and Properties of Solid Surfaces* (Chicago: University of Chicago Press).

Halliday, J. S., Rymer, T. B., and Wright, K. H. R., 1954, *Proc. Roy. Soc.* A, **225**, 548.

Kehoe, R. B., Newman, R. C., and Pashley, D. W., 1954, *J. Sci. Inst.*, **31**, 399.

Laue, von M., 1936, *Ann. Phys.*, **26**, 55; 1937, *Ibid.*, **29**, 211.

Lucas, L. N. D., 1951, *Proc. Phys. Soc.* A, **64**, 943.

Raether, H., 1949, *Z. Naturf.*, 4*a*, 582; 1950, *J. Phys. Rad.*, **11**, 11; 1951, *Ergeb. Exact. Naturwiss.*, **24**, 54.

Schulz, L. G., 1950, *J. Appl. Phys.*, **21**, 942; 1951, *Acta Cryst.*, **4**, 483; 1952 a, *Ibid.*, **5**, 130; 1952 b, *Ibid.*, **5**, 264; 1952 c, *Ibid.*, **5**, 266.

Shishakov, N. A., 1952, *Zh. Eksper. Teor. Fiz.*, **22**, 241.

Tull, V. F. G., 1951, *Proc. Roy. Soc.* A, **206**, 232.

CVII. *The Electromagnetic Field in a Lagrangian Quantum Theory*

By K. V. Roberts
Department of Mathematics, University College, London*

[Received March 21, 1955]

Abstract

The graphical rules of Feynman and Dyson are stated in a very general form, which depends only on the field Lagrangian, and does not explicitly require either the use of field operators or the construction of a Hamiltonian scheme. It is shown that by choosing these rules as a starting-point one is able to quantize the electromagnetic field in a simpler way, since there is no longer any need to modify the classical Lagrangian $\frac{1}{4}F^{\mu\nu}F_{\mu\nu}$ (which does not lead to a Hamiltonian as it stands); to impose a supplementary condition; or to employ an indefinite metric. Dyson's theorem on photon propagation functions is established, and the gauge-invariance of the S-matrix is discussed.

§ 1. Introduction

General Statement of the Feynman–Dyson Rules

It seems to be true that nearly all the techniques so far developed in quantum field theory that are not purely formal, but likely to be of direct interest in practical calculations, can be obtained in a straightforward way from the Feynman–Dyson rules of S-matrix theory (Feynman 1949 a, b, Dyson 1949). (These techniques would include, for instance, the one-particle Dirac equation with radiative corrections, the Bethe–Salpeter equation, and probably also the various Tamm–Dancoff equations.) In other words, a knowledge of these rules is all that is really required to enable any physical quantity to be calculated.

It is also true that the Feynman–Dyson rules can be written down at once in a very simple form, for any particular system of interacting fields, as soon as the *Lagrangian* $\mathscr{L}$ is known. Suppose that $\mathscr{L}$ (expressed as a function of the field operators ϕ^α, their conjugates $\bar{\phi}_\alpha$, and derivatives) has been divided into two parts

$$\mathscr{L}^f+\mathscr{L}^i, \qquad \ldots\ldots\ldots \quad (1)$$

where $\mathscr{L}^f$ is bilinear and represents the free fields, while $\mathscr{L}^i$ describes the interactions. In order to avoid any explicit consideration of the form

* Communicated by the Author.

of $\mathscr{L}$, it is convenient to rewrite each part of the corresponding action function I in such a way that

$$I^f \equiv \int \mathscr{L}^f(x)\,dx = \Sigma \frac{1}{d}\int\int \bar{\phi}_\alpha(x) L_\beta^\alpha(x,y)\phi^\beta(y)\,dx\,dy \quad . \quad . \quad . \quad (2)$$

(one term for each free field), and

$$I^i \equiv \int \mathscr{L}^i(x)\,dx = \Sigma \left(\Pi_j \frac{1}{d_j!}\right)\int \ldots \int \bar{\phi}_\alpha(x_1)\bar{\phi}_\beta(x_2)\ldots$$
$$\times V_{\gamma\delta\ldots}^{\alpha\beta\ldots}(x_1, x_2\ldots; y_1, y_2\ldots)\phi^\gamma(y_1)\phi^\delta(y_2)\ldots dx_1 dx_2\ldots dy_1 dy_2\ldots \quad . \quad (3)$$

(one term for each interaction). This defines a set of *kernels* L_β^α, $V_{\gamma\delta\ldots}^{\alpha\beta\ldots}$, containing δ-functions and their derivatives, together with Dirac matrices and fundamental constants. (For a typical example cf. eqn. (20) below.) The numerical factors d, $d_j!$ are designed to take into account the possibility that a given field operator may be raised to a higher power than the first: thus $d=2$ for self-conjugate fields (photon, neutral meson); $d=1$ for non-self-conjugate fields (representing charged particles, neutrons etc.); d_j is the degree to which the jth field operator (together with its derivatives) occurs in the corresponding term of $\mathscr{L}^i$. The transformation (2) allows the variational equations for each of the free fields to be expressed in a standard 'integral' form

$$\int L_\beta^\alpha(x,y)\phi^\beta(y)\,dy = 0, \qquad \int \bar{\phi}_\alpha(x) L_\beta^\alpha(x,y)\,dx = 0, \quad . \quad . \quad (4)$$

which has the advantage of being valid for differential equations of arbitrary order (and also for integral equations, of course). Equation (4) may be written more concisely as

$$\mathbf{L}\phi = 0, \qquad \bar{\phi}\mathbf{L} = 0, \quad . \quad . \quad . \quad . \quad . \quad . \quad . \quad (5)$$

thus defining a linear operator $\mathbf{L}$.

Since the Feynman–Dyson rules are already well known, in order to bring out their dependence on the Lagrangian it should be sufficient to remark that the correct propagation function $\mathbf{\Omega}_F$ (say) for each *line* can be defined by the formal limiting process

$$\mathbf{\Omega}_F = \mathscr{L}t_{\epsilon\to 0} \frac{-i\hbar}{\mathbf{L} - i\epsilon}, \quad . \quad . \quad . \quad . \quad . \quad . \quad . \quad . \quad (6)$$

where $\epsilon > 0$, and therefore satisfies the inhomogeneous equations associated with (5),

$$\mathbf{L}\mathbf{\Omega}_F = \mathbf{\Omega}_F\mathbf{L} = -ih, \quad . \quad . \quad . \quad . \quad . \quad . \quad . \quad (7)$$

while the factor for each *vertex* is simply $(ih)^{-1}$ times the corresponding operator $V_{\gamma\delta\ldots}^{\alpha\beta\ldots}$, which acts on the propagation functions or wave-functions belonging to the lines just as on the field operators in (3). The definition (6) is equivalent to Feynman's introduction of a negative-imaginary mass increment (Feynman 1949 a, § 6), which ensures that positive-frequency

waves are always radiated into the future, while negative-frequency waves are radiated into the past. (For further details about these rules the reader is asked to consult the papers of Dyson (1949). The fact that the vertices really depend on $\mathscr{L}^i$, rather than on the interaction *Hamiltonian* $\mathscr{H}^i$ (which may contain extra terms), first became apparent from the work of Matthews (1949).)

In using this Lagrangian version of the rules one is able to circumvent nearly all the abstract formalism of quantum field theory (such as canonical coordinates and momenta, commutation rules, state-vector, Hamiltonian, Heisenberg and Schrödinger equations, definition of the vacuum, etc.); all that matters in practice is contained in the Lagrangian $\mathscr{L}$ and in the definition (6). Furthermore, even the *field operators* themselves do not play any essential part, for what one really needs to extract from $\mathscr{L}$ is simply the set of kernels L_β^α, $V_{\delta\gamma\ldots}^{\alpha\beta\ldots}$. Of course the Lagrangian version can only be *justified* at present by deducing it from the usual Hamiltonian scheme, but such a simple and apparently universal formulation of relativistic quantum theory must have a deeper significance than has yet become clear. In this connection it is very instructive to examine a fairly complicated type of field, such as that of the vector meson, where the construction of a Hamiltonian scheme encounters the problem of the 'missing momentum', conjugate to the time component U^0 of the meson potential. In spite of the various manipulations that are necessary if the theory is to be expressed in a covariant Hamiltonian form (e.g. one might begin by eliminating the time-like component $U^\mu n_\mu(\sigma)$, normal to an arbitrary space-like surface σ), the Lagrangian version of the rules is eventually found to be quite unchanged. This is a remarkable fact, and it suggests that *the same rules might even be used when no Hamiltonian scheme exists at all.*

Application to the Electromagnetic Field

A natural application for this idea is provided by the electromagnetic field. The most obvious choice of Lagrangian in classical theory is

$$\mathscr{L}=\tfrac{1}{4}F^{\mu\nu}F_{\mu\nu}=\tfrac{1}{2}(\mathbf{H}^2-\mathbf{E}^2), \qquad (8)$$

where

$$F^{\mu\nu}=\frac{\partial A^\nu}{\partial x_\mu}-\frac{\partial A^\mu}{\partial x_\nu}, \qquad (9)$$

because this leads directly to Maxwell's equations.* The corresponding energy density is

$$T^{00}=\tfrac{1}{2}(\mathbf{H}^2+\mathbf{E}^2). \qquad (10)$$

Unfortunately, there is no Hamiltonian associated with (8), since the momentum conjugate to A^0 does not exist, and the usual procedure in setting up a canonical scheme for quantization has been to modify the original Lagrangian to

$$\mathscr{L}'=\tfrac{1}{4}F^{\mu\nu}F_{\mu\nu}+\tfrac{1}{2}\left(\frac{\partial A^\mu}{\partial x^\mu}\right)^2, \qquad (11)$$

* Upper indices are assumed to be contravariant, and $g_{11}=g_{22}=g_{33}=1$, $g_{00}=-1$; $\Box=-\partial^2/\partial x^\mu\partial x_\mu$, $c=1$.

so that the variational equations become

$$\Box A^{\mu}=0. \quad . \quad . \quad . \quad . \quad . \quad . \quad . \quad . \quad . \quad (12)$$

Maxwell's equations are then restored by imposing a supplementary condition, whose classical formulation would be

$$\frac{\partial A^{\mu}}{\partial x^{\mu}}=0. \quad . \quad . \quad . \quad . \quad . \quad . \quad . \quad . \quad . \quad (13)$$

However, the modification (11) introduces a number of serious difficulties, which have no analogue in the original version of the theory. The energy density is now

$$\tfrac{1}{2}\{(\text{curl } \mathbf{A})^2+\dot{\mathbf{A}}^2+(\text{div } \mathbf{A})^2-\dot{\phi}^2-(\text{grad } \phi)^2\}, \quad . \quad . \quad . \quad (14)$$

which is not positive definite, and the free field has four degrees of freedom instead of two; in quantum theory there are scalar and longitudinal as well as transverse photons, and the scalar photons appear to have negative energy. In particular this makes it difficult to define the free vacuum state in an invariant way; normally one would expect to take

$$A^{\mu+}\Psi_0=0 \quad . \quad . \quad . \quad . \quad . \quad . \quad . \quad . \quad (15)$$

(where $+$ denotes the positive-frequency part), but for negative-energy scalar photons A^{0+} would be an emission operator. This in turn reacts on Dyson's definition of the photon propagation function as

$$D_{F\sigma}{}^{\rho}(x, y)=\overline{\Psi}_0 P(A^{\rho}(x)A_{\sigma}(y))\Psi_0, \quad . \quad . \quad . \quad . \quad . \quad (16)$$

where P is the chronological ordering operator (Dyson 1949).

The most elegant treatment of these problems has been given by Gupta (1950) and Bleuler (1950), who avoid the occurrence of negative energies by introducing an indefinite metric in the Hilbert space of quantum states. This device allows a consistent definition of the vacuum, so that (16) can be given a rigorous meaning, and also makes it possible to prove a theorem of Dyson (1950), which states that the expression (16) may always be replaced by the simpler propagation function

$$D_{F\sigma}{}^{*\rho}(x, y) \equiv \delta_{\sigma}{}^{\rho} D_F(x-y) \quad . \quad . \quad . \quad . \quad . \quad . \quad (17)$$

where

$$\Box D_F(x)=-i\hbar\delta(x). \quad . \quad . \quad . \quad . \quad . \quad . \quad . \quad (18)$$

These authors also show that the correct quantum analogue of the classical condition (13) is

$$\left[\frac{\partial A^{\mu}}{\partial x^{\mu}}\right]^{+}\Psi_0=0, \quad . \quad . \quad . \quad . \quad . \quad . \quad . \quad (19)$$

(in the Heisenberg picture).

In spite of the formal success of the Gupta–Bleuler method, it is hard to give any physical meaning either to the difficulties that arise from the modification (11), or to the technique used for overcoming them, especially since the introduction of an indefinite metric leads to ' negative probabilities '. On the other hand it is known that the original Lagrangian (8) is perfectly satisfactory as it stands in the classical

theory, because the Hamiltonian scheme is never really needed. One would expect it to be equally satisfactory in a Lagrangian version of quantum theory. The main task of this paper will therefore be to apply our version of the Feynman–Dyson rules to the electromagnetic field in the most straightforward way, i.e. using (8) instead of (11), and to show that this procedure leads to consistent and intelligible results, while avoiding the difficulties encountered in the usual method.

This programme will be carried out in § 3. However, the variational equations associated with (8) exhibit some unusual features, which it is necessary to discuss, and so these equations are dealt with in § 2.

§ 2. Structure of the Variational Equations

The ' integral operator ' belonging to (8) is

$$L_\sigma^{\rho}(x, y)=\tfrac{1}{2}\left(\frac{\partial}{\partial x_\mu}\delta_\sigma^{\ \nu}-\frac{\partial}{\partial x_\nu}\delta_\sigma^{\ \mu}\right)\left(\frac{\partial}{\partial y^\mu}\delta_\nu^{\ \rho}-\frac{\partial}{\partial y^\nu}\delta_\mu^{\ \rho}\right)\delta(x-y), \quad . \quad (20)$$

leading to the equations

$$\int L_\sigma^{\rho}(x, y)A^\sigma(y)\,dy \equiv \left(\Box\delta_\sigma^{\ \rho}+\frac{\partial^2}{\partial x_\rho \partial x^\sigma}\right)A^\sigma(x)=0. \quad . \quad . \quad (21)$$

The associated inhomogeneous equations are

$$\left(\Box\delta_\sigma^{\ \rho}+\frac{\partial^2}{\partial x_\rho \partial x^\sigma}\right)A^\sigma=j^\sigma, \quad . \quad . \quad . \quad . \quad . \quad . \quad (22)$$

which of course are equivalent to Maxwell's equations

$$\frac{\partial F^{\rho\sigma}}{\partial x^\sigma}=j^\rho. \quad . \quad . \quad . \quad . \quad . \quad . \quad . \quad . \quad . \quad (23)$$

The pecularities of (22) are conveniently studied by making a Fourier transformation :

$$L_\sigma^{\rho}(k)A^\sigma(k) \equiv (k^2\delta_\sigma^{\ \rho}-k^\rho k_\sigma)A^\sigma(k)=j^\rho(k), \quad . \quad . \quad . \quad (24)$$

$$F^{\rho\sigma}(k) = i(k^\rho A^\sigma(k)-k^\sigma A^\rho(k)) \quad . \quad . \quad . \quad . \quad . \quad (25)$$

where $k^2=k^\mu k_\mu$. $L_\sigma^{\rho}(k)$ is a 4×4 matrix, but it has rank 3, since the four rows and columns are linearly dependent :

$$k_\rho L_\sigma^{\rho}(k)=0, \qquad L_\sigma^{\rho}(k)k^\sigma=0. \quad . \quad . \quad . \quad . \quad . \quad (26)$$

Equation (24) is therefore *a set of inhomogeneous algebraic linear equations with vanishing determinant*, and in accordance with the usual algebraic theory this set will be incompatible, and thus have no solution, unless the vector $j^\rho(k)$ lies in the 3-dimensional subspace V_3 defined by

$$k_\rho j_\rho(k)=0. \quad . \quad . \quad . \quad . \quad . \quad . \quad . \quad . \quad . \quad (27)$$

When (27) is satisfied (24) must possess an infinite set of solutions, since to any one solution $A^\rho(k)$ it is possible to add an arbitrary multiple of the vector k^ρ :

$$A^\rho(k)+\alpha(k)k^\rho. \quad . \quad . \quad . \quad . \quad . \quad . \quad . \quad . \quad (28)$$

However, it is clear from (25) that this arbitrariness cannot affect $F^{\rho\sigma}(k)$, and it may be removed by imposing the condition that $A^\rho(k)$ is to lie

in the same 3-dimensional subspace V_3 as $j^\rho(k)$, i.e. that it is to be orthogonal to k_ρ,

$$k_\rho A^\rho(k)=0, \qquad \ldots\ldots\ldots \quad (29)$$

so that $\alpha(k)=0$. After reduction to V_3 (24) becomes

$$L_\sigma^{*\rho}(k)A^\sigma(k) \equiv (k^2\delta_\sigma{}^\rho)A^\sigma(k)=j^\rho(k), \qquad \ldots\ldots \quad (30)$$

with the unique solution

$$A^\rho(k)=j^\rho(k)/k^2, \qquad \ldots\ldots\ldots \quad (31)$$

unless of course $k^2=0$.

It should be remarked that the orthogonality condition (29) also fails to define $A^\rho(k)$ uniquely when $k^2=0$ (the Lorentz metric is of course indefinite), so that $\alpha(k)\neq 0$, and in addition to the arbitrariness in $F^{\rho\sigma}(k)$ there is a further arbitrariness in the relation between $F^{\rho\sigma}(k)$ and $A^\rho(k)$.

The algebraic method described here is obviously the exact analogue of the usual technique in which the differential eqn. (24) is simplified by imposing the Lorentz condition $\partial A^\mu/\partial x^\mu=0$, but the latter seems at first sight to be a rather *ad hoc* procedure ; it should become much clearer when related to the familiar theory of inhomogeneous algebraic equations. Thus (27) is equivalent to the conservation of charge ; (28) corresponds to the existence of unrestricted gauge transformations

$$A^\rho \to A^\rho + \frac{\partial \phi}{\partial x_\rho}, \qquad (\phi \text{ arbitrary}) ; \qquad \ldots\ldots \quad (32)$$

(29) to the Lorentz condition ; (30) to the usual wave-equation $\Box A^\rho=j^\rho$, and the remaining arbitrariness in $A^\rho(k)$ to the existence of restricted gauge transformations of the form

$$A^\rho \to A^\rho + \frac{\partial \phi}{\partial x_\rho}, \qquad (\Box\phi=0). \qquad \ldots\ldots \quad (33)$$

Finally, it should be pointed out that eqn. (22) is not as strange as it might seem ; the differential operator on the left-hand side can be given a simple interpretation. A 4-vector A^ρ would normally be expected to split up into two components on restriction to the 3-dimensional orthogonal group, belonging to representations with dimensions 1 (scalar) and 3 (vector). $L_\sigma{}^\rho(k)$ is in fact the *projection operator* on to the subspace V_3 (multiplied by k^2), and its purpose is to avoid the unwanted scalar representation automatically. By changing the Lagrangian (8) to (11) one replaces this projection operator by the identity, and so brings in a scalar component, which must then be removed by a suitable supplementary condition.

§ 3. Quantum Theory

A formal application of Feynman's rule (6) to the operator (20), defined by the Lagrangian (8), leads to

$$\left(\Box\delta_\sigma{}^\rho + \frac{\partial^2}{\partial x_\rho \partial x^\sigma} - i\epsilon\delta_\sigma{}^\rho\right) D^\sigma_{F\tau}(x, y) = -i\hbar\delta_\tau{}^\rho\delta(x-y). \qquad \ldots \quad (34)$$

This equation can be solved by first differentiating with respect to x^ρ, which gives

$$\frac{\partial}{\partial x^\sigma} D^\sigma_{F\tau}(x, y) = \frac{\hbar}{\epsilon} \frac{\partial}{\partial x^\tau} \delta(x-y). \quad . \quad . \quad . \quad . \quad . \quad (35)$$

The second term on the left-hand side can then be transferred to the right, and one finds

$$(\Box - i\epsilon) D^\rho_{F\tau}(x, y) = -i\hbar \left(\delta_\tau{}^\rho + \frac{1}{i\epsilon} \frac{\partial^2}{\partial x_\rho \partial x^\tau} \right) \delta(x-y), \quad . \quad . \quad (36)$$

and therefore

$$D^\rho_{F\tau}(x, y) = \left(\delta_\tau{}^\rho - \frac{1}{i\epsilon} \frac{\partial^2}{\partial x_\rho \partial y^\tau} \right) D_F(x-y), \quad . \quad . \quad . \quad (37)$$

where D_F is defined by (18).

Dyson's Theorem

It is clear that Feynman's introduction of a negative-imaginary mass increment has also succeeded in raising the rank of the operator $L_\sigma{}^\rho(x, y)$ to 4, so that it now has a unique inverse. It is true that the propagation function $D^\rho_{F\tau}(x, y)$ defined by (37) becomes singular in the limit $\epsilon \to 0$, but as Dyson (1950) has remarked, in S-matrix theory this function will always act on currents $J_\rho{}^\tau(y, x)$ satisfying

$$\frac{\partial J_\rho{}^\tau}{\partial x_\rho} = \frac{\partial J_\rho{}^\tau}{\partial y^\tau} = 0 \quad . \quad . \quad . \quad . \quad . \quad . \quad . \quad (38)$$

(when summed over all graphs belonging to the same order in e). If one therefore makes the rule that elements of the S-matrix are to be evaluated by multiplying the propagation functions together and summing over all graphs *before* the limiting process $\epsilon \to 0$ is carried out, the second term on the right-hand side of (37) will give zero on integration by parts, and can be omitted altogether. Hence it is permissible to replace (37) by the modified propagation function $D_F \delta_\tau{}^\rho$ that is normally used in electrodynamics. This is just the content of Dyson's theorem.

Photon Wave-Functions

It is convenient to imagine that the initial and final photon wave-functions $\mathscr{A}^\rho$ associated with a given collision process are 'radiated' from sources in the past and future respectively, localized in the small regions of space-time where the initial photons were originally created, or the final photons will eventually be destroyed. These wave-functions will then be defined by

$$\mathscr{A}^\rho(x) = \int D^\rho_{F\tau}(x, y) J^\tau(y)\, dy \equiv \mathscr{L}t_{\epsilon \to 0} \int \left(\delta_\tau{}^\rho - \frac{1}{i\epsilon} \frac{\partial^2}{\partial x_\rho \partial y^\tau} \right) D_F(x-y) J^\tau(y). \quad (39)$$

Since $\partial J^\tau / \partial y^\tau = 0$, (39) is equivalent (after integration by parts) to

$$\mathscr{A}^\rho(x) = \int D_F(x-y) J^\rho(y)\, dy, \quad . \quad . \quad . \quad . \quad . \quad (40)$$

and from this it follows that $\partial \mathscr{A}^\rho / \partial x^\rho = 0$.

There can be no arbitrariness associated with J^ρ, and so one may conclude that each individual photon has a *uniquely defined* 'natural' wave-function or potential $\mathscr{A}^\rho$, and that this potential satisfies the Lorentz condition (as Feynman (1949 b, § 8) has pointed out). Feynman's prescription (6) is therefore more powerful than the classical Lorentz condition by itself, which leaves the potential arbitrary to within a *restricted* gauge transformation of the form (33). (Of course, even in classical theory the arbitrariness (33) is removed if one insists on using retarded potentials, for example.)

Gauge-Invariance of the S-Matrix

Although each of the initial and final photons associated with a given collision has a unique natural potential which is defined by (40) (and therefore depends on conditions in some other region of space-time, where the photon is created or destroyed), in the neighbourhood of the collision itself each photon will propagate like a plane wave satisfying the homogeneous equation, and there will be no way of telling what its natural potential may be. In fact one can make a quite *unrestricted* gauge transformation of the form (32) on the wave-function for each photon separately, without altering the amplitude for any collision process, since in evaluating the S-matrix each photon wave-function is multiplied by a current J_ρ satisfying $\partial J_\rho/\partial x_\rho=0$, so that

$$\int J_\rho \frac{\partial \phi}{\partial x_\rho}\, dx = \int \frac{\partial}{\partial x_\rho}(J_\rho \phi)\, dx - \int \frac{\partial J_\rho}{\partial x_\rho}\phi\, dx = 0.$$

The state of a free photon is therefore completely defined by its 'field' $\mathscr{F}^{\rho\sigma}$ (related to $\mathscr{A}^\rho$ according to (9)), and any wave-function consistent with this field may be used in calculations. It follows from (40) (together with the conservation of charge) that $\mathscr{F}^{\rho\sigma}$ satisfies Maxwell's equations, so that at large distances from the source $\mathscr{E}$ and $\mathscr{H}$ are at right-angles to one another and to the direction of propagation, as in the classical theory.

Energy–Momentum Tensor

Since the graphical method of quantization described in this paper does not use the concept of *field operators* $A^\mu(x)$, it is no longer possible to construct a canonical energy–momentum tensor by the usual variational principle, and the simplest way of defining the energy and momentum associated with a free photon is to vary the metrical tensor $g_{\mu\nu}$. It is well known that in classical field theory a symmetrical energy–momentum tensor can be defined by

$$T^{\mu\nu}(z) = -\frac{\delta I}{\delta g_{\mu\nu}(z)}, \qquad \text{(41)}$$

where I is the action function, and $g_{\mu\nu}$ is equated to its value for flat space-time after the variation has been carried out. In quantum theory

the effect of a change in $g_{\mu\nu}(z)$ will be to introduce a *new type of* 3-*vertex*, with kernal

$$-T_{\sigma}^{\rho,\mu\nu}(x, y\,;\, z) \quad . \quad . \quad . \quad . \quad . \quad . \quad . \quad (42)$$

say, describing the scattering of a photon by the new 'external field' at the point z. Equation (42) may be evaluated by remarking that any small external interaction will modify the photon propagation function from $\mathbf{D}_F$ to $\mathbf{D}_F+\delta\mathbf{D}_F$, where

$$\delta\mathbf{D}_F \equiv \delta\left(\frac{-i\hbar}{\mathbf{L}}\right) = \mathbf{L}^{-1}(i\hbar\delta\mathbf{L})\mathbf{L}^{-1} = \mathbf{D}_F[(i\hbar)^{-1}\delta\mathbf{L}]\mathbf{D}_F. \quad . \quad (43)$$

This is equivalent to introducing a new vertex with kernal $\delta\mathbf{L}$, so that

$$-T_{\sigma}^{\rho,\mu\nu}(x, y\,;\, z) = \frac{\delta}{\delta g_{\mu\nu}(z)}\mathbf{L}_{\sigma}^{\rho}(x, y). \quad . \quad . \quad . \quad . \quad (44)$$

(The interaction terms in the energy–momentum tensor can be obtained in a similar way by functional differentiation of the vertex kernels or V-functions, but these are not of interest for a free photon.)

The result of the variation (44) is most simply stated in the form

$$T^{\mu\nu}(z) \equiv \int\int \overline{\mathscr{A}}_{\rho}(x)T_{\sigma}^{\rho,\mu\nu}(x, y\,;\, z)\mathscr{A}^{\sigma}(y)\,dx\,dy$$

$$= \overline{\mathscr{F}}^{\mu\alpha}(z)\mathscr{F}_{\alpha}{}^{\nu}(z) + \overline{\mathscr{F}}^{\nu\alpha}(z)\mathscr{F}_{\alpha}{}^{\mu}(z) - \tfrac{1}{2}\overline{\mathscr{F}}^{\alpha\beta}(z)\mathscr{F}_{\alpha\beta}(z)g^{\mu\nu}, \quad . \quad (45)$$

which corresponds to the classical energy–momentum tensor, except for an extra factor 2. The expectation value of the energy density associated with a free photon is therefore

$$\overline{\mathscr{E}}\,.\,\mathscr{E} + \overline{\mathscr{H}}\,.\,\mathscr{H}. \quad . \quad . \quad . \quad . \quad . \quad . \quad . \quad (46)$$

By integrating (45) over a space-like surface one can find the total flux of energy and momentum P^{μ} associated with the photon. This enables the wave-function to be normalized correctly.

Equation (45) is invariant under unrestricted gauge transformations of the form (32), since it depends only on the field $\mathscr{F}^{\rho\sigma}$. Hence, there is no energy or momentum associated with a potential $\partial\phi/\partial x_{\rho}$. This might be explained by saying that the energy–momentum operator $T_{\sigma}^{\rho,\mu\nu}(k)$ acts only on the subspace V_3 of § 2.

§ 4. Discussion

It has been shown that by starting from a Lagrangian version of the Feynman–Dyson rules (§ 1), one is able to develop a much simpler treatment of the quantized electromagnetic field than has hitherto been available within the framework of the Hamiltonian theory. The reason for this is that if one uses Feynman's definition (6) for the propagation function, rather than Dyson's definition (16), it is no longer necessary to construct *field operators*, *commutation rules* or the *vacuum state* explicitly, and so it becomes possible to work with a more general kind of Lagrangian, for which a Hamiltonian scheme would not exist. The classical Lagrangian $\frac{1}{4}F^{\mu\nu}F_{\mu\nu}$ happens to be of this kind, and turns out

to be extremely well adapted for describing particles of spin 1 and mass 0 (§ 2). By avoiding the necessity for modifying this Lagrangian one greatly simplifies the gauge-invariance problem.

On the other hand, since the Hamiltonian formalism of relativistic quantum mechanics has been dispensed with altogether in this paper, and a rather abstract method of Lagrangian quantization used instead, it is no longer possible to rely on general theorems in quantum mechanics for establishing either the physical interpretation of the self-consistency of our treatment of the electromagnetic field, and some explicit investigation ought to be made. Actually so far as the electromagnetic field itself is concerned, the new treatment can be justified for all practical purposes by comparing it with the more complicated Gupta–Bleuler method, which leads to the same numerical results. But it would obviously be much better to establish the general validity of Lagrangian quantization by some independent argument.

From this point of view, it may be worth remarking that a new formulation of relativistic quantum theory can be developed, in which the Feynman–Dyson rules themselves are chosen as the axioms. I call this the *Theory of Graphs* (TG), since it starts from the basic idea of ' graphs ' rather than ' fields ' or ' elementary particles '. Roughly speaking, it might be said that TG represents an attempt to provide the simplest posssible logical framework for the intuitive graphical methods of Feynman (1949 a, b), so that these can be justified directly, without appealing either to the Hamiltonian formalism of quantum mechanics, or to the more classical concepts of ' continuous particle paths ' (Feynman 1948) or ' continuous field distributions '. TG is equivalent to quantum mechanics, but there are differences both in the mathematical formalism (which is Lagrangian rather than Hamiltonian), and also in the physical interpretation. It is found that a number of problems can be treated more simply with the help of TG ; in addition to gauge-invariance, these include time reversal, charge conjugation and the derivation of relativistic wave-equations. I hope to publish a paper about this theory shortly.

References

Bleuler, K., 1950, *Helv. Phys. Acta*, **25**, 417.
Dyson, F. J., 1949, *Phys. Rev.*, **75**, 486, 1736 ; 1950, *Phys. Rev.*, **77**, 420.
Feynman, R. P., 1948, *Rev. Mod. Phys.*, **20**, 367 ; 1949 a, *Phys. Rev.*, **76**, 749 ; 1949 b, *Ibid.*, **76**, 769.
Gupta, S. N., 1950, *Proc. Roy. Soc.* A, **63**, 681.
Matthews, P. T., 1949, *Phys. Rev.*, **76**, 1254.

CVIII. *The Nuclear Orientation of Cobalt* 57

By G. R. Bishop, M. A. Grace, C. E. Johnson, A. C. Knipper, H. R. Lemmer, J. Perez y Jorba and R. G. Scurlock

Clarendon Laboratory, Oxford*

[Received May 23, 1955]

Abstract

The isotope ^{57}Co has been studied by the method of nuclear alignment in cobalt rubidium sulphate. By determining the angular distribution of the γ-radiation following its decay and its plane of polarization it is shown that the 123 kev transition is predominantly M1 with a small admixture of E2 ($\delta = +0{\cdot}19 \pm 0{\cdot}02$).

§ 1. Introduction

In an earlier paper (Bleaney *et al.* 1954) a detailed account was given of a method for aligning cobalt nuclei by cooling a single crystal of a paramagnetic Tutton salt to temperatures of about 0·01°K. At these temperatures the lower h.f.s. levels are preferentially populated and an alignment of the nuclei is obtained. The spatial anisotropy of the γ-radiation emitted in the decay of the aligned radioactive isotopes ^{60}Co (Bleaney *et al.* 1954) and of ^{58}Co (Daniels *et al.* 1953) was studied in previous experiments which have now been extended to ^{57}Co.

The general features of the decay scheme of ^{57}Co are shown in fig. 1. The nuclear spin and moment of ^{57}Co which are almost identical with those of stable ^{59}Co have been determined by Baker *et al.* (1953) and identify the state as $f7/2$. The most probable values for the spins and parities in the sequence I_2, I_1, I_0 are $5/2^-$, $3/2^-$, $1/2^-$, the prominent γ-ray transition γ_2 being mainly M1 in character (Lemmer *et al.* 1955). Although the principal features of the decay scheme seemed to be well understood we thought it worthwhile to apply the nuclear alignment method to the study of this nucleus both in order to confirm these assignments and to obtain further information on the decay scheme.

§ 2. Experimental Equipment

Six single crystals of a Tutton salt of the composition (0·01 Co, 0·12 Cu, 0·87 Zn) $Rb_2(SO_4)_2 6H_2O$, were grown from a radioactive solution containing some ^{57}Co which had been prepared about two years previously by 18 Mev

* Communicated by the Authors.

deuteron bombardment of iron. The total ^{57}Co activity in these crystals was about 20 μCurie ; the ^{56}Co activity which was the principal contaminant had, at the time of these experiments, decayed to a low value. These crystals were mounted in parallel crystallographic orientation in the low temperature cryostat. Adiabatic reduction of the magnetic field at 0·9°K from 25 kilogauss to zero caused the temperature of the crystals to fall to between 0·01°K and 0·02°K. Scintillation counters were then placed round the cryostat and the dependence of the anisotropy (ϵ) of

Fig. 1

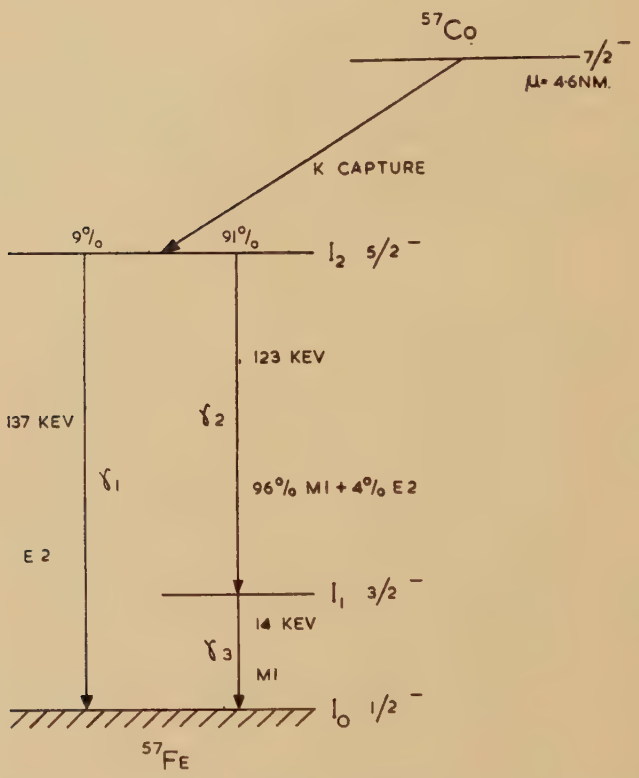

Decay scheme of Cobalt 57.

the γ-radiation ($\gamma_1+\gamma_2$) was observed as the crystal sample returned to 0·9°K ($\epsilon=1-I(\mathrm{K1})/I(\mathrm{K2})$ where I(K1), I(K2) are the γ-ray intensities observed along the magnetic axes K1, K2 of the crystal). The variation of ϵ with $1/T$ is shown in fig. 2 where it is seen that even at the lowest temperature the anisotropy does not exceed 0·004. That this unexpectedly negative result was not due to failure to align the cobalt nuclei was proved by the fact that the hard background radiation from the residual ^{56}Co activity did have an appreciable anisotropy.

§ 3. Theoretical Dependence of Anisotropy on Temperature

The theoretical dependence of anisotropy on temperature for the decay scheme of fig. 1 has been evaluated using the treatment of Steenberg (1952) and is also shown in fig. 2. It is clear that there is a marked discrepancy between theory and experiment of at least a factor of 70. For the calculation four assumptions have been made :

(i) The anisotropy arises from the γ_2-radiation only. Using NaI(Tl) scintillation counters it was not possible to separate the contributions due to the 123 kev γ-ray (γ_2) and the weak 137 kev γ-ray (γ_1). From the known intensities of these γ-rays it can be concluded that the detection of γ_1 will not cause the expected anisotropy to be reduced by more than 25% at any temperature.

(ii) That the h.f.s. is completely anisotropic. Since the slight departure from complete anisotropy of the h.f.s. will alter the expected γ-ray anisotropy by only about 2% (for a discussion see Bleaney *et al.* 1954) this assumption is justifiable.

Fig. 2

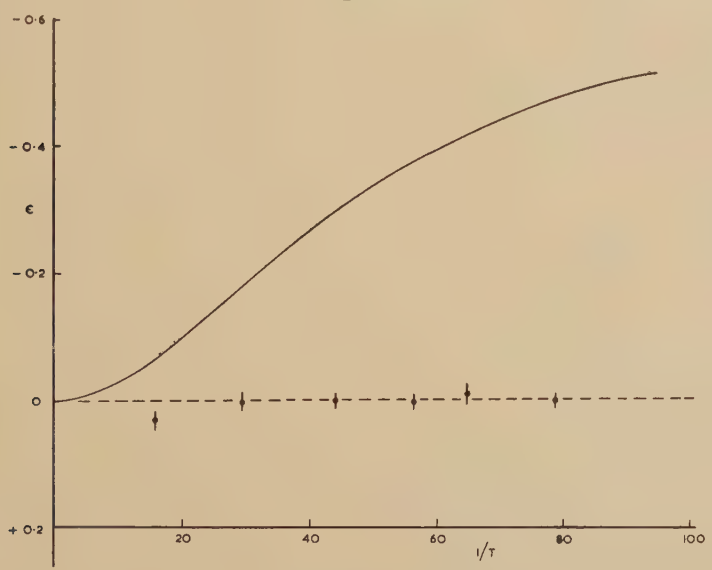

Dependence of anisotropy (ϵ) on $1/T$ and the theroretical curve for a pure M1 transition.

(iii) That the alignment of the state I_2 is not perturbed during its finite lifetime by the influence of extra-nuclear fields. The lifetime of this state can be estimated from the yield of Coulomb excited radiation (Temmer and Heydenburg 1954) and is found to be $5 \pm 2 \times 10^{-9}$ sec. For lifetimes of this order of magnitude perturbations of nuclear states are known to occur.

(iv) That the γ-radiation γ_2 is pure dipole.

Admixtures both of M2 and E1 and of E2 and M1 radiations have been identified in many γ-ray transitions and it would not be surprising if such a mixture was present.

It is therefore clear that the explanation for the discrepancy between the theoretically predicted and the observed behaviour lies in incorrectness of assumptions (iii) or (iv), or both. It is possible to distinguish between the two possible explanations by determining the state of polarization of the γ-radiation from the oriented nuclei. The highest degree of polarization will in general be observed in the radiation emitted at right angles to the axis of alignment. This degree of polarization can be described by the intensities $I_{\parallel}$ and $I_{\perp}$ of plane polarized components of the radiation in the directions parallel and perpendicular to the axis of alignment. If the assumption (iii) is incorrect the perturbation will cause the ratio $p=(I_{\perp}-I_{\parallel})/(I_{\perp}+I_{\parallel})$ to be reduced in direct proportion to the reduction of the anisotropy (ϵ). If, however, it is assumption (iv) which is at fault, and it is assumed that there is an admixture of coherent quadrupole radiation which makes the γ-ray intensity isotropic, it can be shown that the ratio p will remain almost unchanged.

§ 4. Polarization of the γ-radiation

The polarization of the radiation was measured using the apparatus described earlier (Bishop and Perez y Jorba 1955). This was set up so as to detect radiation emitted along the magnetic K3 axis of the crystal, for in this direction the polarization of the radiation should be greatest. The degree of polarization p was found by measuring the number of γ-rays ($N_{\parallel}$ and $N_{\perp}$) scattered in directions parallel and perpendicular to the axis of alignment, the scattering being a maximum in the direction at right angles to the plane of polarization. The degree of polarization p can be determined from the relationship

$$N_{\perp}/N_{\parallel}=[(1+p)+R(1-p)]/[(1-p)+R(1+p)]$$

where R is the analysing ratio for the polarimeter, determined from the geometrical arrangement and the differential Compton scattering cross section for the γ-radiation in question. For 123 kev γ-radiation the value of R is about 6.

Figure 3 shows the dependence of $N_{\perp}/N_{\parallel}$ on $1/T$ and indicates a small but significant polarization at the lowest temperatures. Since $N_{\perp}/N_{\parallel}$ is greater than unity the above expression shows that p is negative. Since the measurements of Alburger and Grace (1954) indicate that this transition is predominantly dipole the sign of the polarization establishes that it must be magnetic (see for instance Steenberg 1953) thus confirming the suggested assignment of parities to these levels. The degree of polarization however is at least 6 times smaller than that to be expected at the temperatures reached and it can be concluded that this reduction is due to perturbation of the state I_2.

§ 5. Discussion

If the transition is both mixed and follows a state which is perturbed the angular distribution of radiation intensity can be written, for dipole transitions, as :

$$I(\theta,\phi)=I+\lambda B_2 U_2(F_2+\delta g_2)P_2(\cos\theta)+\tfrac{1}{2}\sigma\lambda B_2 U_2(F_2-\delta g_2/3)\cos 2\phi P_2^2(\cos\theta)$$

(see Gray and Satchler 1955) where ϕ is the inclination of the electric vector of the radiation to the plane containing both its direction of emission and the axis of alignment, λ is an attenuation coefficient ($\leqslant 1$) describing the perturbation (this is assumed either to be random or to have symmetry about the symmetry axes for the ions), U_2, F_2 and g_2 are coefficients involving the angular momenta of the transitions, B_2 is the population function of the initial state and depends on its magnetic moment and temperature, $P_2(\cos\theta)$, $P_2^2(\cos\theta)$ are the Legendre and the associated Legendre polynomials for $\cos\theta$; δ, which in the above expression is assumed to be small, is the ratio of the amplitudes of quadrupole and dipole in the mixed transition and σ takes the values -1 and $+1$ for electric dipole and magnetic dipole transitions respectively. It can be seen clearly from the above expression why a vanishingly small anisotropy

Fig. 3

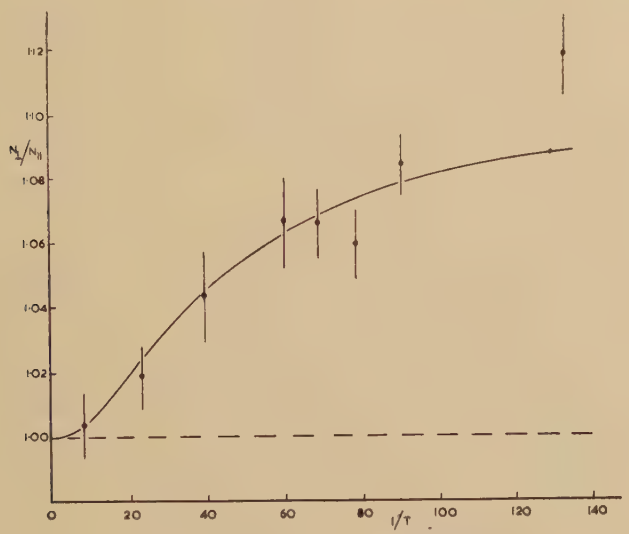

γ-ray polarimeter measurements.
Dependence of $N_\perp/N_\parallel$ on $1/T$ and the theoretical curve for $\lambda=0{\cdot}11$, $\delta=+0{\cdot}19$.

is not necessarily accompanied by vanishing polarization. The reason for this is that the anisotropy, since it is measured with polarization insensitive detectors, is independent of the term containing ϕ. This leads to the condition for zero anisotropy $\delta=-F_2/g_2$; the polarization of the radiation for this value of δ still remains finite and can be predicted for any particular value of λ. Hence λ can be determined since B_2, U_2, F_2 and g_2 are known for this isotope. λ and δ may therefore be determined directly from the values of the polarization p and the anisotropy ϵ obtained at the same temperature.

Using the values of ϵ and p at a temperature of $1/80^\circ$K it is found that δ is $+0{\cdot}19\pm0{\cdot}02$ and λ is $0{\cdot}11$. Account has been taken here of the small effect due to the detection of γ_1. In fig. 3 the theoretical curve using

these values of λ and δ is shown as well as the experimental points. The agreement at temperatures other than 1/80°K gives one confidence not only that this small polarization is significant but also that the interpretation of these results is correct.

§ 6. Conclusions

The residual polarization of the γ-radiation and its nearly isotropic distribution supports the spin and parity assignments shown in fig. 1 and requires an E2/M1 admixture with $\delta = +0{\cdot}19 \pm 0{\cdot}02$. The value of λ (0·11) indicates that the state I_2 is strongly perturbed by extra-nuclear fields. These presumably arise as a result of the K-capture process. The large line widths of the x-ray lines indicate that the lifetimes of K and L shell vacancies are too short for the fields arising from them to influence this nuclear state. It is therefore likely that the perturbing fields originate in vacancies in the outer electron shells.

Acknowledgments

We are very grateful to Dr. N. Kurti for his advice and help in this work and to Professor H. Halban and Professor Sir Francis Simon for their continued interest.

References

Alburger, D. E., and Grace, M. A., 1954, *Proc. Phys. Soc.* A, **67,** 280.
Baker, J. M., Bleaney, B., Bowers, K. D., Shaw, P. F. D., and Trenam, R. S., 1953, *Proc. Phys. Soc.* A, **66,** 305.
Bleaney, B., Daniels, J. M., Grace, M. A., Halban, H., Kurti, N., Robinson, F. N. H., and Simon, F. E., 1954, *Proc. Roy. Soc.* A, **221,** 170.
Bishop, G. R., and Perez y Jorba, J. P., 1955, *Phys. Rev.*, **98,** 89.
Daniels, J. M., Grace, M. A., Halban, H., Kurti, N., and Robinson, F. N. H., 1952, *Phil. Mag.*, **43,** 1297.
Gray, T. P., and Satchler, G. R., 1955, *Proc. Phys. Soc.* A, **68,** 349.
Lemmer, H. R., Grace, M. A., and Segaert, O. J. A., 1955, *Proc. Phys. Soc.* (in course of publication).
Steenberg, N., 1952, *Proc. Phys. Soc.* A, **65,** 791 ; 1953, *Ibid.*, **66,** 391.
Temmer, G. M., and Heydenburg, N. P., 1954, *Phys. Rev.*, **96,** 426.

CIX. *On the Scattering Cross Section of an Obstacle*

By D. S. Jones
Department of Mathematics, University of Manchester *

[Received December 3, 1954]

Summary

Van de Hulst's theorem giving the relation between the scattering cross section and the scattered ' amplitude ' for an obstacle in an incident plane wave is derived by a calculation of the energy flow. In addition it is shown that, when the incident wave is due to a point source, the sum of the scattering and absorption cross sections is determined by the value of a certain field in the neighbourhood of the source.

The argument, which is based on energy considerations, could be applied to many scattering problems, e.g. sound waves or atomic collisions but is given explicitly for the electromagnetic field.

§ 1. Introduction

It has been shown by van de Hulst (1949) that the scattering cross section of an obstacle in an incident plane wave is closely related to the ' amplitude ' of the wave scattered in the direction of the incident wave. (Various special cases of his theorem have been derived by, for example, van de Hulst (1946), Levine and Schwinger (1948, 1950) and by Storer and Sevick (1954). A proof for atomic collisions has been given by Feenberg (1932) and by Lax (1950).) The argument of van de Hulst is that the attenuation of the plane wave after it has passed the obstacle is a measure of the absorption and scattering of the obstacle. Since the scattered field and plane wave do not interfere at infinity except in the direction of the incident field the attenuation can be estimated by considering the neighbourhood of this direction only. The calculation, which involves a difficulty over the convergence of an integral, shows that the attenuation depends only on the ' amplitude ' of the scattered wave in the direction of the incident wave.

In this paper we shall consider firstly the same problem using a somewhat different method which avoids the convergence difficulty. The method, which is based on energy considerations will be given explicitly for the harmonic electromagnetic field, so that polarization effects may be observed but, apart from an alteration of the mathematical equations, most of the statements could be applied to other scattering problems, e.g. those concerned with small-amplitude sound waves or atomic particles.

* Communicated by the Author.

Secondly we shall consider the problem which arises when the incident wave is due to a point source. In this problem the scattered field may be regarded as due to certain sources, situated within the obstacle, radiating into free space. Let the field which is produced by replacing all these sources by equal sinks (which give ingoing waves at infinity) be called the equivalent ingoing field. Then the sum of the scattering and absorption cross sections of the obstacle in the point source field is equal to average rate at which work is done in maintaining the source in the equivalent ingoing field only divided by the average rate at which incident energy is crossing unit area.

Some readers may find this clearer when they see the appropriate mathematical expressions. These will now be given for two particular examples.

Firstly, we consider scalar fields and suppose that the incident field, due to a source at $\mathbf{r}'$, is derived from

$$\nabla^2\phi+k^2\phi=-q\delta(\mathbf{r}-\mathbf{r}')$$

where q is a constant. Then the sum of the absorption and scattering coefficients is

$$-\frac{16\pi^2}{k\sigma\,|\,q\,|^2}\mathscr{I}\{\phi_2(\mathbf{r}')q^*\}$$

where ϕ_2 is the equivalent ingoing field, σ the solid angle subtended by the obstacle at $\mathbf{r}'$ and the star indicates a complex conjugate.

Secondly, consider an electromagnetic field with the incident wave derived from

$$\text{curl}\ \mathbf{E}_0=-i\omega\mu_0\mathbf{H}_0,$$

$$\text{curl}\ \mathbf{H}_0=\frac{ik^2}{\omega\mu_0}\mathbf{E}_0+\mathbf{p}\delta(\mathbf{r}-\mathbf{r}')$$

where $\mathbf{p}$ is a constant vector. Then the sum of the average rates at which energy is scattered and absorbed by the obstacle is equal to

$$-\tfrac{1}{2}\mathscr{R}\{\mathbf{E}_2(\mathbf{r}')\cdot\mathbf{p}^*\}$$

where $\mathbf{E}_2$ is the electric intensity in the equivalent ingoing field.

§ 2. The Incident Plane Wave

Let S be a sphere of radius R which completely encloses the obstacle. Then the average rate at which energy is entering S is the average rate at which energy is absorbed by the obstacle.†

Let $\mathbf{E}$, $\mathbf{H}$ and $\mathbf{E}_0$, $\mathbf{H}_0$ be the electric and magnetic intensities in the total field and incident field respectively, the time dependence exp $(i\omega t)$ being understood. Denote by $\mathscr{A}$ the average rate at which energy is absorbed by the obstacle. Then the above statement about the rate of energy leaving S may be written

$$\tfrac{1}{4}\int_S(\mathbf{E}\wedge\mathbf{H}^*+\mathbf{E}^*\wedge\mathbf{H})\cdot\mathbf{n}\,dS=-\mathscr{A}\quad\ldots\ldots\quad(1)$$

† The corresponding statement for the scattering of a beam of particles by a nucleus is that the number of particles entering S is equal to the number being absorbed.

where the star indicates a complex conjugate and $\mathbf{n}$ is the unit vector along the outward normal to S.

Now the average rate at which the energy of the incident wave only enters S is zero. Hence (1) can be written

$$\tfrac{1}{4}\int_S (\mathbf{E}_1\wedge\mathbf{H}_1^*+\mathbf{E}_1^*\wedge\mathbf{H}_1)\cdot\mathbf{n}\,dS=-\mathscr{A}-\tfrac{1}{4}\int_S (\mathbf{E}_0\wedge\mathbf{H}_1^*+\mathbf{E}_1\wedge\mathbf{H}_0^*+\mathbf{E}_0^*\wedge\mathbf{H}_1 +\mathbf{E}_1^*\wedge\mathbf{H}_0)\cdot\mathbf{n}\,dS \quad . \quad . \quad . \quad . \quad . \quad . \quad . \quad (2)$$

where $\mathbf{E}_1$ and $\mathbf{H}_1$ are the electric and magnetic intensities in the scattered field. The integral on the left of the equation gives the average rate at which energy is scattered by the obstacle. The integral on the right gives a contribution only from a small portion of S because, over most of S, the incident and scattered waves carry energy independently.

To calculate this contribution we observe that, as $R\to\infty$,

$$\left.\begin{aligned}\mathbf{E}_1&=\mathbf{A}_1(\mathbf{n})\exp(-ikR)/R+O(1/R^2),\\ \mathbf{H}_1&=\frac{k}{\mu_0\omega}\mathbf{n}\wedge\mathbf{A}_1(\mathbf{n})\exp(-ikR)/R+O(1/R^2)\end{aligned}\right\} \quad . \quad . \quad . \quad (3)$$

where $\mathbf{n}\cdot\mathbf{A}_1=0$, μ_0 is the permeability of free space and the wavelength is $2\pi/k$. The incident field is given by

$$\mathbf{E}_0=\mathbf{e}_0\exp(-ikR\mathbf{n}\cdot\mathbf{n}_0),$$
$$\mathbf{H}_0=\mathbf{h}_0\exp(-ikR\mathbf{n}\cdot\mathbf{n}_0)$$

where the real constant vectors $\mathbf{e}_0$, $\mathbf{h}_0$, and $\mathbf{n}_0$ are related by

$$\mathbf{e}_0\cdot\mathbf{e}_0=1,\quad \mathbf{n}_0\cdot\mathbf{e}_0=0,\quad \mathbf{n}_0\cdot\mathbf{h}_0=0 \quad \text{and} \quad \mu_0\omega\mathbf{h}_0=k\mathbf{n}_0\wedge\mathbf{e}_0. \quad . \quad . \quad (4)$$

Also there is a lemma (Jones 1952) which states

$$\frac{1}{R}\int_S f(\mathbf{n})\exp(-ikR\mathbf{n}\cdot\mathbf{n}_0)\,dS=\frac{2\pi i}{k}\{f(\mathbf{n}_0)\exp(-ikR) -f(-\mathbf{n}_0)\exp(ikR)\}+o(1)$$

as $R\to\infty$. This lemma enables the integral on the right of (2) to be calculated. After a use of (3) and (4) the limiting value of the integral is found to be

$$\frac{2\pi}{\omega\mu_0}\mathscr{I}\mathbf{e}_0\cdot\mathbf{A}_1(\mathbf{n}_0).$$

It may be remarked that this is contributed by the portion of S (in the direction of the plane wave) which subtends a solid angle of order $(kR)^{-\beta}(1>\beta>\frac{4}{5})$ at the centre of S and thus the attenuation can be measured by an instrument which subtends a solid angle of this order.

The average rate at which energy is scattered by the obstacle is, consequently,

$$-\frac{2\pi}{\omega\mu_0}\mathscr{I}\mathbf{e}_0\cdot\mathbf{A}_1(\mathbf{n}_0)-\mathscr{A}.$$

On dividing by the average rate at which the energy of the incident waves crosses a unit area perpendicular to its direction of propagation

we find that the extinction, i.e. the sum of the scattering and absorption cross sections is equal to

$$-\frac{4\pi}{k}\mathscr{I}\mathbf{e}_0 \cdot \mathbf{A}_1(\mathbf{n}_0)\dagger$$

which is the result obtained by van de Hulst.

§ 3. The Point Source Incident Field

The incident field $\mathbf{E}_0$, $\mathbf{H}_0$ produces a scattered field $\mathbf{E}_1$, $\mathbf{H}_1$, which may be regarded as generated by sources, placed within the obstacle, radiating into free space. Let $\mathbf{E}_2$, $\mathbf{H}_2$ be the equivalent ingoing field, i.e. the field produced when all the sources within the obstacle are replaced by equal sinks. As $R\to\infty$

$$\mathbf{E}_2=\mathbf{A}_2(\mathbf{n})\exp(ikR)/R+O(1/R^2) \quad . \quad . \quad . \quad . \quad . \quad (5)$$

where $\mathbf{n}\cdot\mathbf{A}_2(\mathbf{n})=0$.

In the calculation of $\mathbf{A}_1(\mathbf{n})$ the only important quantity, apart from the source strength, is the phase difference between the position of a source and a plane perpendicular to $\mathbf{n}$. A similar remark is true for $\mathbf{A}_2(\mathbf{n})$ and clearly the phase difference occurring for $\mathbf{A}_2(\mathbf{n})$ is the same as that occurring for $\mathbf{A}_1$ in the direction $-\mathbf{n}$. Hence

$$\mathbf{A}_2(\mathbf{n})=\mathbf{A}_1(-\mathbf{n}), \quad . \quad . \quad . \quad . \quad . \quad . \quad . \quad . \quad (6)$$

i.e. at infinity the amplitude of the equivalent ingoing field can be obtained by rotating the scattered field at infinity through 180°. One consequence of this is that the average rate at which energy is scattered by the obstacle is the same as the average rate at which energy is brought into S (a sphere which encloses the obstacle and the source of the incident field) by the equivalent ingoing field.

Consider now the field $\mathbf{E}_2-\mathbf{E}_0$, $\mathbf{H}_2-\mathbf{H}_0$; the average rate at which energy in this field leaves S', a surface enclosing the obstacle but not the source of the incident wave, is equal to the average rate at which work is done in maintaining the sources and sinks inside S'. In fact, there are only sinks namely those producing the equivalent ingoing field. The average rate at which work is done can be split into two parts (i) that done by maintaining the sinks in the field $\mathbf{E}_2$, $\mathbf{H}_2$ and, (ii) that done by maintaining them in $-\mathbf{E}_0$, $-\mathbf{H}_0$. The first of these is just the average rate at which energy is taken out of S' (or S) by the equivalent ingoing field alone and hence is equal to the average rate at which energy enters S' due to the scattered field alone. This, again, is equal to the average rate at which work is done in maintaining the sources of the scattered field in $-\mathbf{E}_1$, $-\mathbf{H}_1$. In view of the relation between the sources of the scattered field and the sinks of the equivalent ingoing field the combination of this average rate and (ii) gives the average rate at which energy enters S' in the field $\mathbf{E}_0+\mathbf{E}_1$, $\mathbf{H}_0+\mathbf{H}_1$, and this is the average

† The corresponding quantity for small amplitude sound waves, with incident field $\exp(-ikR\mathbf{n}\cdot\mathbf{n}_0)$ and scattered field $A_1(\mathbf{n})\exp(-ikR)/R$, is $-(4\pi/k)\mathscr{I}A_1(\mathbf{n}_0)$.

rate at which energy is absorbed by the obstacle. Therefore, the average rate at which energy leaves S' in the field $\mathbf{E}_2-\mathbf{E}_0$, $\mathbf{H}_2-\mathbf{H}_0$ is equal to $\mathscr{A}$.

Now the average rate at which energy leaves the interior of S' in $\mathbf{E}_2-\mathbf{E}_0$ is equal to the sum of the average rate at which work is done in maintaining the source of the incident wave in the field $\mathbf{E}_2-\mathbf{E}_0$ and the average rate at which energy leaves S. Since the incident wave and equivalent ingoing field do not interfere the average rate at which energy leaves S is equal to the difference between the average rates at which energy leaves S due to the incident wave and scattered field separately. Hence *the sum of the average rates at which energy is scattered and absorbed by the obstacle is equal to the average rate at which work is done in maintaining the source of the incident field in the equivalent ingoing field only.* This is equally true if the incident wave is due to a number of point sources.

Denote by σ the area of the sphere, with centre the source of the incident field and unit radius, which lies within the tangent cone from the source to the obstacle. Define ρ, the average rate at which incident energy is crossing unit area, to be the average rate at which the energy of the incident field is crossing σ divided by σ. Then the scattering cross section is defined to be the ratio of the average rate at which energy is scattered and ρ. With a similar definition for the absorption cross section we find that the extinction is equal to the average rate at which work is done in maintaining the source of the incident wave in the presence of the equivalent ingoing field only divided by ρ.

The cross section, defined in this way, does not become the plane wave cross section as the source tends to infinity. A more suitable quantity, from this point of view, is the scattering coefficient which is defined as the ratio of the average rates at which energy is scattered and at which incident energy is crossing σ. The value of the sum of the absorption and scattering coefficients may be deduced easily from the preceding paragraphs.

When the incident wave is obtained from

$$\text{curl } \mathbf{E}_0 = -i\omega\mu_0\mathbf{H}_0,$$

$$\text{curl } \mathbf{H}_0 = \frac{ik^2}{\omega\mu_0}\mathbf{E}_0 + \mathbf{p}\delta(\mathbf{r}-\mathbf{r}')$$

where $\mathbf{p}$ is a constant vector and δ is the Dirac delta function, the above results show that the sum of the average rates at which energy is scattered and absorbed by the obstacle is equal to

$$-\tfrac{1}{4}\{\mathbf{E}_2(\mathbf{r}')\cdot\mathbf{p}^* + \mathbf{E}_2^*(\mathbf{r}')\cdot\mathbf{p}\}.\dagger$$

If the source is some distance from the obstacle this reduces, on account of (5) and (6), to

$$-\tfrac{1}{4}\{\mathbf{A}_1(-\mathbf{n}')\cdot\mathbf{p}^* \exp(ikR')/R' + \mathbf{A}_1^*(-\mathbf{n}')\cdot\mathbf{p} \exp(-ikR')/R'\} + O(1/R'^2) \quad . \quad . \quad . \quad (7)$$

where $\mathbf{r}' = R'\mathbf{n}'$.

† The corresponding formula for scalar waves is stated in the introduction.

The result of § 2 can be deduced from this. For, if we put $\mathbf{n}' = -\mathbf{n}_0$ and $\mathbf{p} = (4\pi i/\omega\mu_0)\ R' \exp(ikR')\mathbf{e}_0$, the incident wave becomes the plane wave of § 2 in the limit as $R' \to \infty$ and (7) becomes $-(2\pi/\omega\mu_0)\mathscr{I}\mathbf{A}_1(\mathbf{n}_0) \cdot \mathbf{e}_0$ in agreement with the earlier result for the sum of the average rates at which energy is scattered and absorbed.

§ 4. The High Frequency Extinction

When the wavelength is very small compared with the linear dimensions of the obstacle the limiting case of geometrical optics is approached. Only that part of the incident wave which lies within the tangent cone to the obstacle is then affected by the obstacle. If there is no transmission through the obstacle the scattered field inside the tangent cone and on the opposite side of the obstacle from the source must annul the incident field. The incident field itself is either reflected or absorbed by the obstacle. Hence the sum of the average rates at which energy is scattered and absorbed by the obstacle is twice the average rate at which energy is incident inside the tangent cone. Consequently the extinction is twice the geometrical cross section, the geometrical cross section being the area of the unit sphere inside the tangent cone. The sum of the absorption and scattering coefficients is 2.

It may be remarked that this simple result would not hold in general if ρ were defined by the incident energy over the whole unit sphere because the energy of the source is not necessarily radiated uniformly in all directions.

References

Feenberg, E., 1932, *Phys. Rev.*, **40**, 40.

van de Hulst, H. C., 1946, *Recherches Astronomiques de l'Observatoire d'Utrecht*, **11** ; 1949, *Physica*, **15**, 740–6.

Jones, D. S., 1952, *Proc. Camb. Phil. Soc.*, **48**, 733–41.

Lax, M., 1950, *Phys. Rev.*, **78**, 306.

Levine, H., and Schwinger, J., 1948, *Phys. Rev.*, **74**, 958–74 ; 1950, *Comm. Pure and App. Math.*, **3**, 355–91.

Storer J. E., and Sevick, J., 1954, *Journ. App. Phys.*, **25**, 369–76.

CX. *Inelastic Scattering of* 2·5 MEV *Neutrons by* ^{54}Fe *and* ^{56}Fe

By L. E. BEGHIAN, D. HICKS and B. MILMAN
Clarendon Laboratory, Parks Road, Oxford*

[Received May 26, 1955]

ABSTRACT

A NaI(Tl) crystal was used to study the gamma radiations emitted by natural iron, ^{54}Fe, and ^{56}Fe scatterers. Gamma rays of the following energies were observed: from natural iron 0·85±0·03, 1·22±0·05, 1·42±0·05 MEV. The 1·4 MEV gamma ray was not present with the ^{56}Fe scatterer. A 1·37±0·05 MEV line was observed with the ^{54}Fe scatterer. In addition the neutrons scattered from natural iron were studied with a stilbene crystal, and groups corresponding to levels at 0·85±0·03 MEV and 1·45±0·05 MEV were found. On the basis of the above the following levels can be identified: in ^{56}Fe 0·85±0·03 MEV, 2·07±0·05 MEV, in ^{54}Fe 1·40±0·05 MEV.

§ 1. INTRODUCTION

THE gamma ray spectrum associated with the scattering of fast neutrons by natural iron has been extensively studied (Beghian *et al.* 1951, Day 1954, Lafferty *et al.* 1954, Rothman *et al.* 1954, Scherrer *et al.* 1954). Gamma rays of 0·85 MEV, 1·25 MEV, and 1·42 MEV have been reported (Day 1954). The 0·85 MEV and 1·25 MEV lines fit into the level scheme of ^{56}Fe established from the β decays of ^{56}Co and ^{56}Mn. The 1·4 MEV line must either be associated with some level of ^{56}Fe which is not excited in the β decays, or it must originate from one of the other iron isotopes. The present work was carried out to decide between these alternatives, to find which levels are excited in the various isotopes and to establish their mode of decay.

§ 2. MEASUREMENTS WITH NATURAL IRON

A 5 cm diameter, 2 cm thick natural iron scatterer was employed and studies of the neutron groups and gamma rays made by techniques which have previously been described (Eliot *et al.* 1954). As before, pulse height distributions were recorded, on a 25 channel kicksorter, with and without scatterer, and using both a sodium iodide and stilbene crystal as detectors.

The gamma ray spectrum was obtained from the sodium iodide measurements by subtracting (after suitable normalization) the pulse height

* Communicated by the Authors.

distribution taken without scatterer from that made with the scatterer. In this way the effect of background neutrons was eliminated. Gamma rays of $0{\cdot}85\pm0{\cdot}03$ Mev, $1{\cdot}22\pm0{\cdot}05$ Mev and $1{\cdot}45\pm0{\cdot}05$ Mev were observed (see fig. 1). In addition there was a small peak at 2·1 Mev (see § 5).

The neutron spectrum was determined from the stilbene pulse height distributions as before (Eliot *et al.* 1954) by plotting R as a function of pulse height where

$$R=\left(\frac{\text{counts per kicksorter channel with the scatterer}}{\text{counts per kicksorter channel without the scatterer}}\right).$$

Fig. 1

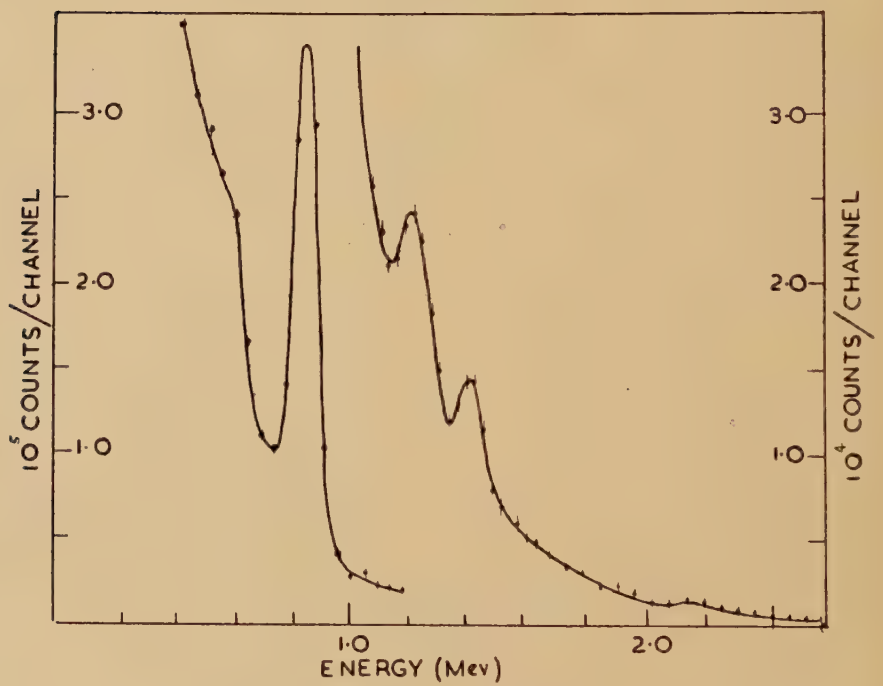

Natural iron scatterer. Gamma ray spectrum.

The resulting ratio plot will, in general, consist of a series of plateaux separated by steps. Each step can be interpreted as a neutron group or gamma ray Compton edge. In the present case the NaI measurements indicate that all the gamma rays are too energetic to produce Compton edges on the ratio plot. Any steps must therefore correspond to neutron groups.

Figure 2 shows the presence of neutron groups exciting levels at $0{\cdot}85\pm0{\cdot}03$ Mev and $1{\cdot}45\pm0{\cdot}05$ Mev. It has been demonstrated in subsidiary experiments (details to be published) that gamma rays of

all energies produce a distortion of the plateaux in the region of low pulse heights. This makes it impracticable to search for neutron groups corresponding to levels of more than 1·7 MeV.

Fig. 2

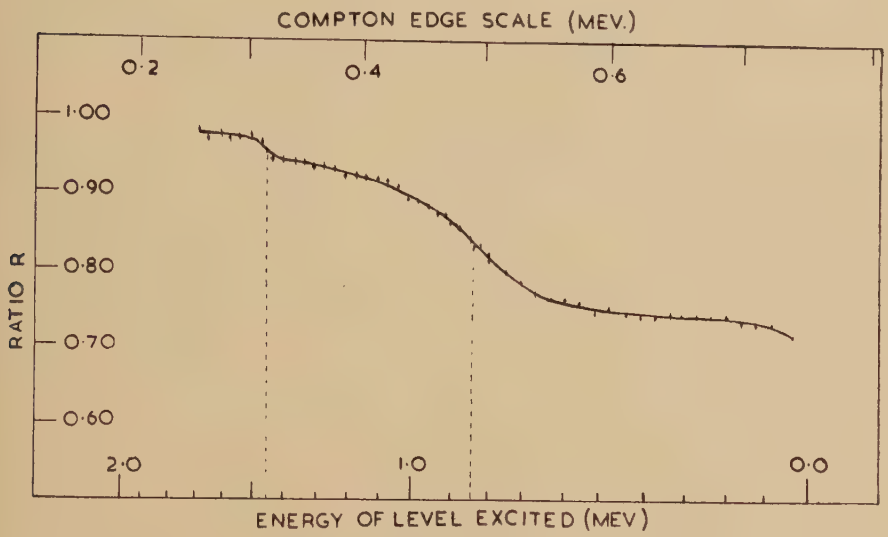

Natural iron scatterer. Ratio plot.

Fig. 3

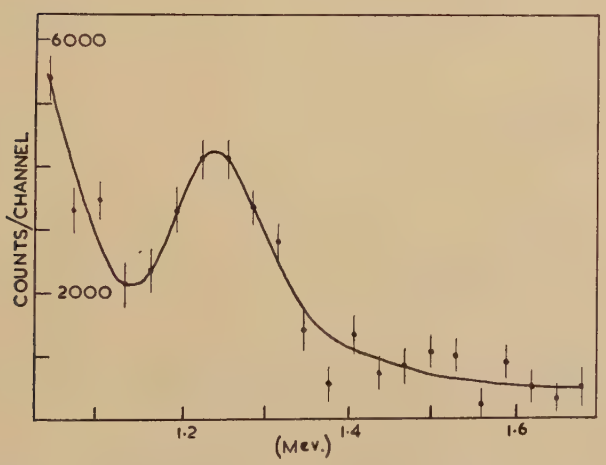

^{56}Fe scatterer. Gamma ray spectrum.

§ 3. Measurements with ^{56}Fe

The scatterer was 29·6 g of 97% ^{56}Fe powder enclosed in a thin (0·1 mm) aluminium can. Gamma ray measurements only were made and it is seen from fig. 3 that the 1·4 MeV gamma ray is absent. The 1·22 MeV gamma ray was still present and can thus be definitely attributed to ^{56}Fe.

§ 4. Measurements with ^{54}Fe

3 g of ^{54}Fe enriched to 67% enclosed in a thin can of aluminium were used as scatterer. Again only the gamma spectrum was observed (see fig. 4). It is seen that a $1{\cdot}37 \pm 0{\cdot}05$ Mev gamma ray was present and within experimental error this can be identified with the $1{\cdot}42 \pm 0{\cdot}05$ Mev line observed with natural iron.

§ 5. Conclusions

It has been shown that the 1·4 Mev gamma ray is associated with ^{54}Fe and the neutron groups from natural iron indicate the presence of an excited state of this energy. It therefore is reasonable to interpret the 1·4 Mev gamma ray as a ground state transition in ^{54}Fe. A similar conclusion has recently been reached by Sinclair (1955) who studied the gamma rays from a 32 g scatterer enriched to 35% ^{54}Fe. The cross section for excitation of the 1·4 Mev level in ^{54}Fe, calculated from the ratio plot, is $1{\cdot}0 \pm 0{\cdot}3$ barns.

Fig. 4

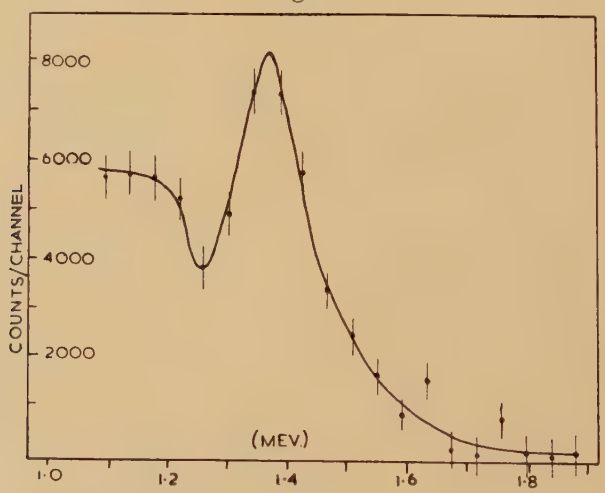

^{54}Fe scatterer. Gamma ray spectrum.

In the measurements with natural iron both the neutron group exciting the 0·85 Mev level in ^{56}Fe and the ground state gamma ray were observed. The isotopic cross section for this level is $1{\cdot}06 \pm 0{\cdot}25$ barns. Since there is no neutron group corresponding to a 1·22 Mev level, the 1·22 Mev gamma ray must be regarded as a cascade transition from a 2·07 Mev level into the 0·85 Mev level. This is consistent with the data on the β decay of ^{56}Co (Sakai *et al.* 1954). The 2·1 Mev peak present in the gamma ray spectrum can be attributed to an addition process in the NaI crystal of the radiations of 1·25 and 0·85 Mev. This interpretation is consistent with the observed intensities but the possibility of a crossover transition cannot be excluded.

The conclusions are summarized in the level schemes of fig. 5. The results obtained with ^{54}Fe show that this technique of measuring gamma spectra is applicable to only a few grams of scattering material and is therefore particularly useful in the case of separated isotopes.

Fig. 5

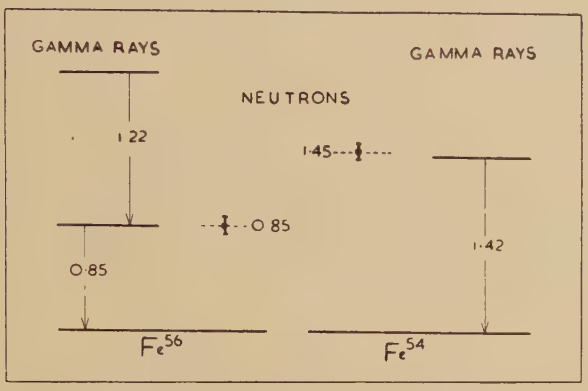

The level schemes of ^{54}Fe and ^{56}Fe.

Acknowledgments

We would like to thank the Director and Dr. M. L. Smith of A.E.R.E., Harwell for providing the separated isotopes, Professor H. Halban for helpful discussions, and Professor Lord Cherwell for extending to us the facilities of this laboratory.

References

Beghian, L. E., Grace, M. A., Halban, H., and Preston, G., 1951, *Phys. Rev.*, **82,** 969.
Day, R. B., 1954, *Phys. Rev.*, **89,** 908.
Eliot, E. A., Hicks, D., Beghian, L. E., and Halban, H., 1954, *Phys. Rev.*, **94,** 144.
Lafferty, D. L., Rayburn, L. A., and Hahn, T. M., 1954, *Phys. Rev.*, **96,** 381.
Rothman, M. A., and Mandeville, C. E., 1954, *Phys. Rev.*, **93,** 796.
Sakai, M., Dick, J. L., Anderson, W. S., and Kurbatov, J. D., 1954, *Phys. Rev.*, **95,** 101.
Scherrer, V. E., Allison, B. A., and Faust, W. R., 1954, *Phys. Rev.*, **96,** 386.
Sinclair, R., 1954, *Bull. Am. Phys. Soc.*, **30,** No. 1, 8.

CXI. *Brittle Fracture and Yielding*

By A. N. Stroh
Cavendish Laboratory, Cambridge*

[Received June 8, 1955]

Summary

The stresses round a piled-up group of dislocations may either initiate a crack or operate a Frank–Read source by pulling it from its locking impurities ; the latter is related to the propagation of a Lüders band. This interpretation leads to results in accord with experiment. The model gives a sharp transition from brittle to ductile behaviour as the temperature is increased.

§ 1. Introduction

The conditions under which the stresses round a piled-up group of dislocations are sufficient to open up a crack have been considered in a previous paper (Stroh 1954) ; to form a crack we require n dislocations piled up under a shear stress σ_s such that

$$n\mathbf{b}\sigma_s = 12\gamma, \quad . \quad . \quad . \quad . \quad . \quad . \quad . \quad . \quad . \quad (1)$$

where $\mathbf{b}$ is the Burgers vector and γ the surface energy. This equation can be put in a form more suitable for comparison with experiment by using the result due to Eshelby, Frank and Nabarro (1951) that the pile-up will occupy a length L of the slip plane given by

$$L = n\mathbf{b}G/\pi(1-\nu)\,\sigma_s, \quad . \quad . \quad . \quad . \quad . \quad . \quad . \quad . \quad (2)$$

where G is the rigidity and ν Poisson's ratio. Eliminating n between (1) and (2) we obtain

$$\sigma_s^2 L = 12\gamma G/\pi(1-\nu). \quad . \quad . \quad . \quad . \quad . \quad . \quad . \quad (3)$$

If the specimen is tested under tension the maximum shear stress is half the tensile stress τ, and, supposing the dislocations to pile up on the grain boundaries, we must take L equal to half the grain diameter d. Then (3) may be written

$$\tau d^{1/2} = 4\{6\gamma G/\pi(1-\nu)\}^{1/2} ; \quad . \quad . \quad . \quad . \quad . \quad . \quad (4)$$

thus the cleavage strength should be inversely proportional to the square root of the grain size, a result first deduced by Orowan (1933) on the basis of Griffith's theory. This proportionality has been verified experimentally by Petch (1953) for ferrite and Greenwood and Quarrel (1954) for zinc. The constant on the right hand side of (4) may also be calculated. For

* Communicated by the Author.

ferrite with $G=8\times10^{11}$ dynes cm^{-2}, $\gamma=1{\cdot}2\times10^{3}$ dynes cm^{-1} and $\nu=0{\cdot}3$ we obtain $\tau d^{1/2}=2{\cdot}0\times10^{8}$, which may be compared with the value $2{\cdot}3\times10^{8}$ from Petch's graph. For zinc, we have $G=3{\cdot}8\times10^{11}$, $\gamma=10^{3}$ and $\nu=0{\cdot}2$, giving $\tau d^{1/2}=1{\cdot}2\times10^{8}$, while Greenwood and Quarrel obtain (at liquid air temperature) $1{\cdot}0\times10^{8}$.

This very satisfactory agreement encourages us to consider how far these ideas may be applied to other problems. In the present paper we discuss the lower yield point of ferrite, and the brittle–ductile transition.

§ 2. The Lower Yield Point

Petch (1953) has emphasized the great similarity in the behaviour of the cleavage strength and the lower yield point of ferrite ; the latter also varies inversely as the square root of the grain size. If we interpret cleavage as resulting from the normal stresses round the pile-up, it is natural to suppose that yielding and the propagation of a Lüders band arise from the shear stresses round the pile-up. Now at a distance r from the head of the pile-up the shear stress, apart from a factor approximately unity but depending on orientation, is

$$\sigma=\sigma_s\,(L/r)^{1/2}. \qquad (5)$$

If slip is to continue, this stress must be great enough to operate the sources in the next grain. These sources will be locked by impurity atoms (Cottrell 1948, Cottrell and Bilby 1949) and to free the dislocation a stress σ_1, equal to the upper yield point is required. In addition the stress on the source must be great enough to bow it out ; if the source has length l the stress needed for this is $G\mathbf{b}/l$. Hence the source will operate if

$$\sigma_s(L/r)^{1/2}=\max\,[\sigma_1,\, G\mathbf{b}/l], \qquad (6)$$

where ' max ' indicates that the greater of the two quantities in brackets is to be taken.

We suppose, now, that there are a number of sources of varying lengths. Those of length l cannot be nearer than a distance l from the pile-up ; in general the nearest sources will be a distance $r=\alpha l$ away, where α is a constant of order, but greater than, unity. With this value of r, (6) may be written

$$\sigma_s(L/\alpha)^{1/2}=\max\,\{\sigma_1 l^{1/2},\, G\mathbf{b}/l^{1/2}\}. \qquad (7)$$

The right hand side of (7) is least when the two terms are equal, or

$$l=G\mathbf{b}/\sigma_1 \qquad (8)$$

and these sources will be the first to operate. With σ_1 equal to the observed upper yield point of about 7×10^{3} dynes/cm (at room temperature), this gives $l=3\times10^{-5}$ cm. Substituting (8) in (7) we have

$$\sigma_s(L/\alpha)^{1/2}=(G\mathbf{b}\sigma_1)^{1/2},$$

or taking L half the grain size d, and σ_s half the tensile stress τ,

$$\tau d^{1/2}=2(2\alpha\sigma_1 G\mathbf{b})^{1/2}=\text{constant}. \qquad (9)$$

The constancy of $\tau d^{1/2}$ is the relation between lower yield point and grain size observed by Hall (1951) and Petch (1953).

At two different temperatures T_1 and T_2 eqn. (9) gives

$$(\tau d^{1/2})_1/(\tau d^{1/2})_2=(\sigma_1 G)_1{}^{1/2}/(\sigma_1 G)_2{}^{1/2}, \quad . \quad . \quad . \quad . \quad (10)$$

where the suffixes refer to the temperatures.

To test this equation we may use the results of Hall at room temperature and of Petch at liquid air temperature. From the graphs in their papers we find that $\tau d^{1/2}$ has the values $0{\cdot}7\times10^8$ at room temperature and $1{\cdot}9\times10^8$ at $-196°$c, the ratio being 2·7. Both experiment (McAdam and Mebs 1943) and theory (Cottrell and Bilby 1949) agree in giving a change in the upper yield point σ_1 by a factor of 4·1 between the temperatures under consideration. The change in G will be about 10%. Then the right hand side of (10) is equal to 2·1, which is of the right order. It is possible that the agreement could be improved by taking into account the rate of straining. Hall used the unusually slow rate of 10^{-4}/min ; Petch does not state his strain-rate but if it were greater, the effect would be to accentuate the difference in temperature.

Finally we may consider the value of the constant in eqn. (9). Using the value $\sigma_1=7\times10^8$ dynes cm^{-2} appropriate to room temperature, we obtain $3{\cdot}3\times10^7\,\alpha^{1/2}$; this agrees with Hall's results provided α is about 4 which seems reasonable. Further the value of $\tau d^{1/2}$ should be the same for all specimens (at one temperature) if σ_1 is the same ; however in all but the very purest specimens of ferrite there will be sufficient carbon atoms present to form a saturated atmosphere round the dislocations so that the locking forces will have a constant maximum value. In fact Petch has found that when the lower yield point is plotted against grain size, even for such different materials as mild steel, ingot iron, and spectrographic iron, the points all lie on a single line with a remarkably small amount of scatter. The point is not a trivial one, as if the value of the yield point depended on some quantity such as the mean size of the dislocation network considerable variation might occur.

Thus the model proposed accounts for the variation of the lower yield point with grain size and temperature, its insensitivity to the nature of the specimen, and, in order of magnitude, for the absolute value of the yield point.

§ 3. Brittle–Ductile Transition

We have seen that the stresses round a pile-up may either initiate a crack or operate nearby sources ; if the former happens the metal is brittle, if the latter, ductile. When the sources are locked by impurity atoms, thermal fluctuations will help free them, and so high temperatures will favour ductile behaviour. At low temperatures no thermal fluctuation great enough to liberate a source may occur in the time taken for the pile-up to grow large enough to initiate a crack ; the material is then brittle. In the present section we attempt to estimate the temperature at which the transition from brittleness to ductility will take place.

Let σ be the stress at time t on a source of length l near the pile-up. The probability that the source will operate in the next interval of time dt, provided it has not done so already, is

$$\nu(l/\mathbf{b}) \exp \{-u(\sigma)/kT\}\, dt,$$

where ν is an atomic frequency of vibration, and $u(\sigma)$ is the activation energy for the source to break away from its locking impurities ; $l/\mathbf{b}$ is the number of points at which the break away can start. If p is the probability that the source has not operated at time t, the probability that it will do so between times t and $t+dt$ is

$$-dp=p\nu(l/\mathbf{b}) \exp \{-u(\sigma)/kT\}\, dt. \quad . \quad . \quad . \quad . \quad . \quad . \quad (11)$$

On integrating (11) we have

$$p=\exp\left[-\frac{\nu l}{\mathbf{b}}\int_{-\infty}^{t} \exp\left\{-\frac{u(\sigma)}{kT}\right\} dt\right]. \quad . \quad . \quad . \quad . \quad . \quad (12)$$

We require the probability that the source will not have operated by the time the pile-up has grown large enough to initiate a crack ; (12) is now taken to refer to this time. The contributions to the integral will come mainly from times at which $u(\sigma)$ is least, which will be when σ is greatest. The integral will be approximately $t_0 \exp \{-u(\sigma)/kT\}$ where t_0 is a time of the order of that required to form the pile-up, and σ now denotes the final value of the stress due to the pile-up on the source. Then (12) may be written

$$p=\exp [-(\nu l t_0/\mathbf{b}) \exp \{-u(\sigma)/kT\}]. \quad . \quad . \quad . \quad . \quad . \quad (13)$$

Because of the double exponential p will change fairly abruptly from 1 to 0 as T increases ; this is in accord with the sharp transition from brittle to ductile behaviour observed. The transition will occur at a temperature

$$T=\frac{u(\sigma)}{k \log (\nu l t_0/\mathbf{b})}. \quad . \quad . \quad . \quad . \quad . \quad . \quad . \quad (14)$$

To estimate $u(\sigma)$ we require the stress on the sources : from (3) and (5) this will be

$$\sigma=\{12\gamma G/\pi(1-\nu)r\}^{1/2}. \quad . \quad . \quad . \quad . \quad . \quad . \quad (15)$$

The considerations of § 2 suggest that the first sources to be operated will be about $1{\cdot}2\times10^{-4}$ cm from the pile-up. With this value of r (15) gives $\sigma=10^{10}$ dynes/cm^2. Taking the yield stress at absolute zero to be 3×10^{10} dynes/cm^2, curve 4 of Cottrell and Bilby (1949), which they consider to be their best, gives u to be about 0·6 ev. Other quantities, which appear only in the argument of a logarithm in (14) are not very critical ; taking $\nu\sim10^{12}$ sec^{-1}, $t_0\sim10^{-6}$ sec, and $l/\mathbf{b}\sim10^3$ we obtain $T=300°$K. This is of the right order, though there is clearly considerable uncertainty as to the exact value. Under the same conditions we find from (13) that p decreases from 0·9 to 0·1 for a rise in temperature of 40°C ; this may be taken as a measure of the width of the transition range.

We may be interested in the spread of a crack instead of in its initiation. In Robertson's experiments (1951) a crack started from a saw cut is propagated through a temperature gradient, and the temperature where it is arrested observed. The moving crack will produce stresses on any sources it passes ; these may or may not then break away from their locking impurities and generate dislocation loops. As before we can find a transition temperature ; this will be given by (14) with t_0 now the time taken for the crack to pass the source, i.e. $t_0 \sim r/v$, where r is the distance of closest approach and v the speed of the crack. This temperature will be of similar magnitude, but not identical with that obtained previously. Below the transition temperature the crack can propagate without disturbing any source and so the material will certainly be brittle. Above the transition temperature the propagation of the crack will be accompanied by plastic flow ; if this absorbs too much of the stored elastic energy the crack will be unable to spread. It seems reasonable then to expect the arrest temperature of the crack will be closely related to our transition temperature.

Acknowledgment

This work was done during the tenure of a Department of Scientific and Industrial Research senior award.

References

Cottrell, A. H., 1948, *Bristol Conference on the Strength of Solids* (London : The Physical Society), p. 134.
Cottrell, A. H., and Bilby, B. A., 1949, *Proc. Phys. Soc.* A, **62,** 49.
Eshelby, J. D., Frank, F. C., and Nabarro, F. R. N., 1951, *Phil. Mag.*, **42,** 351.
Greenwood, J. N., and Quarrel, A. G., 1954, *J. Inst. Metals*, **82,** 551.
Hall, E. O., 1951, *Proc. Phys. Soc.* B, **64,** 747.
McAdam, D. J., and Mebbs, R. W., 1943, *Trans. Amer. Soc. Test. Mat.*, **43,** 661.
Orowan, E., 1933, *Z. Phys.*, **86,** 195.
Petch, N. J., 1953, *J. Iron. Steel Inst.*, **174,** 25.
Robertson, T. S., 1951, *Engineering*, **172,** 445.
Stroh, A. N., 1954, *Proc. Roy. Soc.* A, **223,** 404.

CXII. *Spin–Orbit Coupling and the Density Distribution in Heavy Nuclei*

By R. J. Blin-Stoyle
Clarendon Laboratory, Oxford*

[Received June 23, 1955]

Abstract

The spin–orbit coupling experienced by a nucleon in a nucleus is interpreted in terms of a neutral two-body spin–orbit potential. An expression of the Thomas form is obtained for the effective spin–orbit potential. It is shown that the spin–orbit splitting in heavy nuclei can be explained satisfactorily if the nuclear density distribution has a finite transition region at the surface and if the neutron distribution has a larger radius than the proton distribution.

§ 1. Introduction

The success of the nuclear shell model introduced by Mayer (1949) and Haxel, Jensen and Suess (1949) implies that a nucleon moving in a nucleus experiences a strong spin–orbit force. Recent experiments on the polarization of nucleons scattered by nuclei have served to confirm the existence of such a force and it is therefore of interest to investigate its origin.

To explain the force which manifests itself in the shell model two types of approach have been considered. Firstly, the spin–orbit potential has been interpreted in terms of a sort of Thomas (1926) precession, the potential having the form $\hbar^2/2m^2c^2r\,dV/dr$ $\mathbf{L}.\mathbf{S}$ where m is the nucleon mass. The actual relativistic Thomas precession gives much too small an effect, but suggestions (e.g. Inglis 1953) have been made that spin–orbit potentials of the above form should arise from meson theories. Secondly, the spin–orbit potential has been interpreted in terms of two-body internucleon forces. In particular, Keilson (1951) considered the contribution of tensor forces to the spin–orbit coupling and showed that, subject to the validity of certain approximations, one obtains an effective spin–orbit potential having the form $-K\rho(r)/r\;d\rho/dr$ $\mathbf{L}.\mathbf{S}$ resulting from the interaction of an odd particle with a spin saturated core (here ρ is the nuclear density and K a positive number). Splitting of the right sign is obtained if the odd particle spends most of its time in a region of radially *increasing* core density. However, particles of high angular momentum which are known to experience the largest splitting spend most of their time at the ' surface ' of the nucleus where the core density is radially *decreasing*. Hence it seems unlikely that the tensor interaction is

* Communicated by Professor R. E. Peierls, F.R.S.

responsible for the strong spin–orbit coupling. On the other hand, a two-body spin–orbit force of the form

$$V=J(|\mathbf{r}_1-\mathbf{r}_2|)[(\mathbf{r}_1-\mathbf{r}_2)\wedge(\mathbf{p}_1-\mathbf{p}_2)\cdot(\boldsymbol{\sigma}_1+\boldsymbol{\sigma}_2)]T(\boldsymbol{\tau}_1,\boldsymbol{\tau}_2)$$

has been shown by various authors to give spin–orbit splittings of the right order of magnitude and the correct sign (Hughes and Le Couteur 1950, Blanchard and Avery 1951) provided that the isotopic spin factor $T(\boldsymbol{\tau}_1,\boldsymbol{\tau}_2)$ is suitably chosen. These authors, however, do not attempt to make detailed quantitative comparisons of theory with experiment or to obtain an explicit form for the effective spin–orbit potential. Further, it has been shown by Elliott and Lane (1954) that such an internucleon interaction can also account for the observed increase in splitting in light nuclei as a given shell or sub-shell is filled (e.g. the $1p_{3/2}$—$1p_{1/2}$ splitting in ^{15}N is about twice the $1p_{3/2}$—$1p_{1/2}$ splitting in ^{5}He).

The object of the present paper is two-fold. Firstly, starting from the above two-body force an expression is derived for the effective spin–orbit potential experienced by a nucleon in a nucleus. Secondly, it is shown that this spin–orbit potential can then account in detail for the sign and magnitude of the splitting observed in nuclei in the vicinity of ^{208}Pb and is also consistent with the $1p_{3/2}$—$1p_{1/2}$ splitting in ^{5}He.

§ 2. Deduction of the Spin–Orbit Potential

We consider here the spin–orbit potential experienced by an odd nucleon interacting with a spin saturated core. Because of the necessary anti-symmetrization of the wave functions when the odd nucleon is of the same type as those forming the core there will be both direct and exchange terms to consider in the interaction. Calculations of Blanchard and Avery (1951), however, indicate that the exchange terms are only appreciable in the case of light nuclei and for this reason they are neglected in the following work.

For the two-body spin–orbit interaction we take the neutral form

$$V_{ij}=J(|\mathbf{r}_i-\mathbf{r}_j|)[(\mathbf{r}_i-\mathbf{r}_j)\wedge(\mathbf{p}_i-\mathbf{p}_j)\cdot(\boldsymbol{\sigma}_i+\boldsymbol{\sigma}_j)]$$

since this accounts satisfactorily for the increase in splitting as a given shell is filled (Elliott and Lane 1954).

The potential experienced by an odd nucleon at $\mathbf{r}_j$ in the presence of a spin saturated closed shell (specified by the usual quantum numbers n, l) is given by

$$V_j=\sum_i \int \phi^* V_{ij}\phi \, dV \, d\sigma$$

where ϕ is the wave function for the closed shell.

Since we are dealing with a spin saturated core the expectation values of $\Sigma_i\mathbf{p}_i$ and $\Sigma_i\boldsymbol{\sigma}_i$ will vanish so that

$$\begin{aligned} V_j&=-\sum_i \int \phi^* J(|\mathbf{r}_i-\mathbf{r}_j|)(\mathbf{r}_i-\mathbf{r}_j)\wedge\mathbf{p}_j\cdot\boldsymbol{\sigma}_j \, dV \, d\sigma \\ &=-\left[2\sum_m \int \psi_{nl}^{m*}(\mathbf{r}_i)J(|\mathbf{r}_i-\mathbf{r}_j|)(\mathbf{r}_i-\mathbf{r}_j)\psi_{nl}^{m}(\mathbf{r}_i)dV_i\right]\wedge\mathbf{p}_j\cdot\boldsymbol{\sigma}_j \end{aligned}$$

where $\psi_{nl}^{m}(\mathbf{r})$ is the wave function for a single particle in the state specified by the quantum numbers n, l, m (m=magnetic quantum number).

By symmetry

$$2\Sigma_{m}\int \psi_{nl}^{m*}(\mathbf{r}_i)J(|\mathbf{r}_i-\mathbf{r}_j|)(\mathbf{r}_i-\mathbf{r}_j)\psi_{nl}^{m}(\mathbf{r}_i)\,dV_i$$

will have the form $F(r_j)\mathbf{r}_j$ where

$$F(r_j)=-2\Sigma_{m}\int \psi_{nl}^{m*}(\mathbf{r}_i)J(|\mathbf{r}_i-\mathbf{r}_j|)\left[\frac{\mathbf{r}_i\cdot\mathbf{r}_j}{r_j^2}-1\right]\psi_{nl}^{m}(\mathbf{r}_i)dV_i.$$

Thus, the effective spin–orbit potential is

$$V=F(r)\mathbf{r}\wedge\mathbf{p}\,.\,\boldsymbol{\sigma}$$
$$=F(r)\mathbf{L}\,.\,\boldsymbol{\sigma}$$

where $\mathbf{L}$ and $\boldsymbol{\sigma}$ are the usual orbital angular momentum and Pauli spin operators respectively, and the suffix j has been omitted.

§ 3. Evaluation of $F(r)$

In order to obtain an explicit expression for $F(r)$ we use a method of evaluation valid for short range forces used by Brink (1954).

Denoting

$$-2\Sigma_{m}\psi_{nl}^{m*}(\mathbf{r}')\left[\frac{\mathbf{r}'\cdot\mathbf{r}}{r^2}-1\right]\psi_{nl}^{m}(\mathbf{r}') \quad \text{by} \quad -\rho(\mathbf{r},\mathbf{r}')$$

we have

$$F(r)=-\int J(|\mathbf{r}-\mathbf{r}'|)\rho(\mathbf{r},\mathbf{r}')\,dV'.$$

Writing $\rho(\mathbf{r},\mathbf{r}')=\rho'(\mathbf{s},\mathbf{r})$ where $\mathbf{s}=\mathbf{r}'-\mathbf{r}$ and expanding $\rho'(\mathbf{s},\mathbf{r})$ about $\mathbf{s}=0$ gives

$$F(r)=-4\pi\int J(s)s^2\,ds\,[\rho'(0,\mathbf{r})]-\frac{4\pi}{3!}\int J(s)s^4\,ds\,[\nabla^2\rho'(\mathbf{s},\mathbf{r})]_{\mathbf{s}=0}+\ldots$$

The first term in the expansion of $F(r)$ vanishes since, for $\mathbf{s}=0$, $\mathbf{r}=\mathbf{r}'$ and $\frac{\mathbf{r}'\cdot\mathbf{r}}{r^2}-1=0$. The evaluation of the second term presents no difficulty and one obtains for $F(r)$ to this approximation

$$F(r)=-\frac{2(2l+1)}{3}\left(\int J(s)s^4\,ds\right)\frac{1}{r}\frac{d}{dr}[f_{nl}^2(r)]$$

where $f_{nl}(r)$ is the radial function for a single particle in the state (nl). But if the mean density distribution of particles at a radius r in the closed shell is $\rho_{nl}(r)$, then

$$\rho_{nl}(r)=2f_{nl}^2(r)(2l+1)/4\pi$$

so that

$$F(r)=-\frac{4\pi}{3}\left(\int J(s)s^4\,ds\right)\frac{1}{r}\frac{d\rho_{nl}}{dr},$$

If we now sum over all particles in the nucleus, it follows that we can write $F(r)$ in the form

$$F(r)=K/r\;d\rho(r)/dr$$

where

$$K=-4\pi/3\int J(s)s^4\,ds$$

is a positive quantity (assuming $J(s)$ to be of the usual form for nuclear forces) and $\rho(r)$ is the nuclear density distribution.

Thus it turns out that the radial dependence of the resulting spin–orbit potential is of the same form as the Thomas type except that the nuclear density distribution replaces the potential $V(r)$ in which the nucleon is moving. It is to be expected, of course, that $\rho(r)$ and $V(r)$ will have a similar sort of behaviour. Although one cannot be sure of the effective nuclear potential one has a fairly good idea as to the nuclear density distribution (e.g. from electron scattering experiments) so that the above form of $F(r)$ gives a reasonable guide to the radial dependence of the spin–orbit potential which might be used for calculations in scattering problems. It is interesting to note that the above result is independent of the form of the radial functions used.

§ 4. Calculation of the Nuclear Spin–Orbit Splitting

From the form of $F(r)$ it is clear that shell model spin–orbit splitting of the right sign is obtained in regions of radially decreasing density, i.e. at the surface of the nucleus. Calculation of the splitting to be expected, however, must necessarily be fairly approximate since some assumption has to be made about the radial function of the odd particle. For the purpose of the calculation the following crude assumptions are made :

(i) The nuclear density distribution $\rho(r, t)$ is taken to have the form

$$\rho(r,t)=\rho_0, \qquad 0\leqslant r\leqslant R(1-t)$$

$$\rho(r,t)=\rho_0[R-r]/Rt, \qquad R(1-t)\leqslant r\leqslant R$$

where $t(0\leqslant t\leqslant 1)$ is a parameter measuring the size of the transition region in which the nuclear density decreases from ρ_0 to 0.

(ii) The radial function is taken to be that of a particle moving in an infinite well of radius R.

These two assumptions are consistent in that both the density and the radial function vanish for values of r greater than R. The radius R_0 of the nucleus is conventionally defined as the radius of the uniform density distribution which has the same mean square radius as that of the distribution under consideration. This implies

$$R^2=\beta^2(t)R_0{}^2$$

where

$$\beta^2(t)=3(4-6t+4t^2-t^3)/2(6-15t+20t^2-15t^3+6t^4-t^5)$$

and for a nucleus of atomic number A we take $R_0=r_0A^{1/3}$. Furthermore, the normalization of $\rho(r)$ must be such that

$$4\pi\int_0^R \rho(r)r^2\,dr=A.$$

This gives at once

$$\rho_0=3A/\pi R^3(4-6t+4t^2-t^3).$$

The spin–orbit splitting $\Delta E = E_{j=l-1/2} - E_{j=l+1/2}$ for an odd nucleon in the state (n, l) is then given by

$$\Delta E = -(2l+1)\int_0^R |f_{nl}^2(r)|^2 F(r) r^2\, dr$$

where $f_{nl}(r)$ is the appropriate radial function for a particle in an infinite well of radius R.

But

$$F(r) = K/r\, d\rho/dr = 0 \qquad \text{for} \qquad 0 \leqslant r \leqslant R(1-t)$$
$$= K\rho_0/Rtr \qquad \text{for} \qquad R(1-t) \leqslant r \leqslant R$$

so that

$$\Delta E = (2l+1)K\rho_0/Rt \int_{R(1-t)}^R |f_{nl}(r)|^2 r\, dr$$

which, for an infinite well can be written

$$\Delta E = \gamma_{nl}(t) U A^{-2/3}$$

where

$$\gamma_{nl}(t) = [8(2l+1)I_{nl}(t)]/[\alpha_{nl}|J_{l+3/2}(\alpha_{nl})|^2 t(4-6t+4t^2-t^3)\beta^5(t)]\,;$$

$$U = -\frac{1}{r_0^5}\int J(s) s^4\, ds$$

and

$$I_{nl}(t) = \int_{\alpha_{nl}(1-t)}^{\alpha_{nl}} J_{l+1/2}^2(x)\, dx.$$

Here α_{nl} is the nth zero of the Bessel function $J_{l+1/2}(x)$.

The values of $\gamma_{nl}(t)$ for $t=0{\cdot}1$ to $0{\cdot}7$ for the different shell model states are given in table 1.

Table 1. Values of $\gamma_{nl}(t)$

State	$t=0{\cdot}1$	$t=0{\cdot}2$	$t=0{\cdot}3$	$t=0{\cdot}4$	$t=0{\cdot}5$	$t=0{\cdot}6$	$t=0{\cdot}7$
1p	0·450	1·489	2·857	4·383	5·758	6·896	7·602
1d	1·251	3·630	6·716	9·341	10·961	11·790	11·924
1f	2·056	6·917	11·989	15·171	16·219	16·217	15·787
2p	1·040	3·037	3·989	3·504	3·103	4·395	6·963
1g	4·564	11·527	18·608	21·491	21·381	20·396	19·537
2d	2·358	5·931	6·600	5·239	5·901	9·495	13·053
1h	5·737	17·024	25·278	27·279	25·696	23·910	22·731
2f	4·228	9·409	8·880	7·269	10·377	15·675	18·515
1i	8·400	23·629	32·872	33·296	30·105	27·644	26·207
3p	1·801	3·657	2·914	2·971	4·228	4·232	5·141
2g	6·659	12·941	10·544	10·187	16·136	21·640	23·121
3d	3·632	6·193	4·533	5·841	6·937	6·788	10·933

Since U is positive and $\gamma_{nl}(t)$ is also positive for all values of t it is clear that splitting of the sign required for the shell model is obtained. We now look for values of U and t which give the correct spin–orbit splitting in the region of the double closed shell nucleus ^{208}Pb.

Stripping experiments (Harvey 1953) indicate that the $2g_{9/2}-2g_{7/2}$ and $3d_{5/2}-3d_{3/2}$ splittings for the odd neutron in ^{209}Pb are 2·03 MeV and 0·98 MeV respectively. Further it is possible to make an estimate of the neutron $1i_{13/2}-1i_{11/2}$ splitting (see figure).

Hitherto this splitting has been estimated by reference to the semi-empirical formula (e.g. Harvey 1951). A more accurate estimate is given in the following. At ^{208}Pb the break in neutron binding energy is 3·41 Mev (Wapstra 1953). Apart from the pairing energy $P(3p_{1/2})$ of the last neutrons in ^{208}Pb this can be regarded as the separation in

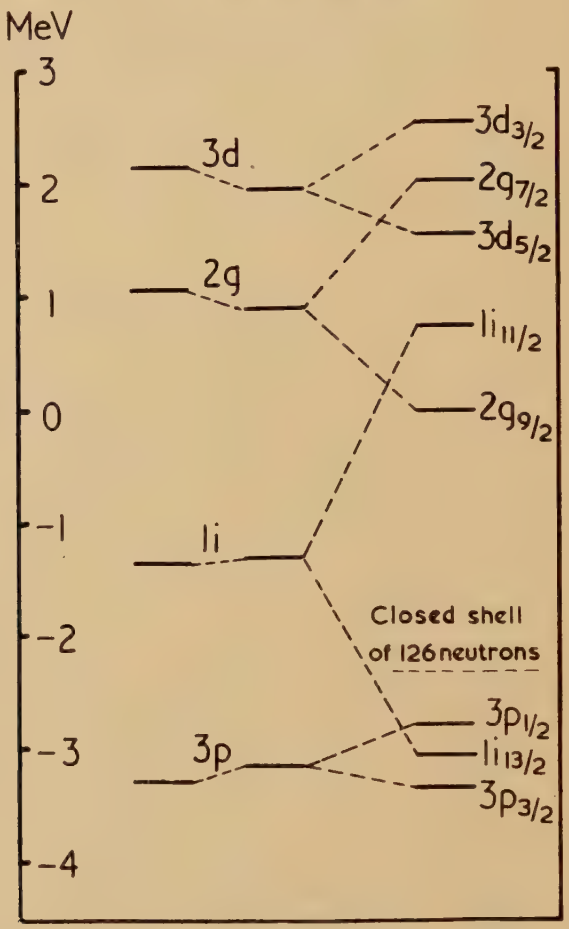

Single particle levels near the closed shell of 126 neutrons. On the left are shown the levels obtained with the potential well referred to in the text. (The $2g_{9/2}$ level is arbitrarily taken as the zero of energy.)

energy of the single particle levels $3p_{1/2}$ and $2g_{9/2}$. Now in ^{209}Pb the $1i_{11/2}$ level has excitation energy 0·75 Mev (Harvey 1953) and in ^{207}Pb the $1i_{13/2}$ level (obtained by excitation of a neutron from $1i_{13/2}$ to $3p_{1/2}$) has energy 1·63 Mev (Stelson and Campbell 1955). The $1i_{13/2}-3p_{1/2}$ single particle level separation is therefore $1{\cdot}63-P(1i_{13/2})+P(3p_{1/2})$. Thus the $1i_{13/2}-1i_{11/2}$ separation is

$$\{0{\cdot}75+[3{\cdot}41-P(3p_{1/2})]+[1{\cdot}63-P(1i_{13/2})+P(3p_{1/2})]\}\ \text{Mev}.$$

But the difference in binding energy between ^{195}Pt and ^{197}Au gives a measure of $P(1i_{13/}$). According to van Patter and Whaling (1954) this difference is about 2 MEV. Thus the $1i_{13/2}-1i_{11/2}$ splitting can be taken to be of the order of 3·8 MEV. Further support for this figure comes from ^{207}Pb where the $1i_{11/2}$ level has excitation energy 3·60 MEV (Stelson and Campbell 1955). This level results from the excitation of a $3p_{1/2}$ particle to the $1i_{11/2}$ state. Using the figure quoted above for the energy of the $1i_{13/2}$ state gives for the $1i_{13/2}-1i_{11/2}$ splitting

$$3{\cdot}60+1{\cdot}63-P(1i_{13/2})+P(3p_{1/2}).$$

Now $P(3p_{1/2})$ can be estimated from the difference in neutron binding energies in ^{207}Pb and ^{208}Pb which, according to Wapstra (1953) is 0·65 MEV. Taking $P(1i_{13/2})=2$ MEV then gives the $1i_{13/2}-1i_{11/2}$ splitting as 3·88 MEV.

Good agreement between theory and experiment is only obtained if we take $U=5{\cdot}5$ MEV and $t=0{\cdot}2$ (see table 2).

Table 2. Experimental and Theoretical Values of the Spin–Orbit Splitting Near ^{208}Pb

State	Experiment	Theory
2g	2·03 MEV	2·03 MEV
3d	0·98 MEV	0·97 MEV
1i	3·8 MEV	3·71 MEV

The postulated single particle levels in the region of ^{208}Pb are shown in the figure. Also shown are the single particle levels from which the spin–orbit doublets result. These levels have been taken at a distance $l/(2l+1)\times$(splitting) from the lower component of the spin–orbit doublet, this being the correct position when the spin–orbit force has the form $F(r)\,\mathbf{L}\,.\,\boldsymbol{\sigma}$. These levels are also compared (as far as spacing is concerned) with those obtained in a spherical well having the form $V(r)=-V_0$ for $r<R$, $V(r)=-V_0\exp[-\alpha\mu(r-R)]$ for $r>R$ with $V_0=34{\cdot}1$ MEV and $\alpha=1{\cdot}83$ with $\mu=1{\cdot}4\times10^{-13}$ cm. Such a well has been deduced by Malenka (1952) from a non-linear meson theory and should be fairly realistic in that it lies in form between a square well and an isotropic oscillator well. The agreement is very good and indicates that a well of this form is reasonable for heavy nuclei. It is also interesting to note that such a well gives a nuclear density distribution very similar to the one assumed here and with $0{\cdot}3>t>0{\cdot}2$.

§ 5. Discussion

(i) *The Value of U*

To see if the value obtained for U is consistent with other experimental data on a two-body spin–orbit force we consider the particular case of $J(s)=SV_0\exp(-ps^2)$. This gives $U=(\pi/p^5)^{1/2}3SV_0/2r_0^5$. Recently Hochberg *et al.* (1955) have fitted the data on the scattering of neutrons by

alpha-particles by using a two-body spin–orbit force of the type considered here. They take $V_0=22{\cdot}5$ MeV and $p=0{\cdot}2657\times10^{26}$ cm^{-2} so that $U=64S$ MeV for $r_0=1{\cdot}45\times10^{-13}$ cm. Thus, in order that this value shall agree with experiment we must take $S=0{\cdot}09$. The above authors find that $S=0{\cdot}1$ fits the scattering data on ^{4}He. The close agreement between these two values of S is satisfactory considering the approximations made in the calculations.

(ii) *The Nuclear Density Distribution*

It is interesting that the spin–orbit coupling data for heavy nuclei can only be fitted if t, which measures the transition region in the nuclear density distribution, is taken as 0·2. That there should be such a transition region is indicated for example by the analysis of high energy electron scattering by nuclei (e.g. Brown and Elton 1954). These experiments suggest a rather larger value for t ($\sim1/3$). It is highly probable, however, that if a more realistic smoothed out density distribution had been used in the present case a larger value for t would have been obtained since the smoothing out at the two ends of the transition region will have small $d\rho/dr$ and will therefore only give a small contribution to the spin–orbit coupling. In view of the lack of knowledge as to the form of the radial functions it was not thought worthwhile to use such a smoothed out distribution.

In the present calculations r_0 has been given the conventional value $1{\cdot}45\times10^{-13}$ cm which is larger than the value ($1{\cdot}2\times10^{-13}$ cm) obtained from electron scattering experiments. This latter value, however, refers only to the proton distribution and it is to be expected (e.g. Swiatecki 1955) that the neutron distribution extends beyond the proton distribution by 10–20% and since ρ refers to the total density it is the larger radius that is relevant. In this connection it is instructive to compare neutron and proton spin–orbit splitting. Unfortunately, in the region of ^{208}Pb such a comparison can only be made for 'holes'. Thus in ^{207}Pb the $3p_{3/2}-3p_{1/2}$ neutron hole splitting is 0·87 MeV and in ^{203}Tl the $2d_{5/2}-2d_{3/2}$ proton hole splitting is 0·4 MeV. The values predicted on the present model for single particles are 0·57 MeV and 0·94 MeV respectively. As pointed out by Elliott and Lane (1954) the hole splitting is expected to be larger than the particle splitting so that in the case of the neutron hole experiment and theory are consistent. This is not so for the proton hole. If it is remembered, however, that the proton radius is smaller than the neutron radius, it follows that the proton will spend less of its time in a region of decreasing core density. Thus if r_0 (proton)$=0{\cdot}9r_0$ (neutron) then for the proton we should take $t\sim0{\cdot}1$ rather than 0·2. In this case the predicted splitting is 0·38 MeV. Since the hole splitting is expected to be about twice the particle splitting this value is probably still too large and suggests that r_0 (proton)$<0{\cdot}9r_0$ (neutron), i.e. r_0 (proton)$<1{\cdot}3\times10^{-13}$ cm in agreement with the electron scattering experiments.

To obtain a more satisfactory comparison of neutron and proton radii it would be useful to compare the splittings of an odd neutron and an odd proton outside the doubly closed ^{208}Pb shell. This would require information about the levels of ^{209}Bi which is not at present available. On the present model for $t=0{\cdot}1$ the predicted $2f_{7/2}-2f_{5/2}$ proton splitting in ^{209}Bi is 0·66 MEV.

(iii) *Splitting of the* 1h *and* 1g *States*

It is interesting to find the order of magnitude of the $1h_{11/2}-1h_{9/2}$ and $1g_{9/2}-1g_{7/2}$ splittings predicted by this model for the neutron magic numbers $N=82$ and $N=50$. For $t=0{\cdot}2$ the values obtained are 3·5 MEV and 3·0 MEV respectively. Work by Harvey (1951) indicates that at the above magic numbers the neutron binding energy drops by about 2 MEV. However, the spin–orbit splitting should be larger than this for similar reasons to those advanced in the case of the $1i_{13/2}-1i_{11/2}$ splitting (e.g. the 51st and 83rd neutrons do not go into the $1g_{7/2}$ and $1h_{9/2}$ states but into $2d_{5/2}$ and $2f_{7/2}$, the $1g_{7/2}$ and $1h_{9/2}$ states lying higher than these). It therefore seems as if the splittings are of the right order of magnitude.

ACKNOWLEDGMENT

The author is indebted to Mr. D. M. Brink for an interesting conversation on the subject matter of this paper.

REFERENCES

BLANCHARD, C. H., and AVERY, R., 1951, *Phys. Rev.*, **81,** 35.
BRINK, D. M., 1954, *Proc. Phys. Soc.* A, **67,** 757.
BROWN, G. E., and ELTON, L. R. B., 1955, *Phil. Mag.*, **46,** 164.
ELLIOTT, J. P., and LANE, A. M., 1954, *Phys. Rev.*, **96,** 1160.
HARVEY, J. A., 1951, *Phys. Rev.*, **81,** 353 ; 1953, *Canad. J. Phys.*, **31,** 278.
HUGHES, J., and LE COUTEUR, K. J., 1950, *Proc. Phys. Soc.* A, **63,** 1219.
HOCHBERG, S., MASSEY, H. S. W., ROBERTSON, H., and UNDERHILL, L. H., 1955, *Proc. Phys. Soc.* A, **68,** 746.
HAXEL, O., JENSEN, J. H. D., and SUESS, H. E., 1949, *Phys. Rev.*, **75,** 1766.
INGLIS, D. R., 1953, *Rev. Mod. Phys.*, **25,** 390.
KEILSON, J., 1951, *Phys. Rev.*, **82,** 759.
MALENKA, B. J., 1952, *Phys. Rev.*, **86,** 68.
MAYER, M. G., 1949, *Phys. Rev.*, **75,** 1969.
STELSON, P. H., and CAMPBELL, E. C., 1955, *Phys. Rev.*, **97,** 1222.
SWIATECKI, W. J., 1955, *Phys. Rev.*, **98,** 204.
THOMAS, L. H., 1926, *Phil. Mag.*, **3,** 1.
VAN PATTER, D. M., and WHALING, W., 1954, *Rev. Mod. Phys.*, **26,** 402.
WAPSTRA, A. H., 1953, *Thesis*, Amsterdam.

CXIII. *The Low Lying Levels of* ^{25}Al

By L. L. Green, J. J. Singh and J. C. Willmott
Nuclear Physics Research Laboratory, University of Liverpool *

[Received May 11, 1955]

Abstract

The γ-ray spectrum at the 825 kev resonance in ^{24}Mg has been investigated and the angular distributions of the three initial γ-rays measured. The spins and parities of the ground state and first excited states are confirmed as $5/2^+$ and $1/2^+$ respectively and the second excited state is shown to be $3/2^+$. Evidence is presented which lends a measure of support to the view that a level exists in ^{25}Al at 1·92 mev.

§ 1. Introduction

The mirror pair ^{25}Al–^{25}Mg are known to have the same parity and spins for their ground states ($5/2^+$) and first excited states ($1/2^+$). The second excited states are both either $3/2^+$ or $5/2^+$ (Goldberg 1953), but which of these values is correct has not been determined so far in either case. The levels above 3·09 mev in ^{25}Al have been studied by the elastic scattering of protons from ^{24}Mg and their properties are well established (Koester 1952). It should be possible to obtain further information about the levels of ^{25}Al lying below the 3·09 mev level by studying the radiation from one of these higher levels.

§ 2. Experimental Method

Two resonances occur in the working range of the Liverpool University H.T. Set, at 418 kev and 825 kev. The resonance at 418 kev has a γ-ray yield which is below the useful working limit, so all the work was carried out on the 825 kev resonance level, the spin and parity of which are known to be $3/2^-$ from the elastic scattering experiments.

A 60 μ-amp resolved beam of protons bombarded a target of electromagnetically separated ^{24}Mg which had been evaporated on to a 0·02 in. copper backing. An insulated target holder enabled the beam current to be measured and integrated. The γ-rays were detected in a 2 in. diameter by 2 in. long thallium activated sodium iodide crystal mounted on a Dumont 6292 photomultiplier. The resultant pulses, after amplification and delay-line shaping, were analysed by a Hutchinson–Scarratt type pulse analyser. Another scintillation counter at 120° to the beam was used to monitor the yield and the pulses from this crystal were fed to a single channel pulse analyser set to accept all pulses corresponding to energy losses in the crystal between 1·5 mev and 3·9 mev.

*Communicated by H. W. B. Skinner.

§ 3. The γ-Ray Spectrum

In order to be certain that all the γ-rays present were correctly identified and to enable a comparison of the relative intensities to be made, the pulse height distribution produced by a single γ-ray was determined for γ-rays in the range 669 kev to 8·06 Mev, with the aid of various radioactive sources and the proton–γ reactions occurring in ^{11}B, ^{12}C, ^{13}C and ^{19}F. By interpolating between these pulse height distributions, the distributions produced by a γ-ray of any energy could be determined. The interpolation was aided by constructing curves of the quantity A/PH versus energy where A is the total area under the curve, P the pulse height of the peak and H the number of counts per channel at the

Fig. 1

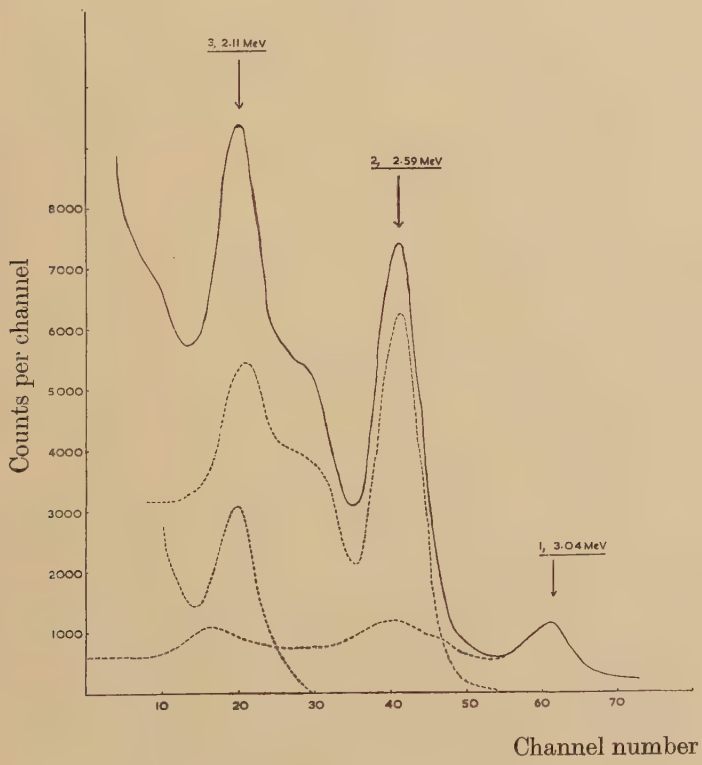

peak, in the manner described by Flack *et al.* (1954). This method was also used for estimating the relative intensities of the γ-rays and has given consistently good results in this and other work in progress.

Knowing the shapes of the spectral distribution produced, the experimentally obtained spectrum was then analysed by starting at the high energy end and successively subtracting the contributions due to the various γ-rays in descending order of energy. An example of this is shown in fig. 1.

The spectrum obtained is shown in figs. 1 and 2. Analysis of this spectrum shows that γ-rays are present as given in table 1, together with their relative intensities corrected for their angular distributions.

Fig. 2

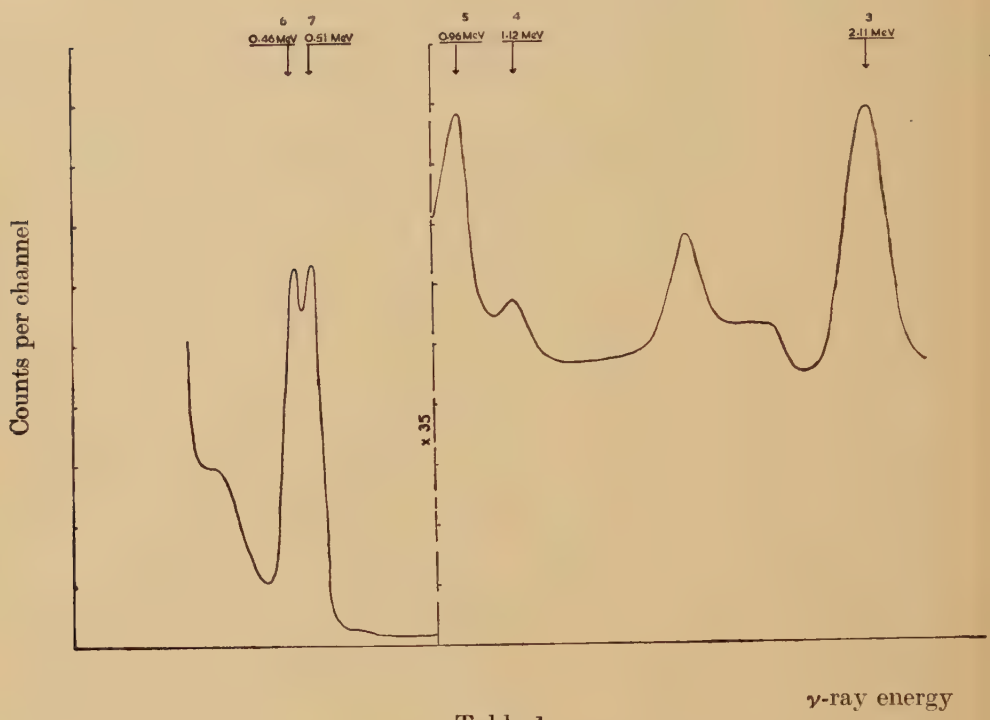

Table 1

	γ-ray Energy Mev	Intensity (Arbitrary Units)
1.	$3{\cdot}04 \pm 0{\cdot}03$	27 ± 2
2.	$2{\cdot}59 \pm 0{\cdot}03$	159 ± 10
3.	$2{\cdot}11 \pm 0{\cdot}03$	19 ± 2
4.	$1{\cdot}12 \pm 0{\cdot}02$	$2 \pm 0{\cdot}5$
5.	$0{\cdot}96 \pm 0{\cdot}02$	11 ± 1
6.	$0{\cdot}460 \pm 0{\cdot}01$	158 ± 10
7.	$0{\cdot}510 \pm 0{\cdot}01$	200 ± 15

The suggested cascade system is shown in fig. 3, where the transitions are numbered according to their energy as in table 1. The 0·51 Mev γ-ray in table 1 is due to annihilation radiation from the positron decay of the ground state. The relative intensities of the 2·11 Mev γ-ray and the 0·96 Mev γ-ray, which are in cascade, show that the 0·96 Mev level decays partially to the ground state and partially to the first excited state at 0·46 Mev. The weak 0·50 Mev γ-ray produced by this latter transition is, of course, lost underneath the combination of the intense 0·51 Mev and 0·46 Mev γ-rays.

The weak 1·12 MEV γ-ray is thought to be due to a transition between the resonance level at 3·04 MEV and a level at 1·92 MEV. Goldberg found a very weak neutron group from the ^{24}Mg(d, n)^{25}Al reaction corresponding to a level at 1·94 MEV. He also found a neutron group corresponding to a level at 1·81 MEV, but a careful search of the spectrum showed no indications of a γ-ray transition to this state. De-excitation of the

Fig. 3

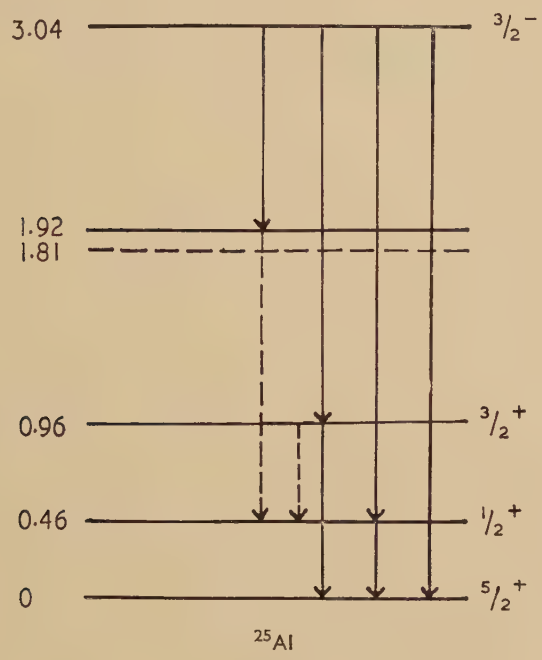

1·92 MEV level could occur to the ground state or either of the first two excited states. All the spectra taken at 6 different angles showed an inflection at 1·45 MEV indicating that the decay probably proceeds at least partially to the 0·46 MEV state. The possibility that the 1·12 MEV γ-ray might be due to a contaminant is unlikely as the most likely contamination would be from ^{25}Mg and ^{26}Mg. The former has a resonance at 820 kev but does not give a γ-ray of this energy and ^{26}Mg has no resonance sufficiently close to this energy region.

§ 4. Angular Distributions

For the angular distribution measurements the pulse amplitude analyser was set to include pulse heights corresponding to energy losses in the crystal from 1·7 MEV to 3·6 MEV. Measurements were made on either side of zero to check the symmetry of the system. Spectra were taken at 6 angles between 0° and 90° in a random order to avoid errors due to slow drifts and deterioration of the target. The spectra were analysed

as described above, the total area under the total capture peak of each of the three initial γ-rays was measured, and the results were then corrected for the varying absorption in the target backing at different angles.

The results obtained are shown in figs. 4, 5 and 6, and in table 2 the best fits to the points are compared with the theoretical formula, modified by the finite acceptance angle ($\pm 10°$) of the scintillator, for electric dipole transitions.

Fig. 4

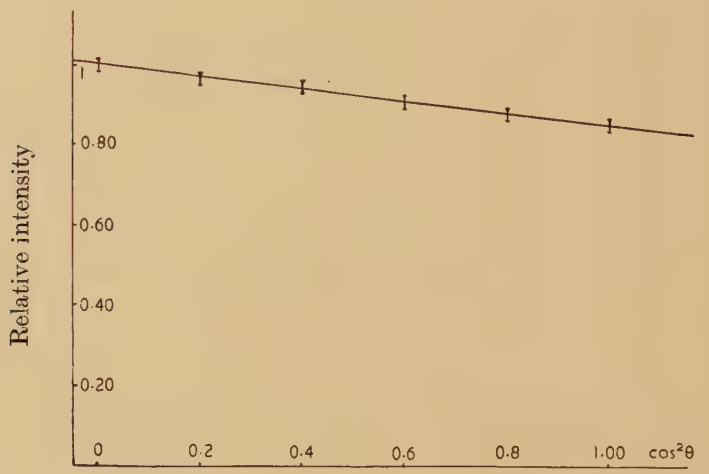

3·04 MeV γ-ray

Fig. 5

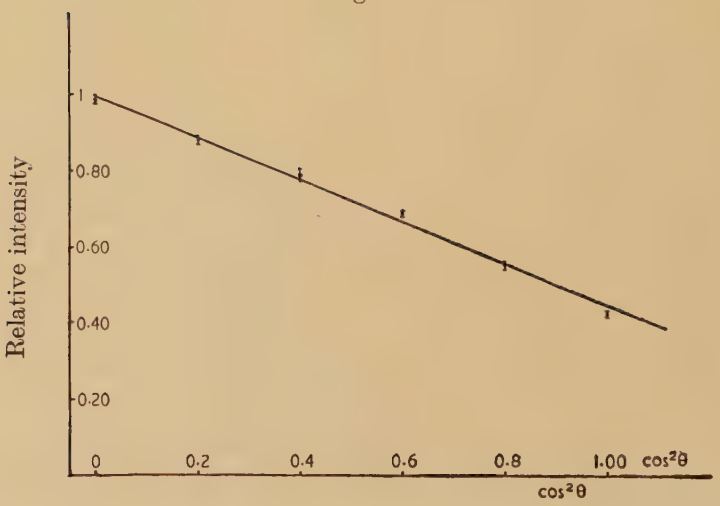

2·59 MeV γ-ray

The results confirm the assignments of $5/2^+$ to the ground state and $1/2^+$ to the 0·46 MeV state and show that the 0·96 MeV state is $3/2^+$.

Table 2

γ-ray Energy	Transition	Theoretical	Experimental
3·04 MeV	$3/2^- \rightarrow 5/2^+$	$1-0{\cdot}14\cos^2\theta$	$1-(0{\cdot}16\pm0{\cdot}025)\cos^2\theta$
2·59 MeV	$3/2^- \rightarrow 1/2^+$	$1-0{\cdot}58\cos^2\theta$	$1-(0{\cdot}55\pm0{\cdot}03)\cos^2\theta$
2·11 MeV	$3/2^- \rightarrow 5/2^+$	$1-0{\cdot}14\cos^2\theta$	$1+(0{\cdot}72\pm0{\cdot}07)\cos^2\theta$
	$3/2^- \rightarrow 3/2^+$	$1+0{\cdot}73\cos^2\theta$	

§ 5. Radiation Width

By knowing the solid angle subtended by the crystal at the source, its efficiency and the integrated beam current, it is possible to calculate the number of γ-ray quanta produced per proton and hence the radiation

Fig. 6

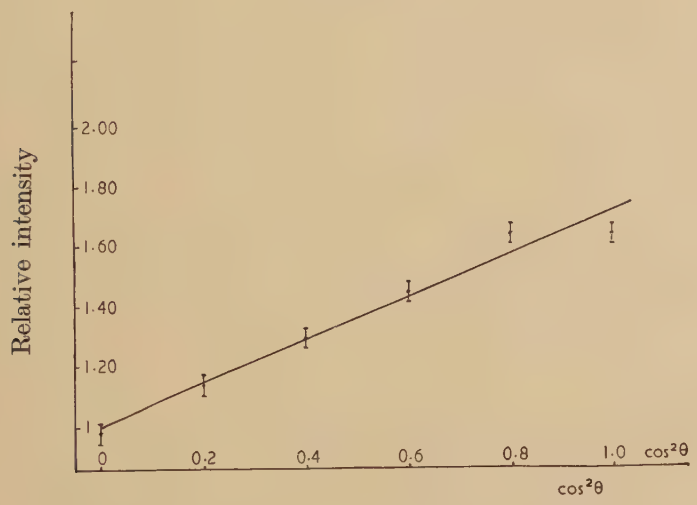

2·11 MeV γ-ray

width Γ_γ of the level at 3·04 MeV, assuming that the energy lost by the protons in traversing the target is several times the total width of the level, which is given by Mooring *et al.* (1954) as 1·5 kev ; our targets were about 5 kev thick. In this way we obtain a value of

$$\Gamma_\gamma = 0{\cdot}08 \pm^{0{\cdot}08}_{0{\cdot}02} \text{ ev.}$$

§ 5. Discussion

The three low lying levels of ^{25}Al are in the order $5/2^+$, $1/2^+$, $3/2^+$ which is the order to be expected from excitation of the odd proton on the shell model. The resonance level at 3·04 MeV is of odd parity and hence, since odd parity levels due to excitation of the $d_{5/2}$ particles would be expected to occur at much higher energy, is probably due to excitation of the ^{16}O core. This view is confirmed by comparison of the observed radiation width with that calculated for single particle transitions by Moskowski (1953) which would lead to a value of approximately 50 ev in this case.

Acknowledgments

We should like to thank Dr. B. Collinge and Mr. K. Aitcheson who built and maintained the pulse analyser. We are indebted to Professor H. W. B. Skinner for much helpful discussion of this paper and one of us (J. J. S.) is indebted to the Punjab Government for leave of absence. Our thanks are due to A. E. R. E. for the ^{24}Mg target.

References

Flack, F. C., Rutherglen, J. G., and Grant, P. J., 1954, *Proc. Phys. Soc.* A, **67,** 973.

Goldberg, E., 1953, *Phys. Rev.*, **89,** 760.

Koester, L. J., 1952, *Phys. Rev.*, **85,** 643.

Mooring, F. P., Koester, L. J., Goldberg, E., Saxon, D., and Kaufmann, S. G., 1951, *Phys. Rev.*, **84,** 703.

Moskowski, S., 1953, *Phys. Rev.*, **89,** 474.

CXIV. *Optical Constants of Metals in the Infra-Red—Conductivity of Silver, Copper and Nickel*

By J. R. Beattie and G. K. T. Conn
Department of Physics, The University, Sheffield*

Summary

The experimental methods used to measure the optical constants of metals at infra-red frequencies have already been described. The conductivity of evaporated aluminium, silver, copper and nickel is reported. Since the penetration depth is small the behaviour is closely related to the nature of the surface of the metal; attention is therefore paid to the preparation of various representative surfaces including hand polished, electrolytically polished and those obtained by evaporating *in vacuo*.

By giving care to the manner of presenting experimental results, the various factors which contribute to the absorption may be discriminated. Figures are given of relaxation times, conductivity and the effective number of free electrons per atom. Elementary interpretations are given.

§ 1. Introduction

The depth of penetration of electro-magnetic waves into metals of high conductivity is of the order of a micron at 10^9 cycles per second and diminishes as the frequency increases. The behaviour may be described using the surface resistance R, defined as the ratio of the electric field gradient to the current per unit square at the surface. It can be shown that

$$R=1/(\sigma\delta)=\sqrt{(2\pi\omega/\sigma c^2)}, \quad . \quad . \quad . \quad . \quad . \quad . \quad (1)$$

where δ is the skin depth, σ is the conductivity and ω is the angular frequency. At the infra-red frequencies, greater than 10^{12} cycles per second, eqn. (1) is inadequate. Since the mean free path of the conducting electrons is limited, the surface impedance Z is complex with real and imaginary components, R the surface resistance and X the surface reactance; $cZ/4\pi$ is the ratio of the electric to the magnetic field strengths at the surface of the metal (Stratton 1941, Reuter and Sondheimer 1948). R may be determined from measurements of the ratio, R_0^2, of the reflected to the incident radiant intensities. To a close approximation

$$1-R_0^2=cR/\pi. \quad . \quad . \quad . \quad . \quad . \quad . \quad . \quad . \quad (2)$$

The early work of Rubens and Hagen (1904) who measured R_0^2 for many metals was interpreted as vindicating eqn. (1) at infra-red frequencies.

* Communicated by Professor W. Sucksmith, F.R.S.

Doubt has been cast on this view which is in conflict with modern theories (Mott and Zener 1934, Dingle 1953). Though R and X are related (Robinson 1952) both must be measured if the investigation is limited to a particular range of frequencies. Indeed the work here reported shows that X is much larger than R so that measurements of R_0^2 alone are of limited value. For example fig. 1 (*a*) shows the surface resistance R and the surface reactance X of a film of aluminium plotted against frequency. The 'theoretical points' are obtained using the dispersion formulae discussed below.

The techniques necessary to examine the characteristics of metals in the infra-red are essentially optical and is natural to frame the experiments and describe the results in terms of a complex refractive index $n-ik$. At a frequency ν the dielectric constant $\epsilon(\nu)$ and the conductivity $\sigma(\nu)$ are then given by (Mott and Jones 1936)

$$n^2-k^2=\epsilon(\nu) \qquad \text{and} \qquad nk\nu=\sigma(\nu). \quad . \quad . \quad . \quad . \quad . \quad (3)$$

Save under certain theoretical conditions discussed by Reuter and Sondheimer (1948) the refractive index is equivalent to the reciprocal of the surface impedance and

$$Z=R+iX=4\pi/\{c(n-ik)\}. \quad . \quad . \quad . \quad . \quad . \quad . \quad (4)$$

Measurements of the complex refractive index of metals at wavelengths greater than 5 μ have not hitherto been reported. In two previous papers (Beattie and Conn 1955 a and Beattie 1955), the difficulties which have restricted such investigations were examined, new experimental methods were described and preliminary results were presented to illustrate the technique adopted. In the present paper observations are reported of silver, copper and nickel at various temperatures and over the range of 2 μ to 12 μ. Since the behaviour is closely bound up with the nature of the surface of the metal, it has been necessary to devote some care and attention to the preparation of various representative surfaces including hand-polished, electrolytically polished and those formed by evaporation *in vacuo*.

If means are adopted of distinguishing the various factors, measurements of optical constants contribute to studies of relaxation effects, phenomena associated with restrictions imposed on the mean free path of conduction electrons, surface oxidation and perhaps internal conversion. Attention is therefore first given to the manner in which numerical values may best be presented to discriminate these phenomena; in particular to ensure that the relaxation and strong absorption of the free electrons do not obscure other information. Elementary interpretations are presented.

§ 2. Framework of Interpretation

In the simple Drude–Lorentz theory of conduction a relaxation time is defined by writing the conductivity in the form

$$\sigma_0=Ne^2\tau/m, \quad . \quad . \quad . \quad . \quad . \quad . \quad . \quad . \quad (5)$$

where N is the number of electrons per unit volume, each of charge e and mass m. The classical dispersion equations are then (Mott and Jones 1936)

$$n^2-k^2-\epsilon_\infty=-\frac{4\pi Ne^2\tau^2}{m}\cdot\frac{1}{(1+\omega^2\tau^2)}, \quad \ldots\ldots\ldots \quad (6)$$

$$2nk=\frac{4\pi Ne^2\tau}{m\omega}\cdot\frac{1}{(1+\omega^2\tau^2)}. \quad \ldots\ldots\ldots \quad (7)$$

ϵ_∞ is the ' static dielectric constant of the atomic cores '. Substitution of (5) in (6) and (7) shows that σ and τ suffice to define the dispersion analytically.

This dispersion has been treated in terms of quantum mechanics by a semi-classical argument (Krönig 1931) and recently by Wolfe (1954 and 1955). The model used by Wolfe to calculate the absorption of a metal is essentially that of photoelectric transition of conduction electrons to higher levels in the same band. Such transitions are forbidden in an ideal lattice and Wolfe examined the case in which lattice irregularities arise from a random distribution of impurity atoms ; he showed that the results of his calculations of the absorption agreed with eqns. (6) and (7) over a wide range. The choice of a random distribution of impurity atoms to give a model of finite conductivity was dictated by analytical convenience and there seems little doubt that formulae of the form (6) and (7) follow in more general cases in which for instance the lattice is disturbed by thermal agitation. We have therefore used these equations as a basis for interpretation of experimental results.

§ 3. Manner of Presentation

The major contribution to the absorption of high conductivity metals in the infra-red is made by the conduction electrons and in seeking means of discriminating the various factors, the primary question is to distinguish this contribution. It is easy to verify that curves of n and k against λ and ν or of n^2-k^2 and $2nk$ against λ or ν are quite insensitive for this purpose. Neglecting ϵ_∞ which is negligible being of the order of unity (Mott and Jones 1936), it follows from (5), (6) and (7) that

$$\epsilon(\nu)=n^2-k^2=-4\pi\sigma_0\tau/(1+\omega^2\tau^2) \quad \text{and} \quad \sigma(\nu)=nk\nu=\sigma_0/(1+\omega^2\tau^2). \quad (8)$$

If an Argand diagram is plotted with $nk\nu$ as ordinate and n^2-k^2 as abscissae a straight line passing through the origin is obtained of slope $-1/(4\pi\tau)$. From such a straight line the relaxation time is easily obtained and the value of σ_0 follows from the numerical values of n^2-k^2 or $nk\nu$.

In practice absorption other than that associated with this metallic dispersion leads to departure of the experimental points from the straight line and to a lateral displacement of the line at long wavelengths. Brief attention is given to this elsewhere (Beattie and Conn 1955 b). It is necessary to take a sufficient number of measurements at long wavelengths to ensure that the slope of the line is known. σ_0 is then obtained by drawing a parallel line through the origin. Several of these Argand diagrams, based on experimental measurements of silver, copper and nickel, are presented below.

Fig. 1

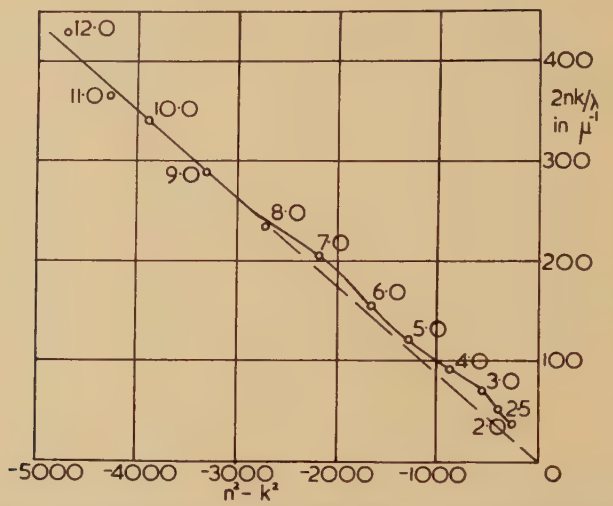

Argand diagram showing $2nk/\lambda$ against n^2-k^2 ; experimental results obtained with evaporated aluminium.

Fig. 1 (*a*)

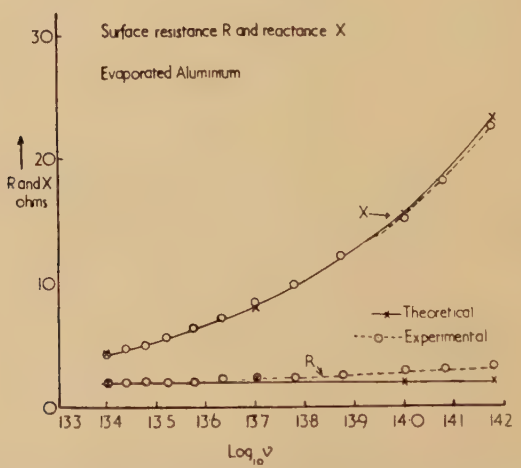

Surface resistance and surface reactance of evaporated aluminium as a function of frequency.

§ 4. Evaporated Aluminium

The form and use of such Argand diagrams is illustrated in fig. 1 in which results obtained with evaporated aluminium are plotted ; the experimental figures have already been published (Beattie 1955). Circles represent the experimental points to which the wavelengths in microns are affixed. The deduced straight line representing the contribution of the conduction electrons is shown by dashes ; the slope of this line indicates

that the relaxation time, τ, is $6{\cdot}1\times10^{-15}$ seconds and hence that the relaxation wavelength, λ_r, is $11{\cdot}5\ \mu$. The fitness of eqns. (8) and (9) to represent the main features is verified by using λ_r and $2nk/\lambda$ and n^2-k^2 at $9\ \mu$, a convenient reference, to calculate values at other wavelengths. The crosses indicate the results of such calculations. It is clear that absorption other than that of conduction electrons may be present at wavelengths less than $8\ \mu$.

Table 1. Characteristics of an Evaporated Aluminium Film

Thickness of film $=1550\pm50$ Å u.

$\tau=6{\cdot}1\times10^{-15}$ sec; $\lambda_r=11{\cdot}5\ \mu$.

λ in μ	8·0	9·0	10·0	11·0	12·0
$\sigma_0\times10^{-17}$ e.s.u.	1·09	1·13	1·19	1·14	1·23

Mean value of $\sigma_0=1{\cdot}16\times10^{17}$ e.s.u.
d.c. conductivity of film $=(1{\cdot}50\pm0{\cdot}10)\times10^{17}$ e.s.u.
d.c. conductivity of bulk aluminium $=3{\cdot}18\times10^{17}$ e.s.u.
Effective number of electrons per atom $=1{\cdot}28$.

Table 1 lists various characteristics of this film. The discrepancy between σ_0 and the conductivity measured with direct currents is a feature of all evaporated films which have been measured; it will emerge that in the case of bulk specimens there is a similar discrepancy. The number of electrons per unit volume is obtained from λ_r and σ_0, eqn. (7); the number per atom, N, is calculated by assuming that the density of bulk aluminium is the same as that of the film the thickness of which was measured by multiple-beam, Fizeau fringes (Tolansky 1948).

It should be emphasized that the construction of an Argand diagram from the experimental results serves primarily to clarify the interpretation; the particular diagram chosen presents the relaxation dispersion in its simplest form and the nature of the experimental absorption is readily grasped. If, as in the present paper, the purpose is restricted to a study of the contribution of the 'conduction electrons', a limited number of measurements at long wavelengths is all that is necessary since these determine λ_r and σ_0.

§ 5. Silver

Three specimens were examined. The first preliminary measurements were made on a small piece of rolled silver sheet, ground with emery and finished with a proprietary polish. The surface was contaminated by abrasive from the polish and only one reflection at 84° incidence was used so these results, listed in table 2, are of qualitative interest only.

Two silver mirrors were then prepared by evaporation from an alundum crucible *in vacuo* and condensed on a glass plate at about 40Å per second; the final thickness was 5200 Å. A study of five reflections showed that

the dispersion formula was closely obeyed though there were indications of an additional resonance absorption in the neighbourhood of 7 μ. Results are listed in table 2.

Attempts to electro-polish large specimens of annealed sheet were only partially successful. Since it is difficult to obtain the critical polishing conditions (Gilbertson and Fortner 1942) over a large area, the finish was marred by a milky etching. A final polish was given by gentle rubbing with chamois leather impregnated with a little magnesium oxide. Figure 2 shows the Argand diagram obtained.

Fig. 2

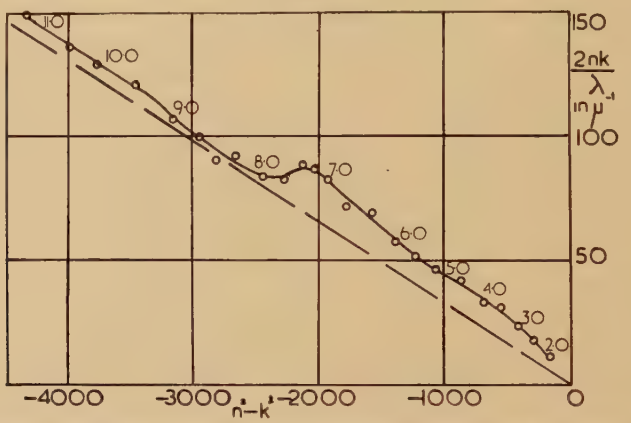

Figures obtained with annealed polished silver plotted on an Argand diagram.

Silver does not readily oxidize and the oxide decomposes above 200°c. An attempt was therefore made to estimate the temperature coefficient of σ_0 by observing the changes at 8 μ when the temperature was raised to 250°c. A section was cut from one of the third. annealed, specimens ;

Table 2. Optical Characteristics of Silver

Treatment	τ in sec	λ_r in μ	σ_0 e.s.u.	σ (d.c.), e.s.u.	σ (d.c.)/σ_0	N per atom
Metal Polish	$2{\cdot}05\times10^{-14}$	38·6	12×10^{16}	57×10^{16}	4·8	0·39
Evaporated	$1{\cdot}75\times10^{-14}$	38·9	$23{\cdot}4\times10^{16}$	33×10^{16}	1·4	0·90
Annealed and polished	$1{\cdot}61\times10^{-14}$	30·4	$19{\cdot}5\times10^{16}$	57×10^{16}	2·9	0·81

Temperature coefficient of σ_0 is of the order of 0·001 per °c.
Temperature coefficient of bulk material is 0·0038 per °c.

details of the arrangements for heating specimens are given in the section devoted to nickel. The temperature coefficient, quoted in table 2 is much smaller than that of the direct current conductivity.

§ 6. Copper

For the study of multiple reflections, pairs of copper specimens were prepared in five different ways ; the purity was better than 99·9%.

(i) Copper was evaporated from an alundum crucible at a pressure of about 5×10^{-6} mm Hg and condensed on a glass plate at about 16Å per second. The thickness was 4900Å.

Specimens of bulk copper were :—

(ii) polished with magnesium oxide by hand, see fig. 3 ;
(iii) buffed, see fig. 3 ;
(iv) electro-polished without annealing, see fig. 3 ;
(v) annealed and then electro-polished, see fig. 4.

Measurements had to be completed within a few hours since copper tarnishes readily. Careful and detailed examination is not possible in this limited time without using a controlled atmosphere. The deviations from a straight line are small in the case of evaporated copper being of the same order as those of evaporated aluminium, see fig. 1 ; in both cases these deviations occur at wavelengths less than 8 μ. The parameters deduced from these specimens are listed in table 3.

Table 3. Optical Characteristics of Copper

Treatment	τ sec	λ_τ in μ	σ_0 e.s.u.	σ (d.c.) in e.s.u.	σ (d.c.)/σ_0	N per atom
Evaporated (i)	$1\cdot41\times10^{-14}$	26·6	$1\cdot54\times10^{17}$	$2\cdot50\times10^{17}$	2·0	0·41
Hand-polished (ii)	$1\cdot06\times10^{-4}$	20·0	$0\cdot49\times10^{17}$	$5\cdot2\times10^{17}$	10·6	0·21
Buffed (iii)	$1\cdot80\times10^{-14}$	33·9	$1\cdot35\times10^{17}$	$5\cdot2\times10^{17}$	3·9	0·35
Annealed and electro-polished (iv)	$1\cdot41\times10^{-14}$	26·5	$0\cdot91\times10^{17}$	$5\cdot2\times10^{17}$	5·7	0·30

The straight lines drawn in figs. 3 and 4 lead to the values listed in table 3. The optical properties are strongly influenced by surface treatment but the results with the four bulk specimens show common features which are believed to be characteristic of copper ; departures from the straight line predicted by dispersion theory are considered elsewhere.

Fig. 3

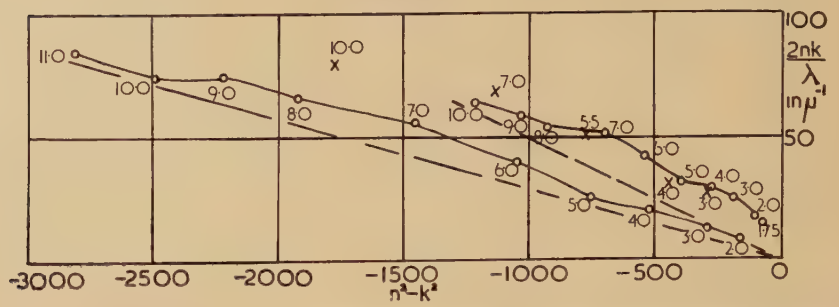

Argand diagram using measurements of copper ; upper curve—hand polished ; lower curve—same specimens buffed. Crosses indicate points obtained when the specimen was electro-polished.

Fig. 4

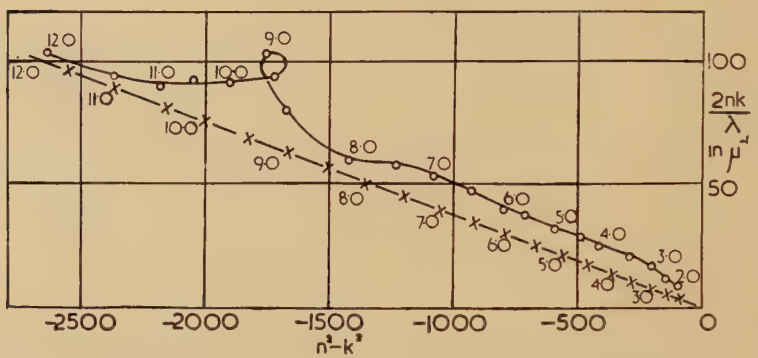

Argand diagram using measurements of annealed and electro-polished copper. The crosses were calculated using the point at 12 μ as reference.

§ 7. Nickel

The manner of preparing the surface of nickel specimens does not appear to have such influence on the measured results as is found with copper. Values of ρ and Δ are less extreme so that a single reflection at 84° by one specimen 2 in. $\times$ 1¼ in. was adequate. Nickel mirrors do not readily tarnish and time is available for detailed study ; they do not oxidize at temperatures below 500°C. Measurements were made above room temperature using specimens in a pyrophyllite holder fitted with a flat nichrome heater and a Pallador thermocouple to measure temperature. To ensure no movement of a specimen during heating, the front face was firmly located against the rounded ends of three quartz rods. To verify that no significant oxidation took place, measurements of the optical constants at 2 μ and 9 μ were repeated after the specimen had cooled again to room temperature. Irreversible changes, when these occurred were caused by contamination of the surface with electrolyte during polishing ; such cases were disregarded.

It is clear from table 4 that the number of electrons per atom, N, remains roughly constant however the surface is prepared. For the reasons given in the footnote below, the second evaporated film cannot be taken to be representative. Figure 6 shows that when the wavelength is less than 5 μ the optical constants are largely independent of temperature ; the contribution of the conduction electrons to the absorption is small and apparently the profile of residual absorption changes little with temperature.

Fig. 5

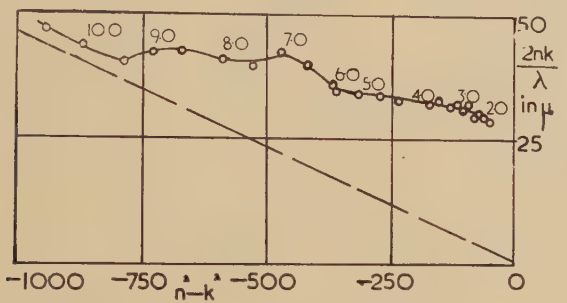

Argand diagram of hand-polished nickel.

Fig. 6

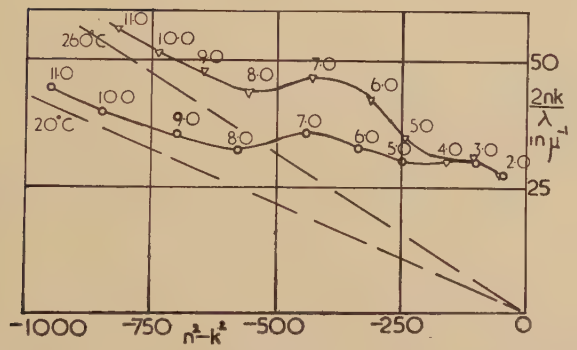

Argand diagram of annealed, electro-polished nickel at 260°C and 20°C.

§ 8. Discussion

There are few data with which present figures may be compared. Ingersoll (1910) extended his measurements of silver, copper and bulk nickel to 2·25 μ while Försterling and Fréedericksz (1913) examined sputtered copper and chemically deposited silver at wavelengths less than 5 μ. The figures of Försterling and Fréedericksz for electro-plated copper are not consistent with their other results. The need to maintain adequate and detailed control of the treatment of the surface confirms that the agreement indicated by typical values listed in table 5 is satisfactory.

Table 4. Characteristics of Nickel

Fig.	Treatment	Temp. °c	τ sec	λ_τ in μ	σ_0 e.s.u.	σ (d.c.) e.s.u.	σ(d.c.)/ σ_0	N/ atom	α
5	Hand-polished	20°c	$1{\cdot}14\times10^{-14}$	21·5	$3{\cdot}72\times10^{16}$	$11{\cdot}5\times10^{16}$	3·1	0·14	
	Buffed	20°c	0·99	18·7	3·80	11·5	3·0	0·17	
	Hand-polished	20°c	0·81	15·2	2·68	11·5	4·3	0·14	0·
		270°c	0·70	13·2	2·50			0·15	
6	Annealed and electro-polished	20°c	1·24	23·4	3·93	11·5	2·9	0·14	0·
		260°c	0·84	15·9	2·72			0·14	
7	Evaporated (i)	20°c	1·02	19·2	3·16	4·6	1·5	0·14	0·
		250°c	0·72	13·6	2·36			0·14	
—	Evaporated (ii)	20°c	0·50	9·38	1·02	1·4	1·4	0·09	0·
		250°c	0·40	7·62	0·88			0·09	

(i) This specimen was evaporated in a vacuum of the order of 5×10^{-6} mm Hg from an alu crucible at about 50Å per second ; the thickness was 3000Å.

(ii) This film 3030Å was formed by slow evaporation less than 10Å per second in a m vacuum of about 10^{-4} mm Hg and is thought to have been contaminated by gettering residual gas. It was unstable, recrystallized after a few days and peeled from the glass b

Fig. 7

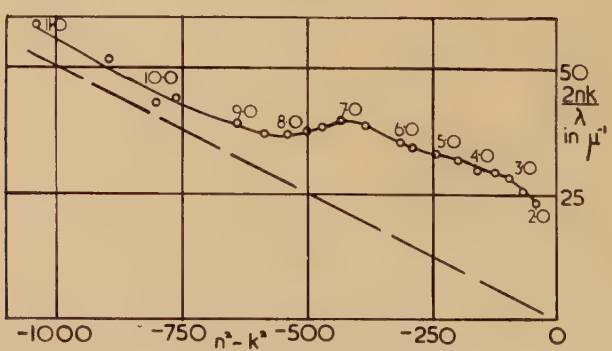

Argand diagram of nickel evaporated at 50Å per second from an alundum crucible ; thickness 3000Å.

Table 5. Comparison of Data

Specimen	Authority	λ in μ	n^2-k^2	$2nk$
Ni (buffed)	Present work	2·0	— 63·1	65·8
Ni (bulk)	Ingersoll	2·0	— 59·1	63·1
Cu (evaporated)	Present work	2·25	—154	15·3
Cu (electropolished)	Present work	2·25	—121	22·2
Cu (bulk)	Ingersoll	2·25	—136	24·1
Cu (sputtered)	Försterling and Fréedericksz	2·25	—130	15·5
Ag (bulk)	Present report	2·0	—166	21·7
Ag (evaporated)	Present report	2·0	—230	16·2
Ag (bulk)	Ingersoll	2·0	—187	18·6
Ag (chemical)	Försterling and Fréedericksz	2·1	—204	28·6
Cu (evaporated)	Present report	5·0	—745	160
Cu (sputtered)	Försterling and Fréedericksz	5·1	—800	169
Ag (evaporated)	Present report	4·0	—710	83·5
Ag (chemical)	Försterling and Fréedericksz	$4{\cdot}0_4$	—821	172

From the experiments figures of three parameters may be obtained, τ, σ_0 and N. These are not independent and it is natural to focus attention on σ_0 and N since these have an obvious physical significance. Caution is required in any general discussion of the present results since the body of experimental data is, as yet, not large.

The effective penetration depth of radiation of wavelength λ into an absorbing medium is $\lambda/4\pi k$ and with most metals this is of the order of 10^{-6} cm in the infra-red. It is therefore to be expected that the manner of preparing a surface influences σ_0 and the results obtained with silver, copper and nickel bear this out. The important factors may be listed for convenience as (*a*) contamination, (*b*) surface topography, and (*c*) crystal size and strain. To these the influence of ' anomalous skin effect ' must be added (Fuchs 1938, Sondheimer 1952 and Dingle 1953). It is not easy to distinguish each since some contribution may be made by all but it is possible to offer certain general comments.

The expressions (6) and (7) leading to (8) which summarize the dispersion of ' free ' or ' metallic ' electrons, do appear to describe adequately the absorption observed at relatively long wavelengths, $\lambda > 8\,\mu$. Figures 1 and 4 in particular illustrate this. At shorter wavelenghts there are significant departures which suggest, particularly in the case of nickel, that there are other factors peculiar to nickel which contribute to the absorption.

The silver surface treated with metal polish yielded a low value of σ_0 because of contamination. All low values of σ_0 cannot however be ascribed to contamination or surface strain ; even a buffed specimen may yield a conductivity as high as that of a specimen which is annealed and electro-polished (see tables 3 and 4). σ_0 may be reduced by surface roughness but even with evaporated films in which there can be little effect from scratches and relatively little contamination from the conditions of condensation, σ_0 is significantly less than the conductivity of the same film measured with direct currents or σ(d.c.). It does appear that σ_0 agrees reasonably well in these cases with the best values obtained with bulk material.

In general σ_0 is less than σ(d.c.) and with the metals reported here σ(d.c.)/σ_0 is of the order of 2·5 or more ; the lowest value of this ratio is furnished by silver (table 2). If measurements of nickel and silver are any guide the temperature coefficient of σ_0 is very small compared with that using direct currents. A simple calculation shows that it is not necessary to assume that the additional contributions to the resistance have any dependence on temperature. These might be attributed to ' imperfections ', a word used in its widest sense, but it is necessary to extend measurements to low temperatures. It is difficult to resist the conclusion that this discrepancy is fundamental and it is natural to seek the cause in current theories of ' anomalous skin effects ' since conductivity at infra-red frequencies is essentially a surface phenomenon. The magnitude of δ/l, l being the electronic mean free path, certainly falls in the appropriate range but direct comparison cannot be made with microwave measurements at low temperatures since the present experiments lie in the region of metallic dispersion. Current theories of anomalous skin effects predict a different frequency dependence from that of classical dispersion. This is not in agreement with experiment. More extensive measurements are required before the demands to be made of theory can be clearly defined.

The values of N are surprisingly low compared with those derived from the Hall effect (Wilson 1953). This cannot be due entirely to the use of the free electronic mass in the calculation. The figure for nickel, 0·15 per atom, presumably refers to the s-electrons since the contribution of the d-electrons to relaxation is negligible. With copper and aluminium, N is low being 0·35 per atom and 1·3 per atom respectively. The figure for silver, 0·9 per atom is more in line with the valency. It may be that simple relaxation theory has been interpreted too closely though it may be noted that with liquid metals (Kent 1919), N is to be identified with the chemical valency to a surprising, and convincing, degree. Measurements of liquid metals made in this laboratory confirm this to a material extent. Whatever the significance of the numerical values, with silver and nickel N does not vary over the range of temperature studied. If a polished surface of silver or nickel is etched, there is little effect on τ but N is significantly reduced.

Acknowledgments

We must acknowledge grants for apparatus from the Research Fund of the University of Sheffield and from the Royal Society.

References

Beattie, J. R., 1955, *Phil. Mag.* (7), **46,** 235.
Beattie, J. R., and Conn, G. K. T., 1955a, *Phil. Mag.* (7), **46,** 222; 1955b, *Ibid.*, in the press.
Dingle, R. B., 1953, *Physica,* **19,** 311 and 348.
Försterling, K., and Fréedericksz, V., 1913, *Ann. d. Phys.*, **40,** 201.
Fuchs, K., 1938, *Proc. Camb. Phil. Soc.*, **34,** 100.
Gilbertson, L. I., and Fortner, O. M., 1942, *Trans. Electrochem. Soc.*, **81,** 199.
Ingersoll, L. R., 1910, *Astrophys. Jnl.*, **32,** 265.
Kent, C. V., 1919, *Phys. Rev.*, **14,** 459.
Kronig, R. de L., 1931, *Proc. Roy. Soc.* A, **133,** 255.
Mott, N. F., and Jones, H., 1936, *Properties of Metals and Alloys* (Oxford: University Press).
Mott, N. F., and Zener, C., 1934, *Proc. Camb. Phil. Soc.*, **30,** 249.
Reuter, G. E. H., and Sondheimer, E. H., 1948, *Proc. Roy. Soc.* A, **195,** 336.
Robinson, T. S., 1952, *Proc. Phys. Soc.* B, **65,** 910.
Sondheimer, E. H., 1952, *Advances in Physics,* **1,** 1.
Stratton, J. A., 1941, *Electromagnetic Theory* (McGraw Hill).
Wolfe, R., 1954, *Proc. Phys. Soc.* A, **67,** 74; 1955, *Ibid.*, **68,** 121.

CXV. *Resonance Absorption of Nickel in the Infra-Red Region*

By J. R. Beattie and G. K. T. Conn
Department of Physics, The University, Sheffield *

[Received May 26, 1955]

Summary

Means are described whereby the absorption in the infra-red of 'free' or 'conduction' electrons may be abstracted from the total which is measured experimentally. When this is done, it is clear that there is residual absorption in nickel which may be caused by electron transitions from the d- to the s-band. The mechanism is being further explored.

The conductivity of silver, copper and nickel in the infra-red has been discussed in a previous paper (Beattie and Conn 1955) where it is shown that the contribution of the conduction electrons, that is those which obey simple dispersion theory (Mott and Jones 1936, Wolfe 1954), gives a straight line through the origin when $2nk/\lambda$ is plotted against n^2-k^2 on an Argand diagram. $n-ik$ is the complex refractive index and λ is the wavelength. With many specimens the experimental points show departures from the simple linear relation particularly at shorter wavelengths. $\lambda<8\,\mu$ and at least in some cases these must be considered to be significant. To assess these additional contributions it is first necessary to dissociate from the measured values the absorption arising from the metallic dispersion. Caution is required in the interpretation because of the influence of the surface examined. It is difficult to avoid the conclusion that with the nickel surfaces, however prepared, there is a real absorption arising from transitions of d-electrons to vacancies in the s-band. Such absorption has been predicted by Mott (1935). The present purpose is to present the experimental evidence for selective or 'resonance' absorption by nickel; confirmation of the interpretation is being sought by examining the behaviour of copper–nickel alloys.

Expressions representing metallic dispersion (Mott and Jones 1936, Beattie and Conn 1955) are commonly described in terms of a relaxation time τ with an associated relaxation frequency, ν_r, and wavelength, λ_r. These are simplified by defining a reduced frequency f so that

$$f=\nu/\nu_r=\lambda_r/\lambda=\omega\tau=2\pi\tau\nu \quad \text{and} \quad \nu_r=1/(2\pi\tau)=c/\lambda_r.$$

$2\pi\nu=\omega$ is the angular frequency and λ is the wavelength. Then

$$n^2-k^2-n_\infty{}^2=-4\pi\tau\sigma_0/(1+f^2) \quad \text{and} \quad 2nk=4\pi\tau\sigma_0/\{f(1+f^2)\}. \qquad (1)$$

---

* Communicated by Professor W. Sucksmith, F.R.S.

n_∞^2 is negligible being of the order of unity so that the straight line through the origin is

$$-(n^2-k^2)=2nkf \qquad \ldots\ldots\ldots \quad (2)$$

and may be used to determine τ and σ_0 (Beattie and Conn, *loc. cit.*). In practice it is not difficult to draw the straight line of eqn. (2) through

Fig. 1

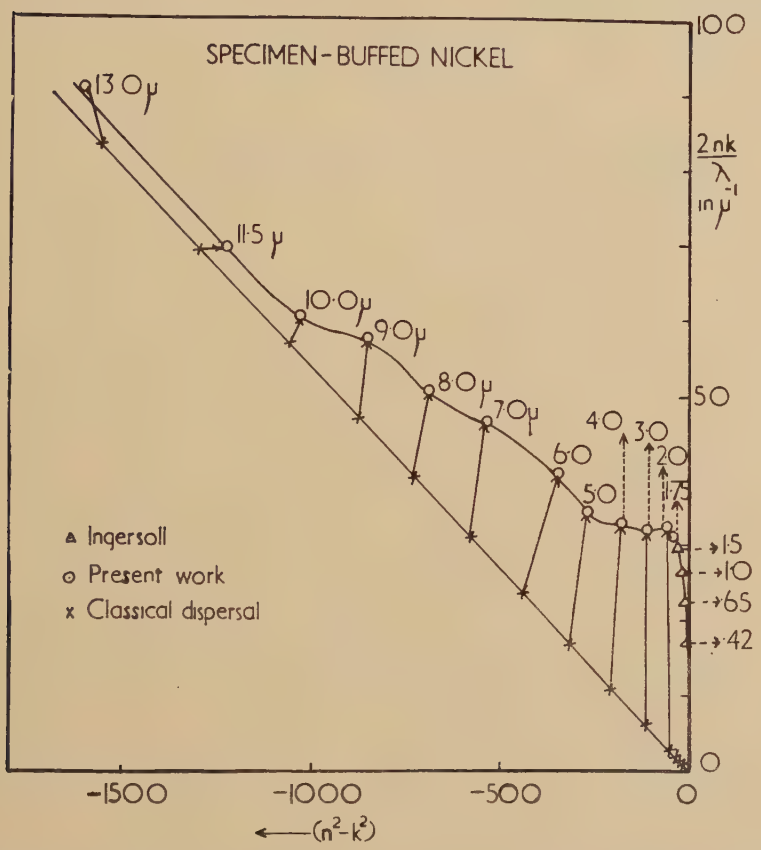

Argand diagram for a buffed nickel surface with $2nk/\lambda$ plotted against n^2-k^2. The straight line is taken to represent the contribution of 'metallic dispersion'; the crosses represent the computed position of the experimental wavelengths associated with the circles on the experimental curve.

the origin and parallel to the run of points at long wavelengths; measurement must be so extended that the linearity is confirmed and the slope determined. Values of $2nk/\lambda$ obtained with buffed nickel are plotted against n^2-k^2 in fig. 1; the present results, measured at the wavelengths indicated, have been extended to shorter wavelengths by using the data of

Ingersoll (1910). The position of points on the straight line which correspond to each of the measured wavelengths can be calculated knowing λ_r ; these are represented by crosses. The additional absorption at each wavelength is given by the lines or vectors joining each cross to the corresponding circle and the components of each vector may be used to construct 'extracted' curves of $2nk$ and n^2-k^2 against ν or λ. The graphs so obtained from fig. 1 are shown in fig. 2. If the additional absorption is caused by resonance there is no contribution to n^2-k^2 at the resonant frequency and the corresponding vector is then parallel to the $2nk/\lambda$ axis. Contours of the residual absorption bands so constructed

Fig. 2

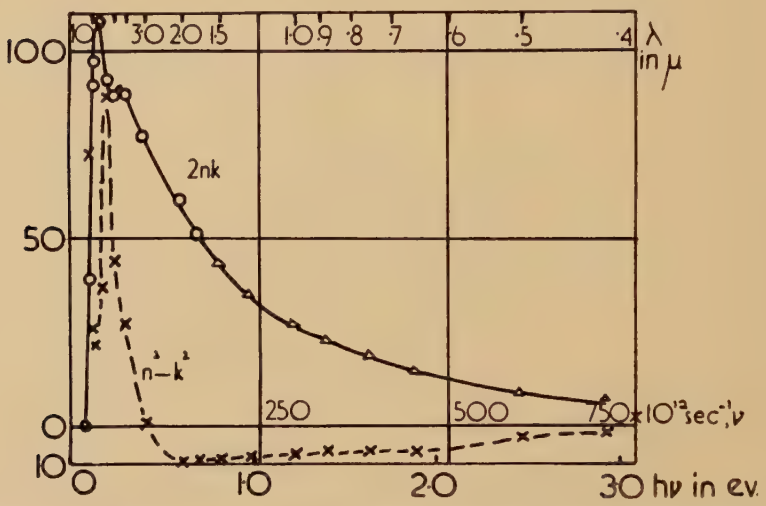

Curves showing, as a function of frequency, residual values of $2nk$ and n^2-k^2 after allowance has been made for metallic dispersion. The specimen was buffed nickel ; see fig. 1.

depend to some little extent on the line drawn to represent relaxation of the conduction electrons but since this must pass through the origin the choice is limited.

The only *a priori* assumption is that relaxation effects can be represented by such a line. The absorption curve is then extracted by calculation using λ_r and the *experimental* values of n^2-k^2 and $2nk$. The errors are therefore those associated with measurement of n^2-k^2 and $2nk$ and with the fitting of the straight line which is very rarely less precise. Since the contribution of metallic dispersion becomes progressively larger at longer wavelengths, small departures from the straight line imply larger changes of $2nk$. The percentage error associated with 'extracted' figures of $2nk$ and n^2-k^2 increases therefore ; the experimental difficulty lies in measurement of the phase difference Δ between the components of the reflected radiation and caution is necessary in interpreting such absorption curves.

Figure 3 shows dispersion curves obtained with two specimens prepared in entirely different ways. For fig. 3 (*a*) a film of evaporated nickel was prepared under good vacuum conditions, the pressure being less than 5×10^{-6} mm Hg and condensed on glass at about 50 Å per second; the thickness was 3000 Å. With unstable specimens prepared under poor conditions, about 10^{-4} mm Hg, similar absorption bands emerged but the

Fig. 3

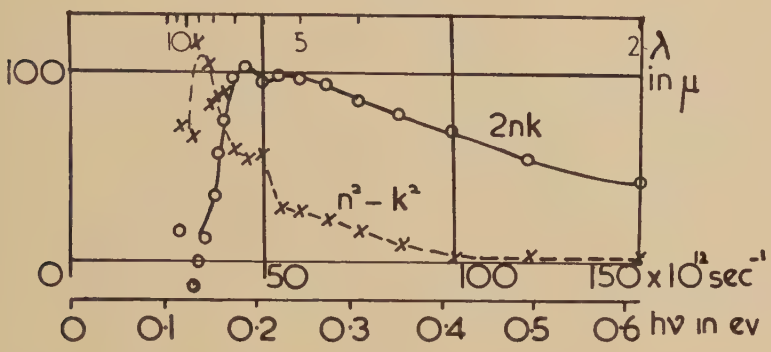

(*a*)

Residual values of $2nk$ and n^2-k^2 plotted against frequency. The specimen was a film of evaporated nickel condensed on glass to a thickness of 3000 Å.

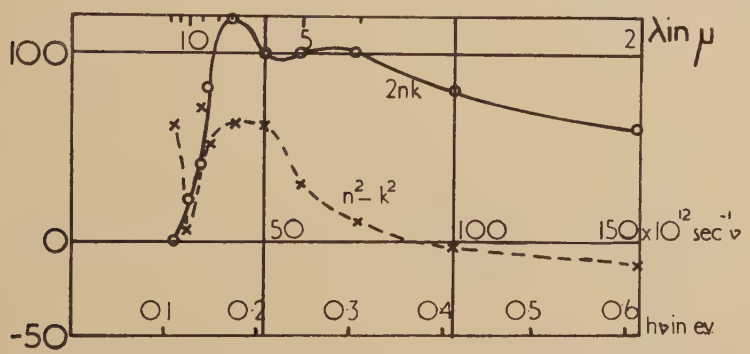

(*b*)

Residual values of $2nk$ and n^2-k^2 plotted against frequency. The specimen was of hand-polished nickel. (It should be noted that the scale of abscissae in figs. 3 and 4 is quite different from that used in fig. 2.)

maximum absorption moves to shorter wavelengths and is less than half the value shown in fig. 3 (*a*). Figure 3 (*b*) illustrates the behaviour of hand-polished nickel. In each case, figs. 2, 3 (*a*) and 3 (*b*), there is a doublet structure near the maximum with a regular fall of $2nk$ as the frequency is increased.

When the effect of temperature is studied the conductivity is changed but the temperature coefficient is much smaller than that of bulk material (Beattie and Conn, *loc. cit.*). Figure 4 was obtained using an annealed,

electro-polished specimen. The broad characteristics of the previous figures are repeated and, most important, the effect of temperature on the band structure is small. At the lowest frequencies it is significant, as is to be expected, but at higher frequencies the influence is negligible.

The present brief communication has two purposes. We wish to report and illustrate the practical possibility of distinguishing the contribution of the free or metallic electrons to the measured values of $2nk$ and n^2-k^2.

Fig. 4

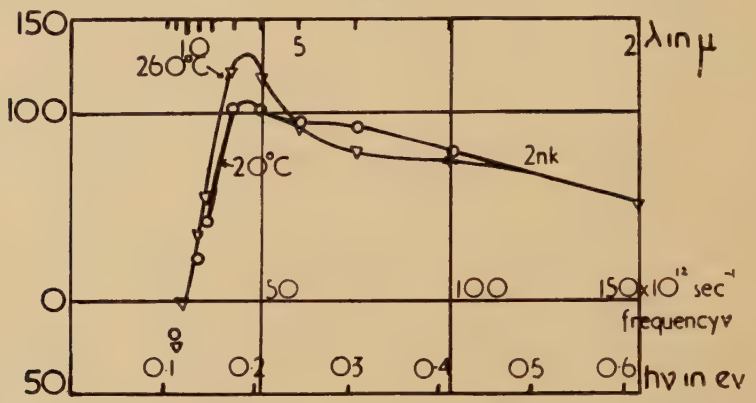

Residual values of $2nk$ plotted against frequency. The annealed, electro-polished nickel was examined at 20°C and 260°C.

Attention may be then directed to residual absorption if this is present. Such absorption may arise from many causes, some associated with the nature of the surface, some characteristic of the material. In the case of nickel it is difficult to avoid the conclusion that there is evidence of resonance absorption. It is natural to ascribe this to transitions between the d- and s-bands ; at the moment there is little profit in detailed quantitative examination of the data. We have preferred to seek confirmation by extending the range of experimental study to alloys of copper and nickel. This work will be reported in the near future.

Acknowledgments

We must acknowledge grants for apparatus from the Research Fund of the University of Sheffield and from the Royal Society.

References

Beattie, J. R., and Conn, G. K. T., 1955, *Phil. Mag.*, **46**, 1002.
Mott, N. F., 1936, *Phil. Mag.* (7), **22**, 287.
Mott, N. F., and Jones, H., 1936, *Properties of Metals and Alloys* (Oxford : University Press).
Wolfe, R., 1954, *Proc. Phys. Soc.* A, **67**, 74 ; 1955, *Ibid.*, **68**, 121.

CXVI. *Vacancies in Monovalent Metals**

By F. G. Fumi†
Cavendish Laboratory, Cambridge‡

[Received April 15, 1955]

Summary

The aim of this paper is to give a simplified calculation of the energy required to form a vacancy in a metal, which is applied to the noble and alkali metals. Although all such calculations are subject to considerable error unless many refinements are introduced, it is felt that such a calculation will give a useful indication of the various factors which determine the energy and the variation from metal to metal.

An outline of the method is as follows. The metal is represented as a large spherical box in which the positive charge of the ions is uniformly distributed and the electrons are free to move. When an ion is removed from the centre of the sphere and spread over its surface, the energy of the free electrons changes by ΔE_{el}, because the electron waves undergo phase shifts in order to screen the vacancy and the volume of the metal box changes. ΔE_{el} is proportional to the Fermi energy of the metal E_F, and is estimated to be about $\frac{1}{6}E_F$. For the noble metals another relevant contribution to the energy needed to create a vacancy is that of the closed-shell repulsion between ions : for Cu this is about $-0{\cdot}3$ ev.

The energy to move a vacancy is also discussed ; the electronic contribution is fairly small and in noble metals the term due to the closed-shell repulsion predominates. This is probably somewhat underestimated if one uses repulsive potentials valid in the neighbourhood of the equilibrium interatomic distance.

The general agreement between the theoretical results and the experimental values for the energies to form and to move a thermal defect in the alkali and noble metals is satisfactory and suggests that vacancies are responsible for the transport of matter also in the alkalis.

§ 1

In recent years there has been considerable interest in the problem of point defects in metals owing to the role that these defects play in the transport of matter within solids. Evidence bearing on these defects

* A preliminary report on this work was given at the Xe Conseil de Physique Solvay (Bruxelles, 1954).

† Permanent address : Istituto di Scienze Fisiche, Università di Milano, Italy.

‡ Communicated by the Author.

has been obtained from widely different experiments, including the study of diffusion, radiation damage and the mechanical properties of metals. In contrast with the fairly large amount of experimental work, the amount of quantitative theoretical work on the problem has been rather limited.

The only detailed calculations of the energies required to form and to move point defects in metals are those of Huntington and Seitz (1942, 1949) and Huntington (1942, 1953) for Cu ; rough estimates have been made by Bartlett and Dienes (1953) for vacancy pairs in Cu and by Paneth (1950) for linearly relaxed interstitials (crowdions) in the alkali metals.* The results of Huntington and Seitz are not in a form which can easily be generalized to other metals. This has recently led Nachtrieb and Handler (1954) to attempt to draw conclusions about the mechanism of transport of matter in metals from an empirical relation between the activation energy for self-diffusion and the latent heat of melting. The underlying assumption of their work is that the vacancy mechanism of self-diffusion should have an activation energy simply related to the latent heat of sublimation ; we shall see that this is not the case.

The purpose of this paper has been to devise a simple model which would allow some physical insight into the processes of creation and motion of vacancies in monovalent metals, and which would make it possible to obtain information of a general nature about the energies involved.

§ 2

To calculate the energy needed to create a vacancy in a monovalent metal, we represent the metal as a large spherical box in which the positive charge of the ions is uniformly distributed and the electrons are free to move. We then compute the change in energy that the electrons undergo when we remove an ion from the centre of the sphere and spread the charge over its surface. For the noble metals we will have to add to the change in the electronic energy computed in this way the change in the energy due to the strong non-coulombic forces between the ions.

With this model the unperturbed wave functions of the free electrons in the perfect metal are of the form $r^{-1}\sin(k_l r-\frac{1}{2}l\pi)$ $(l=0,\ 1,\ 2,\ \ldots)$, while the perturbed wave functions in the metal with the vacancy will have the asymptotic form $r^{-1}\sin(k_l' r+\eta_l-\frac{1}{2}l\pi)$, where η_l is the phase shift of the l waves (Mott and Massey 1950 a) due to the vacancy. The condition that the perturbed and unperturbed wave functions alike

---

* In his estimate Paneth (1950) neglects for instance that the electron gas is pushed out of the volume occupied by the interstitial ion and thus his value for the energy to form a crowdion is bound to be too small by an ev or two (C. Herring, private communication). This contribution to the energy to form an interstitial in a metal has been neglected also by Huntington and Seitz (1942) and by Huntington (1953).

should vanish at the boundary of the spherical box ($r=R$) yields the equations

$$k_l R=n\pi+\tfrac{1}{2}l\pi \qquad (n=1, 2, \ldots), \quad . \quad . \quad . \quad . \quad (1)$$

$$k_l' R=n\pi+\tfrac{1}{2}l\pi-\eta_l \qquad (n=1, 2, \ldots). \quad . \quad . \quad . \quad . \quad (2)$$

It follows that

$$R(k_l'-k_l)+\eta_l=0. \quad . \quad . \quad . \quad . \quad . \quad . \quad (3)$$

The change in energy of an l electron owing to the change Δk_l of its momentum is given by $\hbar^2 k_l \Delta k_l/m$. Therefore the energy change of the free electrons upon removal of an ion from the centre of the metal sphere is equal to

$$\Delta E_{el}'=-2\int_0^{k_F} \Sigma_l (2l+1)\frac{\hbar^2 k \eta_l(k)}{mR}\frac{R}{\pi}dk \quad . \quad . \quad . \quad . \quad (4)$$

where k_F is the momentum of the electrons at the Fermi level and R/π is the density of states for l electrons. The factor 2 originates from the spin.

In the Born approximation (Mott and Massey 1950 b)

$$\eta_l(k)=-\frac{\pi m}{\hbar^2}\int_0^R V(r)\{J_{l+1/2}(kr)\}^2 r\,dr \quad . \quad . \quad . \quad . \quad (5)$$

where $V(r)$ is the perturbing potential, that is the potential field of the vacancy screened by the conduction electrons. Using the addition theorem of Gegenbauer (Watson 1922),

$$\Sigma_l (2l+1)\{J_{l+1/2}(kr)\}^2=\frac{2kr}{\pi},$$

we can rewrite (4) in the following form

$$\Delta E_{el}'=\frac{{k_F}^3}{3\pi^2}\int_0^R V(r)4\pi r^2\,dr. \quad . \quad . \quad . \quad . \quad . \quad . \quad (6)$$

This is the result given by first-order perturbation theory ; the energy change undergone by the electrons is given by the integral of the perturbing potential multiplied by the unperturbed electron density ${k_F}^3/3\pi^2$.

The use of Friedel's theorem (Friedel 1952) for the phase shifts at the Fermi level, still using Born's approximation, allows us to put $\Delta E_{el}'$ in a form independent of $V(r)$. Indeed, following Friedel, we may write

$$\frac{2}{\pi}\Sigma_l (2l+1)\eta_l(k_F)=-1, \quad . \quad . \quad . \quad . \quad . \quad . \quad . \quad (7)$$

since a vacancy in a monovalent metal can be considered as an impurity atom with an excess valence equal to -1. The left-hand side is equal, in Born's approximation, to $-(k_F m/\hbar^2\pi^2)\int_0^R V(r)4\pi r^2\,dr$. Thus

$$\Delta E_{el}'=\frac{\hbar^2 {k_F}^2}{3m}=\tfrac{2}{3}E_F \quad . \quad . \quad . \quad . \quad . \quad . \quad . \quad (8)$$

where E_F is the Fermi energy. To improve on this result which is based on the Born approximation, we shall have to return to eqn. (4) (see § 3).

$\Delta E_{el}'$ is not the entire energy change undergone by the electrons upon creation of a vacancy. We still have to compute the energy change due to the spreading of the ion we have extracted over the surface of the metal sphere ; this causes an expansion of the spherical box in which the electrons are enclosed. The energy of the N electrons in the box is $(3/5)NE_F$, and the Fermi energy E_F is proportional to $V^{-2/3}$ where V is the volume of the box. Thus the change in energy caused by an expansion δV of the box is

$$\Delta E_{el}''=-\frac{2}{3}\frac{3}{5}NE_F\frac{\delta V}{V}=-\frac{2}{5}E_F, \quad . \quad . \quad . \quad . \quad . \quad (9)$$

where the number of atoms in the metal has been taken to be equal to the number N of free electrons (monovalent metal). The increase in surface energy connected with the expansion of the box is negligible being of the order of $N^{-1/3}$.

Thus for the total change ΔE_{el} of the energy of the electrons

$$\Delta E_{el}=\Delta E_{el}'+\Delta E_{el}''=\frac{4}{15}E_F. \quad . \quad . \quad . \quad . \quad . \quad (10)$$

This result neglects the changes in exchange and Coulomb correlation energies of the free electrons. However, as Friedel (1954) has noted, the result is not altered if one includes in the perturbing potential $V(r)$ the change in average exchange energy. Since the volume over which the electrons are distributed is essentially the same in the initial and final states, it is perhaps permissible to neglect also the change in Coulomb correlation.

§ 3

Formula (8), and thus formula (10), have been obtained using the Born approximation for the phase shifts η_l of the free electrons of the metal under the action of the repulsive field of the screened vacancy. This will give too large a value for $\Delta E_{el}'$, and thus for ΔE_{el}, because the Born approximation overestimates appreciably the phase shifts for repulsive fields. It is clearly of interest to see how much the value of $\Delta E_{el}'$ is affected.

To calculate $\Delta E_{el}'$ with exact phase shifts we have to choose a definite form for the repulsive potential of the screened vacancy. We have adopted a constant spherical barrier (Jongenburger 1953, Abelès 1953) for which the exact phase shifts can be expressed analytically. To estimate the error in $\Delta E_{el}'$ caused by the Born approximation it was felt to be sufficient to use exact phase shifts for the s waves which undergo considerably larger shifts than the waves of higher l. The calculation can be done at once for all the monovalent metals, for which

$$r_s k_F=(9\pi/4)^{1/3}=1{\cdot}919$$

(r_s=radius of the atomic sphere).

The potential we use is of the form

$$\left.\begin{aligned} V(r)&=D \quad \text{for} \quad r<a, \\ &=0 \quad \text{for} \quad r>a. \end{aligned}\right\} \quad . \quad . \quad . \quad . \quad . \quad (11)$$

We take a equal to r_s, and we choose D $(=\hbar^2k_0^2/2m)$ using Friedel's condition for the phase shifts at the Fermi level. This condition reads now

$$\frac{2}{\pi}\sum_l(2l+1)\{\eta_l(k_F)\}_{\text{Born}}-\frac{2}{\pi}\{\eta_0(k_F)\}_{\text{Born}}+\frac{2}{\pi}\{\eta_0(k_F)\}_{\text{exact}}=-1 \quad . \quad (12)$$

where

$$\frac{2}{\pi}\sum_l(2l+1)\{\eta_l(k_F)\}_{\text{Born}}=-\frac{2}{3}\frac{r_sk_F(r_sk_0)^2}{\pi} \quad . \quad . \quad . \quad . \quad (13)$$

$$\{\eta_0(k_F)\}_{\text{Born}}=\frac{(r_sk_0)^2}{2(r_sk_F)^2}(\sin r_sk_F\cos r_sk_F-r_sk_F) \quad . \quad . \quad . \quad (14)$$

and (Mott and Massey 1950 a)

$$\{\eta_0(k_F)\}_{\text{exact}}=\tan^{-1}\left[\frac{r_sk_F}{\sqrt{\{(r_sk_F)^2-(r_sk_0)^2\}}}\tan\sqrt{\{(r_sk_F)^2-(r_sk_0)^2\}}\right]-r_sk_F.$$

For $k<k_0$ . . . . (15)

$$\{\eta_0(k)\}_{\text{exact}}=\tan^{-1}\left[\frac{r_sk}{\sqrt{\{(r_sk_0)^2-(r_sk)^2\}}}\tanh\sqrt{\{(r_sk_0)^2-(r_sk)^2\}}\right]-r_sk. \quad (16)$$

$\Delta E_{el}'$ is then obtained by adding the exact energy change for the s waves to the energy change for the higher l waves computed in the Born approximation

$$\begin{aligned}\Delta E_{el}'=\frac{\hbar^2}{mr_s^2}\Bigg[&\frac{2}{9\pi}(r_sk_0)^2(r_sk_F)^3-\frac{1}{\pi}(r_sk_0)^2\left(r_sk_F-\int_0^{r_sk_F}\frac{\sin x\cos x}{x}dx\right)\\&+\frac{2}{\pi}\Bigg\{\frac{(r_sk_F)^3}{3}-\int_0^{r_sk_0}x\tan^{-1}\\&\qquad\times\left(\frac{x}{\sqrt{\{(r_sk_0)^2-x^2\}}}\tanh\sqrt{\{(r_sk_0)^2-x^2\}}\right)dx\\&-\int_{r_sk_0}^{r_sk_F}x\tan^{-1}\left(\frac{x}{\sqrt{\{x^2-(r_sk_0)^2\}}}\tan\sqrt{\{x^2-(r_sk_0)^2\}}\right)dx\Bigg\}\Bigg]. \quad (17)\end{aligned}$$

To obtain ΔE_{el} we have again to add to $\Delta E_{el}'$ the energy $\Delta E_{el}''=-\frac{2}{5}E_F$. The value of r_sk_0 which fits Friedel's condition (12) is found to be approximately 1·64. The resulting value of ΔE_{el} is $\frac{1}{6}E_F$ within the accuracy of the numerical calculation.

The use of exact phase shifts also for $l>0$ would still yield a ΔE_{el} proportional to E_F since the exact phase shifts $\eta_l(k_F)$ depend only on the product r_sk_F; it is difficult to estimate *a priori* the magnitude of the change in the proportionality factor but it appears unlikely that it is sizeable. Thus it does not seem warranted to perform the corresponding numerical calculations owing to the approximations involved in the model itself.

§ 4

In the case of the noble metals, the energy to create a vacancy cannot be taken to be equal to the energy change undergone by the conduction electrons. Important cohesive forces in these metals are the ion–ion closed-shell repulsions (Mott and Jones 1936) and the Coulomb correlations

between conduction electrons and 3d-core electrons (H. Brooks and J. Friedel, private communications); while the former contribute only a small fraction of an ev to the cohesive energy, the latter are thought to contribute more than 1 ev.

The Coulomb correlations between conduction and core-electrons operate inside individual atomic polyhedra and thus should not contribute in a relevant way to the energy needed to transfer an ion from the interior of a metal to its surface.

In the approximation of a rigid lattice, the closed-shell repulsions between ions (central forces) would contribute to the energy to create a vacancy an amount equal to their contribution to the cohesive energy. However, the metal lattice is not rigid and upon removal of a metal ion from the interior the nearest neighbours relax to new positions. The relaxation occurs in such a way as to minimize the energy and thus the repulsive energy decreases more than in a rigid lattice.

To estimate the contribution of the repulsive forces to the work to create a vacancy, allowing for the relaxation of the neighbouring atoms only, we note with Huntington and Seitz (1942) that the creation of a vacancy in a face-centred metal causes the rupture of 6 bonds and the alteration of 84; there are 24 bonds between the nearest neighbours of the vacancy, and only 60 of the 84 bonds between nearest and next-nearest neighbours are altered to a first approximation. The expression for the change in repulsive energy is*

$$\Delta E_R = 12R\{d(1+\lambda)\} + 48R\{d(1+\lambda+\lambda^2)^{1/2}\} + 24R\{d(1-\lambda)\} - 90R(d) \quad (18)$$

where $R(r)$ is the repulsive energy per ion pair at distance r, d is the equilibrium interatomic distance and λd is the inward displacement of the 12 nearest neighbours of the vacancy. If we use for $R(r)$ the Born–Mayer exponential form $A \exp(-r/\rho)$, ΔE_R becomes

$$\Delta E_R = A \exp\left(-\frac{d}{\rho}\right) \times \left\{12 \exp\left(-\frac{d\lambda}{\rho}\right) + 48 \exp\left(-\frac{d}{\rho}\frac{\lambda}{2}\right) + 24 \exp\left(\frac{d}{\rho}\lambda\right) - 90\right\}. \quad (19)$$

To maximize this decrease of repulsive energy, we minimize the λ-dependent part.

We have performed the numerical calculations for copper using the two Born–Mayer potentials recently proposed by Huntington (1953) and the Born–Mayer potential originally used by Huntington and Seitz (1942)

* This expression assumes that each of the 12 nearest neighbours of the vacancy undergoes an equal displacement toward the site of the vacancy. Obviously this is a very special type of relaxation; angular rearrangements may in fact be important (N. Cabrera, private communication). It seems safe to say, however, that the order of magnitude of the repulsive energy gain will not be affected.

in the correct form reported by Huntington (1953).* We found that ΔE_R is about $-7{\cdot}5R(d)$ (with $d=2{\cdot}55$ Å) rather than $-6R(2{\cdot}55$ Å) as it would be in the rigid lattice approximation : λ ranges between 0·015 and 0·020. The numerical values of ΔE_R for the three potentials used are respectively † $-0{\cdot}40$ ev, $-0{\cdot}28$ ev and $-0{\cdot}24$ ev. A reasonable value to take is $-0{\cdot}3$ ev.

For silver and gold no formulae have yet been proposed for the closed-shell repulsion but the order of magnitude of the gain in the repulsive energy upon creation of a vacancy is certainly the same as for copper.

§ 5

The calculation of the energy needed to move one of the nearest neighbours of a vacancy in a monovalent metal from its equilibrium position halfway toward the vacancy, thus reaching the saddle-point configuration, is a difficult problem. We will attempt only some semi-quantitative considerations on the important contributions to this energy.

We note first with Huntington and Seitz (1942) and Huntington (1942) that the saddle-point configuration, in which a metal ion is halfway between two neighbouring vacancies, can be envisaged as a perfect lattice with two neighbouring half-vacancies in it, if one assumes that

---

* It is difficult to say whether any of these potentials is to be preferred. If so, it should be the potential adopted by Huntington and Seitz (1942) in the form reported by Huntington (1953, footnote 14) since its two empirical parameters were determined from the three elastic constants of copper taking proper account of the electrostatic contributions to the shear constants computed by Fuchs (1936). The first repulsive potential proposed by Huntington (1953) (H_1) $R(r)=0{\cdot}053 \exp\{-13{\cdot}9(r-d)/d\}$ ev per ion pair, is based instead on the assumption (Zener 1950) that the actual electrostatic contributions to the shear constants are appreciably smaller than those calculated by Fuchs (1936), owing to a redistribution of the electron gas during the shear distortion. The fact that the values of the shear constants computed by Fuchs (1936) for the alkali metals are in very good agreement with experiment (Mott 1952) appears to indicate that Zener's assumption is unrealistic, and Dr. Huntington (private communication) points out that the calculation that he gave to substantiate it (Huntington 1953, appendix A) is incorrect. The second Born–Mayer potential proposed by Huntington (1953) (H_2) $R(r)=0{\cdot}038 \exp\{-17{\cdot}2(r-d)/d\}$ ev per ion pair, was simply chosen as an opposite extreme to the first, so as to be fairly close to the potential adopted by Huntington and Seitz (1942) (H.S.), which can be written as $R(r)=0{\cdot}032 \exp\{-17(r-d)/d\}$ ev per ion pair. We have not considered the repulsive potential used by Zener (1950), $0{\cdot}078 \exp\{-(19/\sqrt{2})(r-d)/d\}$ ev per ion pair, which is derived on the radical assumption of a vanishing electrostatic contribution to the shear constants, and without using the experimental value of the bulk modulus. It should be mentioned that the repulsive potential attributed by Zener (1950, p. 350) to Huntington and Seitz (1942) is affected by the misprints which occurred in the original paper.

† The last number is given incorrectly by Huntington and Seitz (1942), p. 320, as —0·4 ev.

the moving ion deforms in such a fashion as to fill only spaces which do not belong to the atomic polyhedra of its neighbouring ions.

The electronic contribution to the energy to create two half-vacancies in a monovalent metal can be estimated along the lines of § 2. To a first approximation this energy does not differ from the electronic energy change $(4/15)E_F$ which accompanies the creation of a vacancy ; indeed the ' box expansion ' term $-\frac{2}{5}E_F$ is replaced by two equal terms each amounting to $-\frac{1}{5}E_F$ and similarly the ' phase-shift ' term $\frac{2}{3}E_F$ is replaced by two equal terms each amounting to $\frac{1}{3}E_F$. Roughly we should thus expect no electronic contribution to the energy of movement for a vacancy in a monovalent metal. However, corrections to this first-order estimate should be made, mainly owing to the non-spherical symmetry of the holes in the electronic distribution corresponding to the two half-vacancies (Huntington 1942, section II. 6). These corrections could easily give in the closed-packed metals a contribution of a few tenths of an ev.

For the noble metals one must consider also the contribution of the closed-shell repulsion to the energy of movement of a vacancy. This can easily be estimated following Huntington and Seitz (1942). The saddle-point configuration can be obtained from the perfect lattice by removing two ions from their adjacent lattice sites and placing one of them at the surface and the other at the centre of the rectangle formed by the four ions which are nearest neighbours of both vacancies ; upon the introduction of an ion at the centre of this rectangle, each of the four ions at the vertices displaces itself outwards along the line joining it to the added ion, by an amount equal to its distance from the added ion multiplied by λ. The change in repulsive energy can be considered to be composed of three parts due : (i) to the rupture of 17 bonds (12 to create the first vacancy, 11 to create the second and 6 recovered from the atom placed at the surface), (ii) to the introduction of an ion at the centre of the rectangle formed by the four common nearest neighbours of the two vacancies, allowing only for the relaxation of the ions at the vertices of the rectangle, and (iii) to the relaxation of the remaining 14 neighbours of the two vacancies. The contribution (ii) is given by*

$$\begin{aligned}4[&R(\tfrac{1}{4}a\sqrt{10})+R\{\tfrac{1}{4}a\sqrt{6(1+\lambda)}\}+\tfrac{1}{2}R\{\tfrac{1}{2}a(2+4\lambda)^{1/2}\}+2R\{\tfrac{1}{2}a(2+\lambda)^{1/2}\}\\&+2R\{\tfrac{1}{2}a(2-\lambda)^{1/2}\}+R\{\tfrac{1}{2}a(2-2\lambda)^{1/2}\}\\&+2R\{\tfrac{1}{2}a(2-3\lambda)^{1/2}\}-7{\cdot}5R(\tfrac{1}{2}a\sqrt{2})]. \quad . \quad . \quad . \quad . \quad . \quad . \quad (20)\end{aligned}$$

For (iii) we take with Huntington and Seitz (1942) a ratio 14/12 of the decrease in repulsive energy caused by the relaxation around a single

---

* This formula is given incorrectly by Huntington and Seitz (1942), eqn. (6) ; instead of

$$\tfrac{1}{2}R\{\tfrac{1}{2}a(2+4\lambda)^{1/2}\}+2R\{\tfrac{1}{2}a(2-\lambda)^{1/2}\}+R\{\tfrac{1}{2}a(2-2\lambda)^{1/2}\}$$

they write

$$\tfrac{1}{2}R\{\tfrac{1}{2}a(2+2\lambda)^{1/2}\}+3R\{\tfrac{1}{2}a(2-\lambda)^{1/2}\}.$$

vacancy which we considered in § 4. The contribution of the closed-shell repulsion to the energy of movement of a vacancy is obtained by subtracting from the sum of (i), (ii) and (iii) the repulsive energy gain which accompanies the creation of a single vacancy (see § 4).

We have performed the numerical calculations for copper as we did in § 4 and we have again used the two Born–Mayer potentials proposed by Huntington (1953) (H_1 and H_2) and the Born–Mayer potential adopted by Huntington and Seitz (H.S.) (1942) as reported by Huntington (1953). The values of (i), (ii) and (iii) for the three potentials are given below (in ev) :

	(i)	(ii)	(iii)
H_1	−0·91	1·12 (λ=0·047)	−0·09
H_2	−0·65	1·06 (λ=0·052)	−0·07
H.S.*	−0·55	0·90 (λ=0·052)	−0·06

The final result turns out to be fairly insensitive to the particular form of potential used, ranging from 0·52 ev for the H_1 potential to 0·62 ev for the H_2 potential.

This value for the contribution of the closed-shell repulsion to the energy of movement of a vacancy in copper may be somewhat too small. The Born–Mayer potentials that we have used to calculate it are really valid only in the neighbourhood of the equilibrium interatomic distance. A rather approximate analysis of the (27°C) pressure-volume isotherm for copper up to pressures of 0·5 megabar (Walsh and Christian 1955), following the lines of Zener (1950), suggests that the repulsive energy per ion pair at distances appreciably smaller than the equilibrium distance (such as the distance $r=a\sqrt{6}/4$ which appears in the repulsive energy contribution to the energy of the vacancy saddle point) may be larger than that estimated from the equilibrium forms of the repulsive potential by a factor of a few units. This implies that the contribution (ii) may be underestimated, while the same will not be true for the contributions (i) and (iii) in which one deals respectively with the equilibrium distance and with distances differing only slightly from it. It is tempting to stress the analogy with the case of NaCl where the values that Mott and Littleton (1938) computed for the energies of movement of Na^+ and Cl^- vacancies in NaCl (0·5 ev for Na^+ vacancies ; 0·6 ev for Cl^- vacancies) are well below the experimental values (Etzel and Maurer 1950, Aschner 1954, Seitz 1954) (0·85 ev for Na^+ vacancies, >1 ev for Cl^- vacancies) while the values they computed for the energies of formation are in fair agreement with experiment. It is natural to attribute the inaccuracy of the theoretical energies of movement to the repulsive energy as Mott and Littleton did, since the remaining contributions should be computed with considerable accuracy in an ionic solid.

---

* These numbers are incorrectly given by Huntington and Seitz (1942), Table II as −0·69, 0·51 and −0·19 respectively.

§ 6

The experimental values for the energies to create and to move point defects in monovalent metals are at present uncertain, particularly for the case of the noble metals, and it should be stressed that theoretical results cannot be a decisive element in these disputes owing to the approximations which are made to perform the calculations.

Accurate values for the activation energy for self-diffusion are available for lithium (Holcomb and Norberg, private communication) and for sodium (Nachtrieb, Catalano and Weil 1952), while an approximate value is available for rubidium (Holcomb and Norberg, private communication). Values have been reported also for the energies needed to create thermal defects in the alkali metals (Carpenter 1953, MacDonald 1953, 1955) and the reasonable assumption has been made that the defects created are the defects responsible for self-diffusion ; in this way, the activation energies for self-diffusion have been separated in an energy of formation and an energy of movement. The available results are summarized in table 1. The more probable values appear to be those

Table 1. Experimental Values for the Activation Energy for Self-diffusion (U) and for the Energy to form (U_1) and to move (U_2) a Thermal Defect in the Alkali Metals (in ev)

	Li	Na	K	Rb	Cs
U	0·57	0·45	—	0·41	—
U_1(MacDonald 1953)	0·40	0·39	0·39	—	—
(MacDonald 1955)	—	—	0·39	—	—
(Carpenter 1953)	—	0·26	0·24	—	—
U_2(MacDonald 1953)	0·17	0·06	—	—	—
(Carpenter 1953)	—	0·19	—	—	—

which MacDonald has obtained by measurements of electrical resistance (MacDonald 1953) and of specific heat (MacDonald 1955) at high temperatures. Thus the thermal defects in the alkali metals appear to have a very small energy of movement. This checks well with our discussion of the energy of movement of a vacancy in the alkali metals (see § 5) which gave a zero value. The theoretical values for the energy of formation of a vacancy in the alkali metals that we computed in §§ 2 and 3 are shown in table 2 ; for Li, the only alkali metal for which the effective mass m^* of the conduction electrons is known to be appreciably different from the free electron mass m, we have introduced in E_F the correcting factor $m/m^*=0{\cdot}69$ (Brooks 1954). The values $\frac{1}{6}E_F$ agree well with the more probable experimental values for the energy of formation of a thermal defect, even if they are still slightly too large. It seems reasonable to conclude that the thermal defects responsible for matter transport in the alkali metals are vacancies.

For the noble metals, accurate values for the activation energy for self-diffusion are available (Kuper, Letaw, Slifkin, Sonder and Tomizuka 1954—Copper; Slifkin, Lazarus and Tomizuka 1952—Silver; Gatos and Kurtz 1954—Gold) and vacancies are normally accepted as the defect responsible for the transport of matter, owing to the theoretical results of Huntington and Seitz (1942, 1949) and the experimental observation of the Kirkendall effect (Seitz 1950, Zener 1950). However, alternatives have been proposed for the way in which the total activation energies should be divided into the energies of formation and of movement of a vacancy (Manintveld 1952, 1953, Meechan and Eggleston 1954, Kauffman and Koehler 1955). These experimental values are given in table 3. On the ground of the available experimental evidence the more probable values appear to be those which give an energy of movement for the vacancy larger than the energy of formation (Seeger 1955). The theoretical values for the energy of formation of a vacancy are reported in table 4 and favour such an assignment. The value we estimated in § 5 for the energy of motion of a vacancy in Cu (*c.* 0·6 ev) appears then to be too small by a factor 2; as we noted in § 5, this is not unreasonable.

Table 2. Theoretical Values for the Energy (U_1) to form a Vacancy in the Alkali Metals (in ev)

	Li ($m/m^*=0{\cdot}69$)	Na	K	Rb	Cs
E_F†	3·30	3·20	2·14	1·83	1·58
$U_1^{Born}=(4/15)E_F$ (§ 2)	0·88	0·85	0·57	0·49	0·42
$U_1=(1/6)E_F$ (§ 3)	0·55	0·53	0·36	0·31	0·26

For copper, our theoretical results are in good agreement with the results of Huntington and Seitz (1942) and Huntington (1942). Indeed Huntington and Seitz (1942) obtain an energy of formation for a vacancy ranging from 1 to 1·5 ev, and the more detailed calculations by Huntington (1942) effectively give an energy of about 1 ev. Huntington's calculations (1942) give also an upper limit of about 1·8 ev for the energy of movement of a vacancy. It is frequently stated in the literature that the results of Huntington (1942) give an energy of formation definitely larger than the energy of movement and that the latter is computed to be about 1 ev: these statements, however, should be corrected. The high value (1·8 ev) for the energy of formation that Huntington (1942) reports as the result of his calculations is faulty since it includes twice the electrostatic interaction of the shielded vacancy with its nearest neighbours: the interaction is included already in the calculation leading to the value of 1·2 ev

† The values of the Fermi energy E_F for the alkali metals quoted in the literature differ somewhat (cf. Kittel, C., 1953, *Introduction to Solid State Physics* (Wiley), p. 240; and Wilson A. H., 1953, *Theory of Metals* (Cambridge), p. 270). The values reported in this table have been computed anew with the equation $r_s k_F=(9\pi/4)^{1/3}$ adopting the following values for the lattice parameter: Li, 3·48 Å; Na, 4·25 Å; K, 5·20 Å; Rb, 5·62 Å; and Cs, 6·05 Å.

(Huntington 1942, p. 332), and should not be added again as Huntington (1942) does in Table II of his paper. The actual value for the energy of formation which follows from Huntington's calculation is about 1 ev, since one must subtract from the quoted value of 1·2 ev the gain in repulsive energy which accompanies the breakage of six bonds : according to Huntington (1942), there is no relaxation around a vacancy in copper because the net electrostatic field of the shielded vacancy at its nearest neighbours is repulsive, a result which is likely due to the neglect of the phase shifts for l greater than 2. For the energy of movement, it should be stressed that the value of about 1 ev which can be obtained from Huntington's calculation (1942) by subtracting the energy to form a vacancy (1 ev) from the estimate of the energy of the saddle point (1·6+0·4) ev* is a lower limit, since a relevant contribution to the energy of the saddle point has been neglected as Huntington (1942, section II. 6) emphasizes.

Table 3. Experimental Values for the Activation Energy for Self-diffusion (U) and for the Energy to form (U_1) and to move (U_2) a Vacancy in the Noble Metals (in ev)

	Cu	Ag	Au
U	2·03	1·96	1·96
U_1 (Meechan and Eggleston 1954)	0·90	—	0·67
(Seeger 1955)	0·90	*c.* 0·8	0·67
(Manintweld 1952, 1953)	1·15	1·27	1·27
(Kauffman and Koehler 1955)	—	—	1·28
U_2 (Meechan and Eggleston 1953)	1·13	—	1·29
(Seeger 1955)	1·13	*c.* 1·2	1·29
(Manintweld 1952, 1953)	0·88	0·69	0·69
(Kauffman and Koehler 1955)	—	—	0·68

Table 4. Theoretical Values for the Energy (U_1) to form a Vacancy in the Noble Metals (in ev)

	Cu	Ag	Au
E_F	7·04	5·51	5·54
$\Delta E_{el}^{Born}=(4/15)E_F$ (§ 2)	1·88	1·47	1·48
$\Delta E_{el}=(1/6)E_F$ (§ 3)	1·17	0·92	0·92
ΔE_R (§ 4)	−0·3	*c.* −0·3	*c.* −0·3
$U_1=\Delta E_{el}+\Delta E_R$	0·9	*c.* 0·6	*c.* 0·6

* The value 1·6 ev stands for the value 1·57 ev which actually follows from Huntington's calculation (1942, section II. 5) (through a misprint 1·57 is given as 1·55). The value 0·4 ev is an estimate of the repulsive energy contribution to the energy of the saddle point which is obtained by considering only the contributions (i) and (ii) of § 5 : according to Huntington (1942) there is no relaxation around a vacancy and thus (iii) is zero. The values of the nearest neighbour contribution quoted by Huntington (1942, Table III) suffer from the same fault discussed in the text just above.

A final comment should be made on the widespread opinion that the energy to form a vacancy in a metal would be related to the heat of sublimation (see, for instance, Nachtrieb and Handler 1954). This is, of course, true for a rigid lattice bound by central forces but there is no reason to expect it to be true for a metal, where the main contribution to the energy to form a vacancy comes from the change in energy of the conduction electrons ; as we have seen, this change in energy is related to the Fermi energy of the metal and not to the heat of sublimation. In this connection it is interesting to consider the case of the noble metals where the latent heat of sublimation and the latent heat of melting have different trends ; while the heat of sublimation of copper is smaller than that of gold, the opposite is true for the heat of melting (Slater 1939). The energy of formation of a vacancy, related to E_F, follows the trend of the heat of melting, and not that of the heat of sublimation ; of course the correspondence between the energy of formation of a vacancy and the heat of melting is purely qualitative.

Acknowledgments

It is a real pleasure to thank Professor N. F. Mott, who suggested this approach to the problem of vacancies in metals, and Dr. J. Friedel for helpful discussions. The writer is indebted to the Council of the Royal Society for a Mr. and Mrs. J. Jaffe Donation, and to the Italian National Research Council for a Fellowship.

References

Abelés, F., 1953, *C.R. Acad. Sci.*, **237,** 796.
Aschner, J. F., 1954, *Ph.D. Thesis*, University of Illinois.
Bartlett, J. H., and Dienes, G. J., 1953, *Phys. Rev.*, **89,** 848.
Brooks, H., 1954, cited by Pines, D., 1954, *Report to the X^e Conseil de Physique Solvay (Bruxelles)*.
Carpenter, L. G., 1953, *J. Chem. Phys.*, **21,** 2244.
Etzel, H. W., and Maurer, R. J., 1950, *J. Chem. Phys.*, **18,** 1003.
Friedel, J., 1952, *Phil. Mag.*, **43,** 153 ; 1954, *Advances in Physics*, **3,** 446.
Fuchs, K., 1936, *Proc. Roy. Soc.* A, **153,** 622 ; *Ibid.* A, **157,** 444.
Gatos, H. C., and Kurtz, A. D., 1954, *J. Metals*, **6,** 616.
Huntington, H. B., and Seitz, F., 1942, *Phys. Rev.*, **61,** 315 ; 1949, *Ibid.*, **76,** 1728.
Huntington, H. B., 1942, *Phys. Rev.*, **61,** 325 ; 1953, *Ibid.*, **91,** 1092.
Jongenburger, P., 1953, *Applied Scientific Research* (B), **3,** 237.
Kauffman, J. W., and Koehler, J. S., 1955, *Phys. Rev.*, **97,** 555.
Kuper, A., Letaw, H., Slifkin, L., Sonder, E., and Tomizuka, C. T., 1954, *Phys. Rev.*, **96,** 1224.
MacDonald, D. K. C., 1953, *J. Chem. Phys.*, **21,** 177, 2097 ; 1955, *Report of the Conference on Lattice Defects in Crystalline Solids held at Bristol, July* 1954 (London : The Physical Society), p. 383.
Manintveld, J. A., 1952, 1953, reported by Broom, T., 1954, *Advances in Physics*, **3,** 26.
Meechan, C. J., and Eggleston, R. R., 1954, *Acta Met.*, **2,** 680.

Mott, N. F., and Jones, H., 1936, *Properties of Metals and Alloys*, chapter IV, § 3.2 (Oxford : Clarendon Press).
Mott, N. F., and Littleton, M. J., 1938, *Trans. Faraday Soc.*, **34,** 485.
Mott, N. F., and Massey, H. S. W., 1950 a, *The Theory of Atomic Collisions*, 2nd ed., chapter II ; 1950 b, *Ibid.*, chapter VII (Oxford : Clarendon Press).
Mott, N. F., 1952, *Progress in Metal Physics*, vol. 3 (London : Pergamon Press Ltd.), p. 93.
Nachtrieb, N. H., Catalano, E., and Weil, J. A., 1952, *J. Chem. Phys.*, **20,** 1185.
Nachtrieb, N. H., and Handler, G. S., 1954, *Acta Met.*, **2,** 797.
Paneth, H. R., 1950, *Phys. Rev.*, **80,** 708.
Seeger, A., 1955, *Z. Naturforsch.*, **10**a, 251.
Seitz, F., 1950, *Acta Cryst.*, **3,** 356 ; 1954, *Rev. Mod. Phys.*, **26, 7.**
Slater, J. C., 1939, *Introduction to Chemical Physics* (New York : McGraw-Hill), Table XVI—1.
Slifkin, L., Lazarus, D., and Tomizuka, C. T., 1952, *J. Appl. Phys.*, **23,** 1032.
Walsh, J. M., and Christian, R. H., 1955, *Phys. Rev.*, **97,** 1544.
Watson, C. N., 1922, *A Treatise on the Theory of Bessel Functions* (Cambridge : University Press), p. 366.
Zener, C., 1950, *Acta Cryst.*, **3,** 346.

CXVII. CORRESPONDENCE

Effect of Heat Treatment on the Internal Friction of Aluminium Crystals

By M. Levy
The Haloid Company
and M. Metzger
University of Illinois

The strengthening of metal single crystals by increasing the rate of cooling after an elevated temperature anneal has recently been observed in simple shear tests of zinc crystals (Li, Washburn and Parker 1953) and in tensile tests on aluminium crystals over a wide range of purity (Maddin and Cottrell 1955). Maddin and Cottrell proposed that the strengthening is due to the restraint on the motion of dislocations resulting from the condensation of vacancies on the dislocation lines to form jogs which move with difficulty and increase the applied stress necessary for the nucleation of slip. The purpose of this note is to cite additional evidence in support of this proposal based on measurements of the damping of aluminium crystals in forced longitudinal oscillation in the kilocycle range. The strain amplitude dependent damping observed in these studies, which results from the periodic motion of dislocations (Read 1940), is related to the earliest stage of plastic flow before dislocation multiplication has begun. A low damping corresponds in a general way to a high yield stress. In this sense, the results of these studies are in good agreement with the results of Maddin and Cottrell.

The measurements were made using the composite oscillator method described by Read (1940). Principal attention was devoted to maximum strain amplitudes from 10^{-6} to something more than 10^{-5} (the upper part of the obtainable range) since the effects of heat treatment were more pronounced in this range. The specimens were 4 mm diameter single crystal rods about 8 cm long of 99·992 or 99·996% aluminium grown from the melt. The decrement (the fraction of the vibrational energy lost per half cycle) was measured at room temperature after various heat treatments carried out with the specimen supported in an alundum boat. It was not necessary to remove the oxide film since the decrement was found not to be affected by its presence.

A marked effect on the decrement of the rate of cooling after an anneal had been observed in preliminary work by J. Intrater and S. Shapiro (unpublished), and this was investigated in some detail for a one day anneal at 640°C. Although in each case there was some decrease in the decrement with time at room temperature, the decrements characteristic

of each cooling rate remained in the same relation to one another. In fig. 1 are shown measurements made after one to three days at room temperature when the changes with time had become very slow. These data are typical of those obtained for several crystals as regards both the effect of cooling rate and the magnitude of the decrement. Both the magnitude of the decrement and the rate of its dependence on strain amplitude are seen to be greatest for furnace cooling, intermediate for air cooling and least for water quenching. The broken curve in fig. 1, which represents an earlier water-quenching test, is given to provide an indication of the reproducibility of the data. The reproducibility was always satisfactory, even after a number of intervening annealing treatments, so that the structure of a crystal after annealing at 640°c was independent of thermal history so far as these measurements were concerned.

Fig. 1

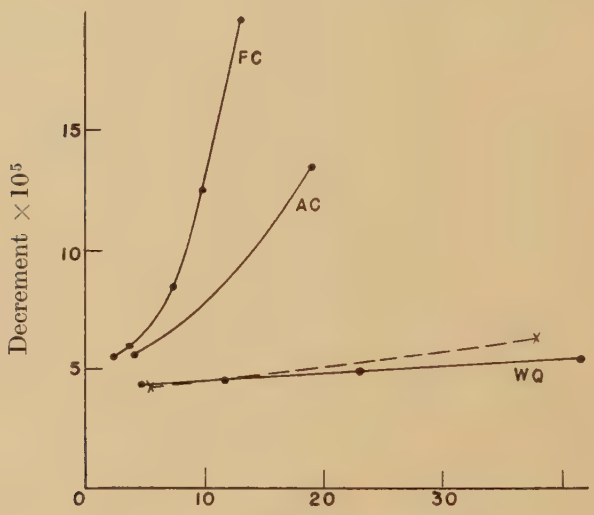

Decrement at 34 kc of a single crystal of 99·992% aluminium as affected by the rate of cooling after annealing 1 day at 640°c. FC=furnace cooled at 50°c hr^{-1} (test No. 6); AC=cooled in still air (test No. 5); WQ= water quenched (test No. 7). The broken curve represents an earlier water quenching test (test No. 3).

The condition of a specimen after furnace cooling may be taken for the moment as reference since a slow cool after annealing has been the traditional practice in damping studies. Now, the effect of increasing cooling rate to depress the damping is not a trivial one due to the strains produced by rapid cooling since it has been observed that the damping of a specimen is lower when it is furnace cooled at 50°c per hour than when it is furnace cooled at a much slower rate. Nonetheless, a word of justification is required with regard to the use of a quenching treatment

in this work since, even though it was performed with care, this is a drastic treatment where measurements of a highly structure-sensitive property are concerned. It is to be noted that the thermal and mechanical shock to which the crystal is subjected during the quench do not appear responsible for the very low decrement observed after quenching since, in the vicinity of room temperature, both these factors markedly increase the decrement of these crystals. It is believed that the effect of these factors is obscured by the opposite and much stronger effect which depresses the damping, and thus the low decrement after quenching is believed to result from the same phenomenon which produces a decrease in the decrement with increased rate of cooling in the range of low cooling rates.

The measurements made in the range where amplitude dependence is substantial show hysteresis, i.e., the decrement remeasured at a given strain amplitude immediately after an intervening exposure to a higher strain amplitude is now higher than the first reading. This is attributed to the breakaway of the dislocation line at some of the sites where it was pinned and is consistent with the conditions treated by Koehler (1952). He considered the dependence of the decrement on the average free length of dislocation line and showed the decrement to vary inversely as a power of the linear density of pinned sites. Then, since the properties of the aluminium crystals studied in this investigation did not change non-reversibly in the course of successive anneals, the general dislocation configuration is considered to have remained unaltered and the effects of heat treatment are considered to have resulted from reversible changes in the density of pinned sites.

The observed effects of cooling rate cannot be ascribed to the redistribution of sites pinned by impurity atoms since the Cottrell or Suzuki atmospheres of the dislocations would be dispersed at 640°c and would be most efficiently reformed to give the lowest decrement at the slowest cooling rate, contrary to observation. It is believed, in agreement with the proposal of Maddin and Cottrell, that the major part of the effects observed can be attributed to the condensation on dislocations of lattice vacancies which are unable to reach the crystal surface during the time the crystal is cooling to room temperature after the anneal. The argument, briefly stated, is that a vacancy has an associated dilatational stress and would be attracted to the edge part of an extended dislocation, and the jog produced would move with difficulty thus serving to pin the dislocation at low stresses ; the stable vacancy pairs formed after quenching (Bartlett and Dienes 1953) have associated shear stresses and could interact with the screw part with similar results.

The number of vacancies available was estimated by using Nowick's (1951) estimate of the volume self-diffusion coefficient of aluminium as $0{\cdot}45\ [\exp(-1{\cdot}43/kT)]\ \mathrm{cm^2\,sec^{-1}}$ and by taking 65% of the activation energy as the energy required for vacancy formation in accordance with the results of Kauffman and Koehler (1955) for gold. The energy to

form a vacancy in aluminium is thus estimated as 0·9 ev and the fraction of vacant sites at 640°c as 10^{-5}. A network of intersecting dislocations is postulated having a density of the order of 10^8 lines per cm^2 corresponding to a value of 10^{-4} cm as the possible free length of the dislocation lines, as required from consideration of the plastic properties of soft single crystals (Cottrell 1953). Thus, the ratio of the length of dislocation line per unit volume to the number of vacancies per unit volume at 640°c is estimated to be of the order of 10^{-9} cm per vacancy. The number of vacancies originally present is therefore so large that, even if many escape to the crystal surface during the quench or combine with one another to form larger groups, there will still be a sufficient number migrating to the dislocations and producing jogs to reduce the average free length of the dislocation lines to a value much below 10^{-4} cm and thus to account for the low decrement observed after quenching.

Effect of Final Annealing Temperature before quenching on the Decrement at 35 kc of a 99·996% Aluminium Crystal. In each case the Crystal was initially annealed one day at 640°c

Test No.	Subsequent heat treatment	Decrement $\times 10^5$ at a maximum strain amplitude of 5×10^{-6}		
		8–11 min. after quench	40–42 min. after quench	1–3 days after quench
1	quenched directly	5·0	3·8	3·7
2	cooled in 5 days to 550°c—quenched	13		9·2
3	cooled in 6 days to 450°c—quenched	19		13·3
4	quenched directly	4·6	3·6	3·8
5	cooled in 10 days to 350°c—quenched	32	21	17

If, instead of quenching from 640°c, the crystal were quenched from a lower final annealing temperature where the equilibrium vacancy concentration is smaller, the decrement would be expected to be higher. This was observed to be the case, as indicated by the data given in the table, both soon after quenching and after one to three days when the decrement was no longer changing at an observable rate. For each test in this series, the crystal was first annealed at 640°c, then it was cooled very slowly in the furnace in order to permit the excess vacancies to migrate to the crystal surface and the equilibrium concentration of vacancies to be approximately maintained, and finally it was quenched from the desired temperature. The magnitude of the decrement after quenching is believed to have been determined by the relative extent to which damping was decreased due to vacancy condensation and increased as a result of thermal and mechanical shock. The large decrement observed after

quenching from 350°C suggests that the latter effect was then predominant. The estimated concentration of vacancies at 350°C (which is 1/200 of the concentration at 640°C) still appears high enough for the vacancies to have been able to exert some influence.

A further test of the vacancy hypothesis is afforded by observations of the rate of decrease in the decrement with time at room temperature after quenching. Maddin and Cottrell had noted that the critical shear stress measured soon after quenching was lower than that obtained after the crystal had remained at room temperature for a few days. They attributed this to the gradual migration to the dislocations of those vacancies which were still dispersed immediately after quenching. In the present work, the decrement after quenching fell rapidly with time, as indicated in the table by the values obtained in three of the tests 40–42 minutes after quenching. The major part of the change was accomplished within a few hours in all crystals quenched from elevated temperatures. Now, the diffusion coefficient for vacancies can be obtained by dividing the volume self-diffusion coefficient by the equilibrium fraction of vacancies (Bardeen and Herring 1952). The present estimates of these quantities lead to an estimate of the vacancy-diffusion coefficient at room temperature as greater than 10^{-10} cm^2 sec^{-1}. This is large enough for diffusion over distances of the order of 10^{-4} cm in a few hours to be nearly complete, i.e., the diffusion parameter $x/2D^{1/2}t^{1/2}$ is about 0·1, and is thus consistent with the view that the decrease in the decrement with time is due to the diffusion of vacancies. This effect cannot be due to the diffusion of impurity atoms to the dislocations; the volume chemical diffusion coefficients for solute atoms in aluminium range from 10^{-22} to 10^{-24} at room temperature as calculated from Nowick's (1951) estimates, and even if the diffusion of the solute atoms were enhanced by the excess vacancies present after quenching, the solute atoms could not have effective diffusion coefficients even within several orders of magnitude of 10^{-10}.

This work was done at Columbia University and was supported in part by the Office of Ordnance Research.

References

Bardeen, J., and Herring, C., 1952, *Imperfections in Nearly Perfect Crystals* (London: Chapman and Hall, Ltd.), p. 261.

Bartlett, J. H., and Dienes, G. J., 1953, *Phys. Rev.*, **89**, 848.

Cottrell, A. H., 1953, *Dislocations and Plastic Flow in Crystals* (Oxford: Clarendon Press), p. 103.

Kauffman, J. W., and Koehler, J. S., 1955, *Phys. Rev.*, **97**, 555.

Koehler, J. S., 1952, *Imperfections in Nearly Perfect Crystals* (London: Chapman and Hall, Ltd.), p. 197.

Li, C. H., Washburn, J., and Parker, E. R., 1953, *Trans. Amer. Inst. Min. and Met. Engrs.*, **197**, 1223.

Maddin, R., and Cottrell, A. H., 1955, *Phil. Mag.*, **46**, 735.

Nowick, A. S., 1951, *J. Appl. Phys.*, **22**, 1182.

Read, T. A., 1940, *Phys. Rev.*, **58**, 371.

Impurity Diffusion in Polar Crystals

By J. Teltow
Institut für Kristallphysik, Deutsche Akademie der Wissenschaften, Berlin

[Received June 3, 1955]

In a previous paper submitted to this journal, A. B. Lidiard* has given a very lucid and elegant statistic analysis of the diffusion of divalent ions in monovalent ionic crystals, e.g. Cd^{++} in AgBr. The same problem was treated by Schöne, Stasiw and the author a few years ago, starting from general thermodynamic transport equations. The purpose of this note is to show that, with a slight simplification, these calculations still remain valid and, in Lidiard's special case, lead to the same result.

Lidiard's principal objection concerns our use of a diffusion coefficient D_C for unassociated Cd^{++} ions, of effective charge $+1$, as distinct from the diffusion coefficient D_k for associated pairs of cadmium ions and silver ion vacancies. Owing to their neutrality, the diffusion of the latter is not influenced by the Nernst diffusion potential, in contrast to the behaviour of the unassociated Cd^{++}. Assuming that the divalent impurity ions can move only by jumps into adjacent vacancies, this kind of double-line description of an essentially uniform diffusion mechanism seems somewhat unsatisfactory.

The D_C term was introduced by us to account for the ideal case of 'no association' when only accidental meetings of cadmium ions and silver ion vacancies occur. Diffusion of the cadmium will then still be possible. Meanwhile it has become clear that instead of putting the number per cm³ of pairs $n=0$, this ideal case is described correctly by the vanishing of the free energy of association ΔG. According to the association equilibrium (Stasiw and Teltow 1947, Teltow 1949)

$$\frac{N_+ n}{(N_i - n)N_v} = K_2 = 12 \exp(\Delta G/kT), \quad . \quad . \quad . \quad . \quad . \quad (1)$$

this is equivalent to $K_2=12$ or $n=12\ N_iN_v/(N_+ + 12N_v)$. Here N_+, N_i and N_v are the numbers of cation sites, totally added Cd^{++} ions and silver ion vacancies per cm³, respectively, and 12 is the number of nearest cation neighbours of a cation site in a face centred cubic (NaCl type) lattice. For small degrees of disorder, $12N_v \ll N_+$ and $n \simeq 12N_iN_v/N_+$ which agrees with direct statistic computation. Thus the D_k term alone gives rise to a non-vanishing macroscopic diffusion coefficient D in this case too.

---

* The author is very much indebted to Dr. Lidiard for receiving a preprint of this paper.

This ideal case should not be confounded with the extreme case ' no pairs at all ', characterized by $\Delta G \to -\infty$ (strong repulsive forces between the partners), and therefore $K_2=0$, $n=0$ and $D=0$.

We therefore agree with this part of Lidiard's criticism and shall obtain a correct description of the AgBr–Cd case by putting $D_C=0$ in our calculations (see below). This procedure automatically rules out the influence of the diffusion potential. It must be emphasized, however, that the general equations with $D_C \neq 0$ are still valuable in cases where diffusion of the impurity ions proceeds by two different mechanisms. This has been demonstrated by Schöne, Stasiw and the author for the diffusion of cuprous ions in AgBr, which partially move via interstitial sites. In such cases, the diffusion potential has an important bearing on the migration of the impurity ions. It will even, to a small amount, modify the probabilities of the orientation jumps of the pairs in the AgBr–Cd case and thus involve the diffusion coefficient. This effect, though presumably negligible, should be examined in a refined analysis.

From eqn. (12) of our paper (Schöne, Stasiw and Teltow 1951), then, we obtain by putting $D_C=0$, in Lidiard's notation

$$D=D_0 \frac{2nN_v}{2N_iN_v-(N_i-n)^2} \quad . \quad . \quad . \quad . \quad . \quad . \quad . \quad (2)$$

where $D_0=D_k$, by a reasoning analogous to eqns. (2), (3) and (5) of our paper, is given by

$$D_0=4a^2w_2/12=a^2w_2/3. \quad . \quad . \quad . \quad . \quad . \quad . \quad . \quad (3)$$

Here a is the nearest anion–cation separation (half lattice constant), and w_2 is the number of jumps of the cadmium ion into an adjacent vacancy per sec. If w_2 is not small compared with the jump probability w_1 of the vacancy to another attached cation position, then in (3) w_2 has to be replaced by $w_1w_2/(w_1+w_2)$. This has been stated already by Schottky (1950).

Equation (2) includes the more general case of the number of thermal defects being comparable with the number of impurity ions (e.g. silver halides above 300°C with additions of about 0·1%). To obtain Lidiard's result, we only have to specialize by neglecting the thermal disorder, i.e. $N_v=N_i-n$. Evaluation of n from (1) and insertion in (2) then leads immediately to

$$D=D_0[1-(1+4K_2N_i/N_+)^{-1/2}] \quad . \quad . \quad . \quad . \quad . \quad . \quad (4)$$

which is Lidiard's final equation. If, on the other hand, the thermal defects have to be accounted for, the calculation of N_v, n and N_p (number of positive lattice defects, e.g. interstitial cations (Frenkel type) or anion vacancies (Schottky type)) by means of the eqn. (1),

$$N_v-N_p=N_i-n \qquad \text{(neutrality condition)}, \quad . \quad . \quad . \quad . \quad . \quad (5)$$

and

$$N_+^2/N_vN_p=K_1 \qquad \text{(law of mass action for thermal disorder)} \quad (6)$$

yields, upon insertion in (2), no simple relation. Nevertheless, this procedure is sometimes indispensable. As an example we take the approximate proportionality of D with N_i resulting from (4) if $4K_2N_i/N_+ \ll 1$. It follows from (1), (2), (5) and (6) that this is no more valid when N_i/N_+ becomes as small as $K_1^{-1/2}$. For still smaller additions N_i the diffusion coefficient is, expanding to the linear term

$$D=D_0(1-L+K_2L^3N_i/N_+ + \ldots),$$

where $L=(1+K_2K_1^{-1/2})^{-1}$. It should be kept in mind that the whole association model is only an approximation for very small (thermal or foreign ion induced) disorder of the lattice. Escaping towards the range of higher impurity concentrations in order to simplify the equations may be sometimes of doubtful practical value.

References

Lidiard, A. B., 1955, *Phil. Mag.* (in the press).
Schöne, E., Stasiw, O., and Teltow, J., 1951, *Z. Phys. Chem.*, **197**, 145.
Schottky, W., 1950, *Forschungen und Fortschritte*, **26**, 3. Sonderheft, 6.
Stasiw, O., and Teltow, J., 1947, *Ann. d. Physik* (6), **1**, 261.
Teltow, J., 1949, *Ann. d. Physik* (6), **5**, 71. In this paper, eqn. (26) relating K_2 and $W_a=R\Delta G/k$ contains an obvious sign mistake. Consequently the true value of W_a is 3600 cal/mole.

Strain-Hardening of a Metal by Laminar or Turbulent Flow

By W. A. Wood
Metallurgy Research Department, University of Melbourne

[Received June 3, 1955]

The theories of strain-hardening due to G. I. Taylor and Mott suggest that the more a metallic structure is disordered the more is it likely to develop barriers to free dislocations and the more rapidly therefore is it likely to strain-harden. Cottrell (1952) has generalized this view by distinguishing between a turbulent flow that disorders the structure during deformation and a laminar flow which does not; turbulent flow hardens more effectively.

It is therefore of interest to test by experiment how effective different forms of disordering may be in practice. One form particularly amenable to experiment is produced in polycrystalline metal by uni-directional deformation. This is the disorientation of the grains that gives rise to x-ray asterisms.

Tests on this particular disordering, summarized in the present note, show rather surprisingly, however, that it has little effect. All it affects is the stability of the hardened structure.

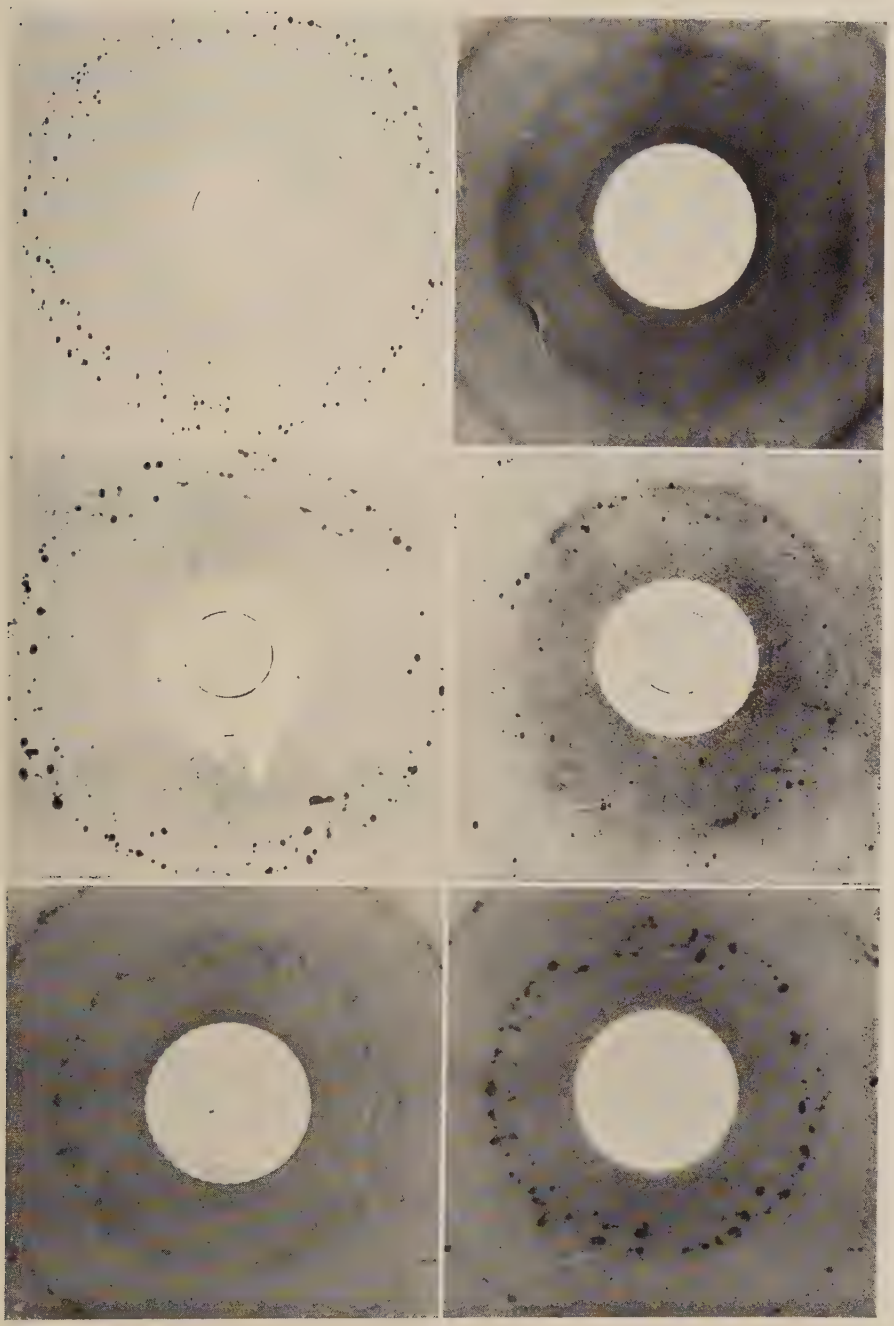

X-ray back-reflection (400) rings from copper. (1) As annealed ; (2) after 5% stretch, hardness 66 VPN ; (3) after cyclic stress, hardness 67 VPN ; (4) after heating stretched specimen, softening by recrystallization ; (5) a specimen hardened cyclically to 63 VPN ; (6) same specimen after heating, softened to 44 VPN without recrystallization (same spots as before heating).

These points may be demonstrated by x-ray back-reflection photographs from polycrystalline copper.

Figure 1 (figs. 1–6, Plate 19) is typical of the structure in the undisordered state after annealing and before deformation. The perfection of the grains is shown by the sharpness of the reflection spots. The hardness in this state was 35 VPN.

Figure 2, from the same material after 5% extension under a tensile stress of 7 tons/m^2, is typical of disordering by uni-directional deformation. The grains reflect over an extended angular range, causing the reflections to diffuse into the continuous rings. Each grain is therefore reduced to differently oriented domains. This flow, evidently turbulent, raised the hardness to 66 PNV.

Figure 3 is from the same material hardened to the same degree, 67 VPN, but by 10^5 cycles of alternating tension–compression at ± 7 tons/in.^{2} applied in a Haigh fatigue-testing machine. This is typical of the alternating deformation about a mean zero stress that is commonly used in fatigue testing. Clearly this hardening occurs without significant disorientation of the grains, or in fact any detectable disordering, for the reflection spots are virtually as sharp as they were initially. Thus we have the same hardening by flow that relative to the foregoing is laminar.

The comparison, then, demonstrates the first point that disordering by disorientation is not essential to strain-hardening.

Its influence on stability was examined by heating specimens such as the above in stages of one hour at 200°, 250°, 300°C . . . and subjecting them after each stage to hardness and x-ray tests. The disordered and undisordered states then responded differently as follows.

Disordered state. Here (i) the disorientation is only removed by recrystallization ; (ii) the strain-hardening also is removed only by recrystallization ; (iii) this recrystallization sets in and is completed at a relatively low temperature.

Thus fig. 4 from the disordered specimen after heating at 350°C is typical of the first signs of softening. New reflection spots from recrystallized grains appear in the still continuous rings. The spots multiply at the expense of the rings until recrystallization is complete, in this case at 400°C.

Undisordered state. Here (i) the strain-hardening may disappear largely before recrystallization ; (ii) recrystallization is postponed to a higher temperature.

These features may be illustrated by a fatigue specimen first hardened to 63 VPN at ± 7 tons/in.^{2}. This specimen was so held that the same areas could be x-rayed before and after heat-treatment and the same reflection spots thereby kept under observation. In this way a sensitive and non-destructive test for recrystallization is obtained, for new grains and therefore new reflection spots are produced as soon as recrystallization sets in. Figure 5 shows the reflection spots in the initially hardened state of 63 VPN. Figure 6 shows that the same spots persist after

heating to 600°C, when the hardness fell to 44 VPN. Hence this softening has occurred before recrystallization. In this instance recrystallization did not occur until the temperature was raised to the relatively high value of 650°C.

These further tests show, then, that the disordered state is the less stable, since it recrystallizes first.

It is believed that these observations are of interest in showing that hardening of the same pure metal can occur by different dislocation-arrays according to the mode of deformation.

Thus, on the one hand, the array responsible for strain-hardening under the turbulent uni-directional deformation might be interpreted on Mott's theory as a relatively coarse array of piled-up groups, each containing many unit dislocations ; for the main slip bands produced by such deformation are spaced widely, and the slip jumps are avalanches of many unit slip movements. Further it would appear that these piled-up groups are located on the network of sub-boundaries delineating the disoriented domains ; for both disorientation and strain-hardening, removal of which implies a dispersing of the pile-ups, disappear together on heating.

On the other hand the array produced by the alternating deformation is more likely to be a finer distribution of smaller pile-ups, on the following grounds. The criterion for the comparatively laminar flow in the fatigue specimens is that the stress cycle should initially be built up by alternating increments that are small, preferably producing not more than about $\pm 0{\cdot}1\%$ strain, so that the stress never produces any large uni-directional strain (Wood and Davies 1953). A strain of $0{\cdot}1\%$ in a grain of say 10^{-3} cm means an extension of 10^{-6} cm. Thus the criterion is that the plastic strain should be restricted to slip jumps of less than some 10^{-6} cm, that is, to what may be classed as ' fine ' slip. In this case, therefore, the pile-ups must consist of fewer unit dislocations ; and since they are capable of hardening as effectively as the coarser pile-ups, they must be more closely spaced. Whether they also are located on sub-boundaries it is not possible on the evidence to say, since such fine slip does not significantly disorient the grain.

On this view the disoriented structure becomes more unstable because of the higher stress concentrations associated with the larger pile-ups. Recrystallization occurs before they can disperse in any other way.

It is suggested that experiments of this kind, dealing with pure metal hardened to the same degree but by different internal changes, may help in a much-needed physical interpretation of the dislocation-arrays postulated by the theories of strain-hardening.

References

Cottrell, A. H., 1952, *Dislocations and Plastic Flow in Crystals* (Oxford : University Press).

Wood, W. A., and Davies, R. B., 1953, *Proc. Roy. Soc.* A, **220**, 255.

Upper Limits for the Lifetimes of the Excited States of Titanium 46

By R. E. Azuma
Department of Natural Philosophy, The University, Glasgow*

[Received July 4, 1955]

Recent beta-spectrometer studies of the ^{46}Sc decay (Keister and Schmidt 1954) give an indication of the order of emission of the two gamma-rays ; the decay scheme is shown in fig. 1. The spins and parities have been determined by angular correlation and polarization experiments (Brady and Deutsch 1948, 1950). Both gamma-rays are expected to be electric quadrupole. Weisskopf's (1951) theoretical relation for the lifetimes of gamma-ray transitions yield lifetimes of 1×10^{-11} sec and 7×10^{-11} sec for the 1·12 MeV and 0·89 MeV transitions respectively. The results of delayed coincidence experiments (Murdoch and Webb 1954, Whittle and Porter 1953) place an upper limit of $1{\cdot}5\times10^{-9}$ sec on the lifetimes of the states in ^{46}Ti.

Fig. 1

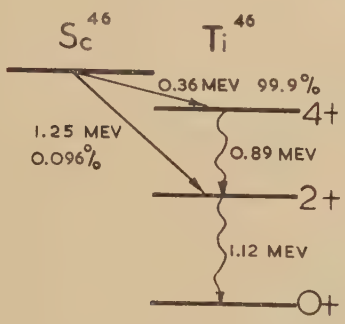

Decay scheme of ^{46}Sc.

Experiments have been carried out in this laboratory to examine more closely the lifetimes of these states in ^{46}Ti. A fast coincidence apparatus similar to that described by Bell, Graham and Petch (1952) with a resolving time $\tau_0\approx2{\cdot}5\times10^{-9}$ sec was used. In this case we have used separate side channels with a display on a cathode ray tube (see Ferguson and Lewis 1953, Azuma and Lewis 1955) to effect the necessary pulse height selection. Three coincidence experiments were performed: (1) a γ–γ coincidence experiment with ^{46}Sc using ^{60}Co to provide prompt coincidences for comparison, (2) a β–γ, γ–γ 'self-comparison' experiment involving only the ^{46}Sc source, (3) a β–γ coincidence experiment in which the ^{46}Sc decay was compared with that of ^{60}Co.

The first experiment determines the lifetime of the intermediate state of ^{46}Ti by 'comparing' the γ–γ coincidence resolution curve with that of ^{60}Co. The two counters used plastic phosphors (from Pilot Chemical Inc.) in the form of right circular cylinders, 1 in. diameter by 1 in. long,

* Communicated by Professor P. I. Dee, F.R.S.

surrounded by magnesium oxide and contained in aluminium cans thick enough to stop all beta particles, and mounted on E.M.I. photomultipliers Type 6262. The side channel kicksorters accepted energy bands 100 kev wide with one side accepting only pulses due to the 1·12 Mev gamma-ray from ^{46}Ti, the other side accepting pulses from both gamma-rays. The positions of these bands were set to include regions of similar pulse height distribution from each source, and also to exclude coincidences due to Compton back-scattered quanta. The ^{60}Co lifetime has been found to be less than 10^{-11} sec (Bay *et al.* 1955) ; but even supposing the lifetime to be as large as 5×10^{-11} sec this source provides a ' prompt ' comparison since either counter can accept the first gamma-ray, and the two γ-rays are detected with almost equal efficiencies. For these reasons a slight broadening of the resolution curve rather than a shift of the centroid is produced. A series of coincidence resolution curves were obtained, the curves for each source being taken alternatively, with one run consisting of a group of four curves. The shifts of the centroids give directly a measurement of the lifetime (Bay 1950). The result of three runs gave a lifetime of less than 5×10^{-11} sec, which is regarded as the limit of stability of the apparatus.

Since the lifetime of the intermediate state of ^{46}Ti is less than 5×10^{-11} sec, a ' self-comparison ' method was used to determine an upper limit for the lifetime of the second excited state. The plastic phosphor on one counter was replaced by a 1 cm cube of *trans*-stilbene for the detection of both beta and gamma rays. The output from the other counter, the gamma-counter, was passed through a discriminator rather than a kicksorter, and was biased to accept pulses from both gamma-rays. Thus a β–γ coincidence resolution curve modified by about 20% γ–γ prompt coincidences was obtained. Since the gamma-counter accepts pulses due to both gamma-rays, the β–γ resolution curve contains contributions from the lifetimes of both excited states of ^{46}Ti. The γ–γ prompt curve was obtained by inserting a 270 mg/cm^2 aluminium absorber between the source and the β-counter. The side channel kicksorter ' windows ' were again set in positions where the shapes of the pulse height distributions were similar for each source. A lead absorber, 0·5 cm thick, was placed between the source and the gamma-counter to attenuate back-scattered quanta. Several runs, again in groups of four, were obtained and showed that the excited state lifetimes of ^{46}Ti are both less than 5×10^{-11} sec.

To confirm the two above results, a third measurement was made by comparing the β–γ cascade of ^{46}Sc with that of ^{60}Co, which is known to have lifetimes of less than 10^{-11} sec (Bay 1955). A thin stilbene crystal, 1·5 mm thick, was used on the beta-counter, and to reduce further the effects of back-scattering a 0·5 cm lead absorber was placed between the source and the gamma-counter. A comparison of the coincidence resolution curves for the two sources shows that the lifetimes of the two excited states of ^{46}Ti are both less than 5×10^{-11} sec, thus confirming the above results. Figure 2 shows a set of coincidence resolution curves for this experiment.

Fig. 2

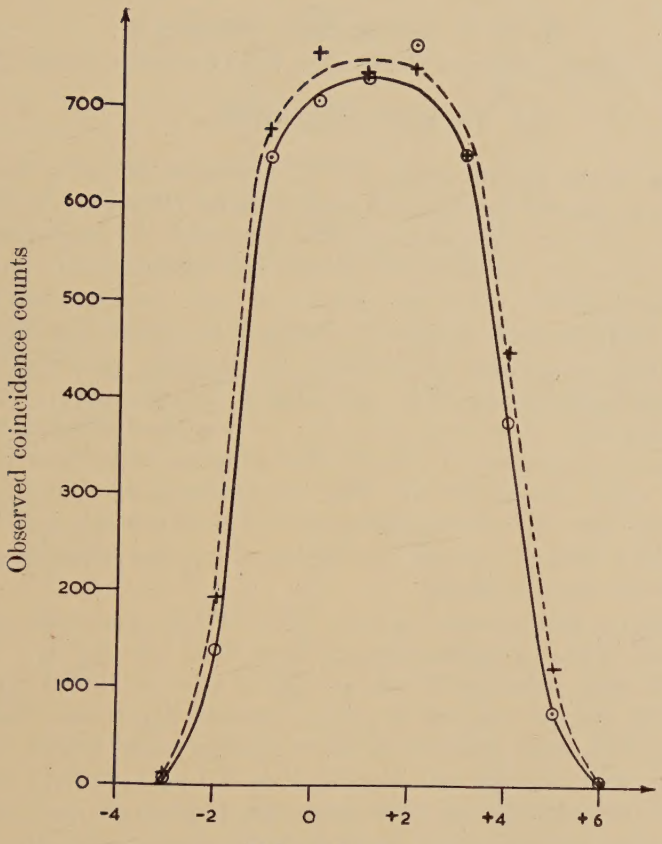

β–γ coincidence resolution curves for ^{46}Sc and ^{60}Co.
—— ⊙—— ^{46}Sc – – + – – ^{60}Co

The author would like to thank Dr. G. M. Lewis for many helpful discussions. He is also indebted to Professor Dee for the interest shown in this work, and to the Nuffield Foundation for a Studentship.

References

Azuma, R. E., and Lewis, G. M., 1955, *Phil. Mag.*, **46,** 1034.
Bay, Z., 1950, *Phys. Rev.*, **77,** 419.
Bay, Z., Henri, V. P., and McLernon, F., 1955, *Phys. Rev.*, **97,** 561.
Bell, R. E., Graham, R. L., and Petch, H. E., 1952, *Canad. J. Phys.*, **30,** 35.
Brady, E. L., and Deutsch, M., 1948, *Phys. Rev.*, **74,** 1541; 1950, *Ibid.*, **78,** 558.
Ferguson, A. T. G., and Lewis, G. M., 1953, *Phil. Mag.*, **44,** 1339.
Keister, G. L., and Schmidt, F. H., 1954, *Phys. Rev.*, **93,** 140.
Murdoch, H. S., and Webb, A. J., 1954, *Proc. Phys. Soc.* A, **67,** 286.
Weisskopf, V. F., 1951, *Phys. Rev.*, **83,** 1073.
Whittle, C. E., and Porter, F. T., 1953, *Phys. Rev.*, **90,** 498.

The Lifetime of the First Excited State of Thallium 203

By R. E. Azuma and G. M. Lewis
Department of Natural Philosophy, The University, Glasgow*

[Received July 4, 1955]

The lifetime of the 280 kev state of ^{203}Tl, produced following the β-decay of ^{203}Hg, was shown by Deutsch and Wright (1950) to be less than 3×10^{-9} sec. Conversion coefficient data suggested the transition was an M1, E2 mixture (cf., for instance, Wilson and Curran 1951, Rose *et al.* 1951). Lifetimes of 2×10^{-12} sec and 5×10^{-9} sec are expected from the Weisskopf (1951) formula for pure M1 and pure E2 transitions respectively. The resonance scattering experiments of Metzger and Todd (1954), Metzger (1954), involving ^{203}Tl, indicated a lifetime ($T\gamma$) of the state against γ-emission, of between $(10\pm4)\times10^{-10}$ sec and $(9\pm4)\times10^{-10}$ sec. This heightens the interest of a direct determination which was in progress here and which we report in this communication. Comparison by results of the two methods has hitherto only been possible for ^{198}Au and then only in a limited manner, the region of overlap being in general a difficult one for both methods.

A coincidence unit of resolving time $\sim2\times10^{-9}$ sec was employed, using two selected E.M.I. photomultipliers type 6262 (cf. fig. 1). The fast mixing unit with delay cable was similar to that of Bell, Graham and Petch (1952), but the two sets of pulses, contributing to the coincidences finally observed, were selected to lie in narrow pulse height bands by kicksorting after mixing (cf. Ferguson and Lewis 1953). At a fast coincidence, the cathode ray tube beam was brightened, and lengthened pulses from the dynodes of the two counters were applied to the X and Y deflecting plates respectively causing brightened spots to appear. Spots appearing on a small selected area of the display activated an auxiliary photomultiplier, operating a scaler. This apparatus allows comparisons to be made of the coincidence resolution curves involving radiations of different kinds.

A delayed coincidence curve was obtained for the β–γ rays of ^{203}Hg. It was compared with a prompt curve for coincidences between the two simultaneous quanta from the annihilation of positrons, generated by a ^{22}Na source enclosed in aluminium. A stilbene crystal, 1 cm cube, was used on one counter. A plastic scintillator, 1 in. long, 1 in. diam. (from Pilot Chemical Inc.) surrounded by a $\frac{1}{8}$ in. thickness of magnesium oxide in a $\frac{1}{32}$ in. aluminium container, on the other counter, detected γ-radiations only. The source lay between the two scintillators. The narrow energy channels were positioned to eliminate coincidences involving Compton back scattering or x-rays, at settings where the respective pulse height distributions of the radiations of ^{203}Hg and ^{22}Na were similar in shape.

---

* Communicated by Professor P. I. Dee, F.R.S.

Fig. 1

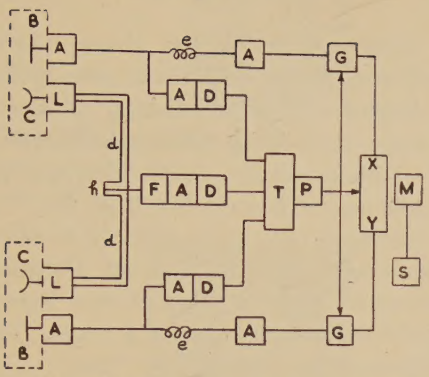

C, photomultiplier collector ; B, dynode ; L, limiter ; A, amplifier ; d, main delay cable ; h, stub ; F, fast crystal mixer ($\sim 2\times10^{-9}$ sec) ; D, discriminator; T, slow coincidence unit ($\sim 1\,\mu$ sec); P, pulse former; e, $1\,\mu$ sec delay ; G, gate and lengthener ; XY, cathode ray tube ; M, auxiliary multiplier ; S, scaler.

Fig. 2

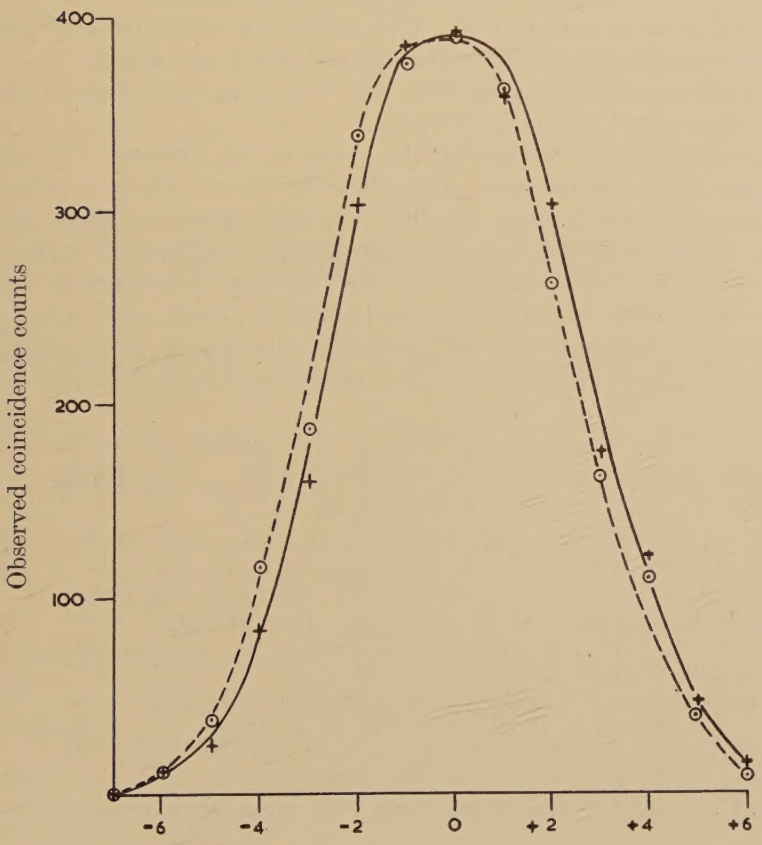

Coincidence counts as a function of delay.
——+—— ^{203}Hg β–γ coincidences.
– – ⊙ – – prompt coincidences between annihilation quanta.

A lead sheet $\frac{1}{10}$ in. thick with a hole $\frac{1}{5}$ in. diam. was inserted between the source and the stilbene as an additional precaution against Compton back scattering. Following pile irradiation of mercury the radioactive mercury had been allowed to decay ubefore se to remove isomers of ^{197}Hg. For a prompt coincidence run in which ^{22}Na was substituted for ^{203}Hg the counters were each moved 5 cm in line from the ^{22}Na source, so that the 1·28 MEV γ-ray contributed only very slightly to the coincidence count; the small delay times associated with it (cf. Ferguson and Lewis 1953) were then of no account. Several pairs of runs were taken in succession. Figure 2 shows results for one such set of 4 runs. The observed centroid shifts, giving the lifetime, lay near 3×10^{-10} sec.

As a check on these results, comparison of the delayed coincidence curve for the β–γ rays of ^{203}Hg was made with the delayed coincidence curve for the β–γ rays of ^{198}Au. ^{198}Au yields a state of half-life $(1\cdot0\pm1\cdot7)\times10^{-11}$ sec (Graham and Bell 1951), which can be considered prompt for this experiment. A stilbene crystal, 1·5 mm thick, was employed on the β-side. The narrow energy channels were used as previously also the lead screen. The results for many pairs of runs in succession showed similar centroid shifts to those found above.

The lifetime of the excited state of ^{203}Tl is, on the basis of all the measurements here $(3\pm1)\times10^{-10}$ sec.

Because of internal conversion the value of the lifetime ($T\gamma$) against γ-emission, of the 280 kev state, determined by the resonance experiments quoted earlier, will exceed by 20% the corresponding figure for the lifetime of the excited state. The lifetime of the excited state from the resonance method $(8\pm3\cdot2, 7\cdot2\pm3\cdot2)\times10^{-10}$ sec, is therefore in a range above that found directly here, the limits of error just adjoin. In conclusion, comparison with the Weisskopf formula shows a substantial electric quadrupole component in the transition.

One of us (R. E. A.) is indebted to the Nuffield Foundation for a Studentship.

References

Bell, R. E., Graham, R. L., and Petch, H. E., 1952, *Canad. J. Phys.*, **30**, 35.
Deutsch, M., and Wright, W. E., 1950, *Phys. Rev.*, **77**, 139.
Ferguson, A. T. G., and Lewis, G. M., 1953, *Phil. Mag.*, **44**, 1339.
Graham, R. L., and Bell, R. E., 1951, *Phys. Rev.*, **84**, 380.
Metzger, F. R., 1954, *Proc. Glasgow Conference on Nuclear and Meson Physics* (Pergamon Press), p. 201.
Metzger, F. R., and Todd, W. B., 1954, *Phys. Rev.*, **95**, 627.
Rose, M. E., Goertzel, G. H., Spinrad, B. I., Herr, J., and Strong, P., 1951, *Phys. Rev.*, **83**, 79.
Weisskopf, V. F., 1951, *Phys. Rev.*, **83**, 1073.
Wilson, H. W., and Curran, S. C., 1949, *Phil. Mag.*, **40**, 631.
